

THÈSE

présentée pour obtenir le grade de docteur
de l'École Nationale Supérieure des Télécommunications

Spécialité: **Électronique et Communications**

Andrea ANCORA

**Techniques de réception avancées pour systèmes
de télécommunications cellulaires sans-fils de type
3GPP LTE**

Soutenue le 26 Novembre 2010 devant le jury composé de:

<i>Président :</i>	David GESBERT	- Eurecom
<i>Rapporteurs :</i>	Luc DENEIRE	- Université de Nice
	Merouane DEBBAH	- Supélec
<i>Directeur :</i>	Dirk SLOCK	- Eurecom
<i>Invité :</i>	Giuseppe MONTALBANO	- ST-Ericsson

Acknowledgments

To my parents, who brought me down from the sky to the earth with their incredible creative energy.

To my Audrey, who everyday brings me to heaven with her unconditional love.

To Professor Slock, who is source of endless inspiration and conduct.

To my colleagues, who always supported me in every sense throughout this incredible journey.

Abstract

Achieving enhanced spectral efficiency and increased reliability are the leading objectives of upcoming wireless systems. In the pursuit of these objectives, it is imperative to devise strategies taking into account the practical constraints so that the ensuing solutions are implementable in the real world. Our focus in this thesis is therefore on the practical communication systems.

In the first introductory part of the thesis, we discuss the classical Orthogonal Frequency Division Multiplexing (OFDM) principle highlighting its advantages such as low-required decoding complexity in case of multipath propagation channel together with its well-known limitations induced by impaired reception. Furthermore, we carefully examine its application to next generation 3GPP Long Term Evolution (LTE) wireless telecommunication system. In this sense, LTE OFDMA physical-layer system parameters are detailed and their dimensioning explained from the 3GPP standard perspective.

In the second part of the thesis, we first consider the design of Reference Signals in LTE and the wireless propagation channel model. We then approach the Channel Estimation problem. In particular, we study the impact of LTE system parameters on common linear channel estimation techniques and introduce several new methods applicable in this specific context. Furthermore, we propose a general framework for the performance analysis of classical and proposed methods.

In the last part of the thesis, we consider impaired OFDM reception in the case of selective channels. As a first step, we deal with linear OFDM equalization in highly doubly selective channels. In order to avoid complex matrix inversion entailed by straightforward application of linear equalization, we develop iterative equalization methods which show to be very attractive from an implementation point of view. Exploiting Basis Expansion Model of the frequency-selective time-varying channel and preconditioning, we show that the complexity of such methods are roughly linearly proportional to the OFDM FFT order but yet attaining MMSE equalizer performance within an acceptable performance loss. Finally, we discuss Alamouti block-code reception for OFDM in case highly selective channel. We determine useful Maximum Likelihood (ML) detection bounds and then revise linear

and non-linear detection approaches. To overcome known sub-optimality of such methods, we present a Lattice Reduction aided near-ML technique which reveals to offer optimal diversity-order detection performance with negligible coding gain loss.

Resumé

Atteindre une meilleure efficacité spectrale et une fiabilité accrue sont les objectifs principaux des systèmes sans fil à venir. Dans la poursuite de ces objectifs, il est impératif d'élaborer des stratégies tenant compte des contraintes d'ordre pratique afin que les solutions qui en découlent soient applicables dans le monde réel. Dans cette thèse, l'accent est donc mis sur les systèmes de communication ayant une dimension pratique et réalisable.

Dans la première partie introductive de la thèse, nous discutons le principe du Multiplexage Orthogonale en Fréquence (OFDM) en soulignant ses avantages comme la faible complexité nécessaire à sa détection dans le cas de canal de propagation multi-trajet et aussi les désavantages dérivants de la violation des assumptions de réception pour ce type de modulation. En particulier, on examine dans le détail son application aux systèmes de nouvelle génération 3GPP LTE. Dans ce sens, on détaille les paramètres de la couche physique de LTE OFDMA et leur dimensionnement dans la perspective du standard 3GPP.

Dans la deuxième partie de la thèse, on considère d'abord le principe utilisé pour les Signaux de Référence en LTE et la modélisation du canal sans-fil. On aborde ensuite le problème de l'estimation de canal en étudiant l'impacte des paramètres système LTE sur les méthodes classiques d'estimation de canal linéaires. On introduit plusieurs nouvelles techniques applicables dans le contexte spécifique du LTE et on analyse leurs performances en proposant un cadre général commun.

Dans la dernière partie de la thèse, on considère la détection du signal OFDM détérioré par des canaux hautement sélectifs. Dans un premier temps, on se penche sur l'égalisation linéaire du signal OFDM dans le cas de canaux doublement sélectifs. Pour éviter la complexité élevée engendrée par l'application directe de l'égalisation linéaire, on développe de méthodes itératives qui montrent un intérêt dans l'applicabilité dans le monde réel. En exploitant la Modélisation par Expansion en Bases du canal et le pre-conditionnement, on démontre que la complexité de ces méthodes est grossièrement proportionnelle à l'ordre de la FFT tout en offrant des performances très proches de l'égalisation par Minimisation de l'Erreur Quadratique Moyenne. Finalement, on discute la réception des codes à blocs Alamouti pour

OFDM dans le cas de canaux sélectifs. On détermine également les limites de performances atteignables lors de détection par Maximum de Vraisemblance. Ensuite, on révisé les approches de détection linéaires et non linéaires. Pour surmonter la sous-optimalité connue de ces méthodes, on présente une méthode dite presque-MV basée sur Réduction de Treillis qui se révèle exploiter d'une façon optimale l'ordre de diversité du code avec une perte négligeable en terme de gain de codage.

Thesis Contributions

- Contributions
 - We propose a general approach to pilot-aided linear channel estimation
 - * We perform among the few and first comprehensive overview of FD channel estimation methods for (LTE) OFDMA
 - * We offer an insight on the impact of LTE system parameters
 - * We suggest several novel schemes for robust LS based on down-sampling and approximated MMSE methods
 - * *The publication related to this contribution was selected in IEEE Com. Soc. LTE Tech-focus, sponsored by Anritsu*
 - We conduct a comprehensive study of preconditioned iterative ICI cancellation
 - * We suggest an original approach to equalization of TV channels by means of fast-converging iterative techniques based on preconditioning
 - * We invented an optimal receiver structure in the MMSE sense subject to limited-complexity constraint
 - We investigate the Alamouti block codes detection over selective channels
 - * We derive ML detection bounds of Alamouti codes over selective channels
 - * We propose novel detection schemes among which an approach based on Lattice-Reduction
- The work done throughout the thesis allowed the filing of over 15 patents

- Publications

- Articles

- * “Down-Sampled Impulse Response Least-Squares Channel Estimation for LTE OFDMA”, A. Ancora, C. Bona and D. T. M. Slock - ICASSP 2007.
 - * “Performance analysis of general pilot-aided linear channel estimation in LTE OFDMA systems with application to simplified MMSE schemes”, S. Omar, A. Ancora and D. T. M. Slock - PIMRC 2008
 - * “Preconditioned Iterative Inter-Carrier Interference Cancellation for OFDM Reception in Rapidly Varying Channels”, A. Ancora, G. Montalbano and D. T. M. Slock - ICASSP 2010
 - * “Performance Analysis of Preconditioned Iterative Inter-Carrier Interference Cancellation for OFDM”, A. Ancora, G. Montalbano and D. T. M. Slock - ICC 2010
 - * “Bayesian Foundations of Channel Estimation for Smart Radios” R. Couillet, A. Ancora and M. Debbah - Advances in Electronics and Telecommunications, Vol. 1, No. 1, April 2010
 - * “Adaptive equalization at HSDPA symbol level”, A. Bastug, A. Ancora and D. T.M. Slock - MACOM 2009

- Book chapters

- * “Chapter 5: Orthogonal Frequency Division Multiple Access (OFDMA)” in “LTE, The UMTS Long Term Evolution : From theory to practice”, Wiley, S. Sesia, I. Toufik and M. Baker (Ed.) - Wiley, February 2009
 - * “Chapter 8: Reference signals and channel estimation” in “LTE, The UMTS Long Term Evolution : From theory to practice”, S. Sesia, I. Toufik and M. Baker (Ed.) - Wiley, February 2009
 - * “Chapter 11: UE demodulation performances” in “LTE for UMTS - OFDMA and SC-FDMA Based Radio Access”, H. Holma and A. Toskala (Ed.) - Wiley, June 2009

Contents

1	Orthogonal Frequency Division Multiplexing in LTE	3
1.1	Introduction	3
1.1.1	History of OFDM Development	4
1.2	OFDM	5
1.2.1	Orthogonal multiplexing principle	5
1.2.2	PAPR and sensitivity to nonlinearity	8
1.2.3	Sensitivity to carrier frequency offset and time-varying channel	12
1.2.4	Timing offset, multi-path channels, and guard interval dimensioning	14
1.3	MIMO and OFDM	16
1.4	OFDMA	17
1.4.1	Parameter Dimensioning	17
1.4.2	Physical Layer Parameters for LTE	19
1.5	Conclusion	20
2	Channel Estimation in LTE	31
2.1	Introduction	31
2.2	Design of Reference Signals in LTE	33
2.2.1	Cell-Specific Reference Signals	33
2.2.2	UE-Specific Reference Signals	36
2.3	RS-Aided Channel Modeling and Estimation	38
2.3.1	Time-Frequency Domain Correlation: The WSSUS Channel Model	38

2.4	Frequency-domain Channel Estimation	41
2.4.1	Channel Estimation by interpolation	42
2.4.2	General approach to linear channel estimation	44
2.4.3	Simulation results	52
2.4.4	Iterative MMSE Channel Estimation	55
2.5	Time-Domain Channel Estimation	60
2.5.1	Finite and Infinite Length MMSE	60
2.5.2	Normalized Least-Mean-Square	62
2.5.3	Kalman filter	63
3	Detection techniques in selective channels	65
3.1	OFDM Detection in Rapidly Varying Channels	65
3.1.1	Introduction	65
3.1.2	Signal and System Model	66
3.1.3	Channel BEM Representation	68
3.1.4	Linear Equalization	69
3.1.5	Iterative ICI Cancellation	70
3.1.6	Simulation results	79
3.2	Analysis of Preconditioned Iterative IC	80
3.2.1	Preconditioned Iterative Reception	80
3.2.2	Iteration-Dependent Preconditioned Iterative Reception	83
3.2.3	Sparse Preconditioning Derivation	85
3.2.4	Performance evaluation	87
3.2.5	Simulation results	88
3.3	Alamouti Detection Over Selective Channels	90
3.3.1	Signal model definition	91
3.3.2	Diversity analysis of Maximum Likelihood detection	93
3.3.3	Decision-Feedback detection	96
3.3.4	Lattice-Reduction Near-ML detection	97
3.3.5	OFDM SFBC and STBC extension	100

3.3.6	Simulation results	101
A	Résumé de thèse	105
A.1	Estimation de canal en LTE	106
A.1.1	Estimation de canal par interpolation	107
A.1.2	Une approche général à l'estimation linéaire de canal	109
A.1.3	Résultats de simulation	117
A.2	Détection OFDM avec canal variant rapidement	122
A.2.1	Introduction	122
A.2.2	Modèle du système et du signal	123
A.2.3	Représentation BEM du canal	125
A.2.4	Égalisation Linéaire	126
A.2.5	Cancellation itérative de l'ICI	127
A.2.6	Resultats de simulation	136
	Bibliography	141

List of Figures

1.1	Spectral efficiency of OFDM compared to classical multi-carrier modulation: (a) classical multi-carrier system spectrum; (b) OFDM system spectrum	4
1.2	OFDM System Model	22
1.3	Serial-to-parallel conversion operation for OFDM	23
1.4	Effect of channel on signals with short and long symbol duration . . .	23
1.5	OFDM cyclic prefix insertion principle	23
1.6	PAPR distribution	24
1.7	Non-linear device equivalent model.	25
1.8	OFDM sub-carriers orthogonality loss due to frequency offset	25
1.9	P_{ICI} for generic Doppler distribution, Jakes profile and deterministic CFO.	26
1.10	SNR_{ICI} for generic Doppler distribution, Jakes profile and deterministic CFO.	27
1.11	Power of signal, ICI and ISI in case of offened guard interval.	27
1.12	SNR in case of offened guard interval.	28
1.13	General MIMO-OFDM scheme	28
1.14	LTE OFDMA resource allocation example.	29
1.15	LTE OFDM symbol and cyclic prefix lengths.	29
1.16	LTE OFDMA spectrum allocation.	30
2.1	A simple transmission model.	31
2.2	Cell-specific reference symbol arrangement in the case of normal CP length for one antenna port.	34

2.3	Cell-specific RS arrangement in the case of normal CP length for two antenna ports.	36
2.4	Cell-specific RS arrangement in the case of normal CP length for four antenna ports.	37
2.5	Normalized PSD for Clarke’s model.	40
2.6	Frequency-domain channel estimation performance, band-edge behavior.	54
2.7	CTF TNMSE vs. SNR.	55
2.8	CTF TNMSE vs. SNR.	56
2.9	BER vs. SNR.	57
2.10	Performance of iterative MMSE channel estimation.	59
2.11	Time-domain channel estimation performance.	62
3.1	BEM representation of OFDM received signal	69
3.2	Preconditioned iterative ZF receiver	72
3.3	Condition number for diagonal and BEM-MMSE preconditioning	75
3.4	Stationary polynomial BEM-MMSE preconditioned iterative receiver	75
3.5	Non-stationary BEM-MMSE preconditioned iterative receiver	76
3.6	Time-domain PIC iterative decoder	77
3.7	Preconditioned Conjugate Gradient algorithm	78
3.8	Performance comparison of iterative methods with 1 iterations, $L_{\text{FIR}} = 5$	79
3.9	Performance comparison of iterative methods with 3 iterations, $L_{\text{FIR}} = 5$	80
3.10	Performance comparison of iterative methods with 1 iterations, $L_{\text{FIR}} = 3$	81
3.11	Performance comparison of iterative methods with 3 iterations, $L_{\text{FIR}} = 3$	82
3.12	Iteration-Dependent Iterative ICI cancellation receiver	84
3.13	Performances of ID-P-IT receiver with $L_{\text{FIR}} = 3$	89
3.14	Performances of P-IT-ZF receiver with $L_{\text{FIR}} = 3$	90
3.15	Performances of P-IT-ZF receiver with $L_{\text{FIR}} = 3$ and FC mechanism	91

3.16	Undisturbed received signals and decision regions of: (a) Maximum-Likelihood, (b) Linear ZF, (c) Decision-Feedback, (d) Lattice-Reduction aided ZF and (e) Lattice-Reduction aided Decision-Feedback detection.	98
3.17	Complex Lattice Reduction LLL algorithm	99
3.18	Performance of SFBC detectors in selective Rayleigh channel ($\rho = 0$).	102
3.19	Performance of SFBC detectors in selective Rayleigh channel ($\rho = 0.5$).	103
3.20	Performance of SFBC detectors in selective Rayleigh channel ($\rho = 0.9$).	103
3.21	Performance of SFBC detectors in selective Rayleigh channel ($\rho = 0.9$).	104
A.1	Perfromances des estimation de canal, comportement aux bords de la bande.	119
A.2	CTF TNMSE versus SNR.	120
A.3	CTF TNMSE versus SNR.	120
A.4	BER versus SNR.	121
A.5	Représentation BEM du signal OFDM reçu	126
A.6	Recepteur itératif ZF pré-conditionné	129
A.7	Nombre de conditionnement pour preconditionnement diagonal et BEM-MMSE	132
A.8	Recepteur itératif polynomial preconditionné BEM-MMSE	132
A.9	Recepteur à Cancellation Iterative Non-stationnaire de ICI par preconditionnement BEM-MMSE	133
A.10	Détecteur dans le domaine du temps de type PIC	135
A.11	Algorithme du Gradient Conjugué Preconditionné	136
A.12	Comparaison de performances des methodes iteratives avec 1 iteration, $L_{\text{FIR}} = 5$	137
A.13	Comparaison de performances des methodes iteratives avec 3 iterations, $L_{\text{FIR}} = 5$	138
A.14	Comparaison de performances des methodes iteratives avec 1 iteration, $L_{\text{FIR}} = 3$	138
A.15	Comparaison de performances des methodes iteratives avec 3 iterations, $L_{\text{FIR}} = 3$	139

List of Tables

2.1	LTE OFDMA parameters.	41
A.1	Paramètres de OFDMA en LTE.	106

Chapter 1

Orthogonal Frequency Division Multiplexing in LTE

1.1 Introduction

The choice of an appropriate modulation technique for wireless data communications is a critical issue due to the adverse influence of the dispersive and mostly time variant mobile radio channel. The interest in multi-carrier modulation for wireless transmissions has revived. In general multi-carrier schemes, the channel spectrum is parsed into a number of parallel sub-channels (Figure 1.1-a) and, under the best circumstances, independent and ideally frequency non-selective. An implementationally attractive approach to multi-carrier modulation is the Orthogonal Frequency Division Multiplexing (OFDM). In OFDM, the frequency selective wide-band channel is divided into many overlapping but orthogonal frequency non-selective narrow-band sub-channels (Figure 1.1-b). Unlike classical multi-carrier modulation, where the carriers are placed sufficiently further apart by means of guard-bands to avoid interference leakage between sub-channels - as can be seen in Figure 1.1, OFDM uses spectral overlapping between sub-carriers and allows for perfect sub-channel separation at the receiver because of the Fourier waveforms orthogonality. This makes of OFDM a highly spectral efficient multi-carrier modulation with a reasonable required receiver complexity and thus attractive for high rate mobile data transmission such as the UMTS Long Term Evolution (LTE).

The advantage of separating the transmission into several sub-channels cannot itself translate into robustness against multi-path time-varying channels if no channel coding is employed. LTE, as other systems, make use of diversity offered by the channel coding such as Turbo codes to overcome the deep fading channel situations and can then be regarded to as so called *Coded* OFDM systems. This attribute is

is not considered within the scope of this chapter and it is covered instead in [61].

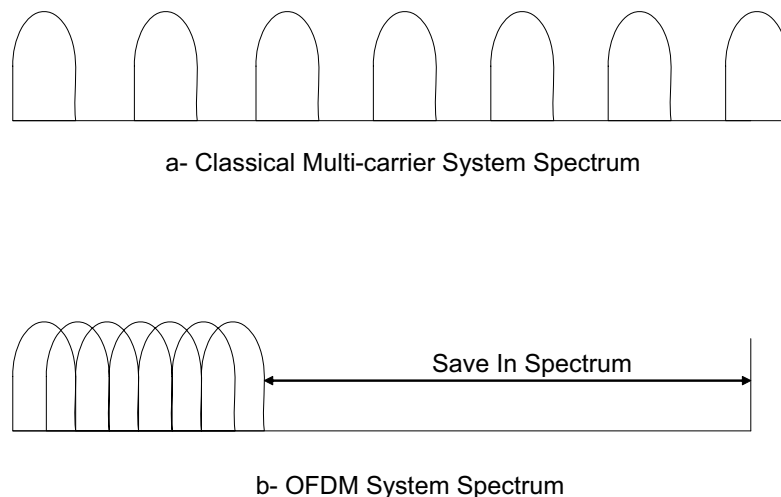


Figure 1.1: Spectral efficiency of OFDM compared to classical multi-carrier modulation: (a) classical multi-carrier system spectrum; (b) OFDM system spectrum

1.1.1 History of OFDM Development

Multi-carrier communication systems were first introduced about 50 years ago by Chang in [1] through the first OFDM patent filed in US at Bell Labs in 1966. A first analysis on this parallel system was done in 1967 [2]. At that time only analog design was proposed. The employment of the discrete Fourier transform (DFT) to replace the banks of sinusoidal generators and the demodulators was suggested by Weinstein and Ebert [3] in 1971, which made OFDM implementation cost effective. Furthermore, the complexity could drastically be reduced by the application of reduced computational complexity algorithms such as the Winograd Fourier Transform (WFT) or the Fast Fourier Transform (FFT) in 1980 by Peled [4]. In [6] authors proposed a cellular mobile radio system based on OFDM. Since then, the processing power of modern digital signal processors has increased allowing OFDM, after more than thirty years of research and development, to find its way into commercial use. OFDM became then the modulation of choice for many applications for both wired and wireless systems. OFDM systems already available in the market comprise Asymmetric Digital Subscriber Line (ADSL), Digital Video Broadcasting (DVB), Wireless Local Area Network (WLAN), Digital Audio Broadcasting (DAB) and now OFDM is considered as the modulation technology for 3GPP LTE down-link. The introduction of OFDM into the cellular world was driven by two main

benefits: the low-complexity equalization and the OFDM spectrum flexibility coming from its ability to operate in different frequency bands and with different channel bandwidths allowing possible deployment in existing spectrum. For LTE, bandwidth ranging from 1.4MHz (suitable for the initial migration of CDMA2000 for example) to 20MHz are envisaged.

1.2 OFDM

1.2.1 Orthogonal multiplexing principle

A high data rate stream of complex symbols faces the problem of having a symbol period much smaller than the channel delay spread. In *serial* broad-band transmissions, the symbol duration T is shorter than the channel delay spread T_d generating a strong ISI impairment which can be undone only with complex equalization procedure. In the general case, the equalization complexity grows as the square of channel memory size.

In OFDM, the high-rate streams of data symbols is first serial-to-parallel converted for modulation onto M parallel sub-carriers as shown in Figure 1.3. This increases the symbol duration on each sub-carrier by a factor approximately M , such that it becomes significantly longer than the channel delay spread.

This operation, while imposing the time-varying channel to stay constant over the transmission of the modulated symbol, has the important advantage of requiring a much less complex equalization procedure. Figure 1.3 sketches the serial-to-parallel operation and figure 1.4 depicts the ISI *virtually* unaffected long symbol duration low-rate signal compared to highly corrupted short symbol duration high rate waveform.

The figure 1.2 shows the typical block diagram of an OFDM system. The signal to be transmitted is defined in the frequency domain. A Serial to Parallel (S/P) converter collects serial data symbols into a data block $S = [S_1, S_2, \dots, S_M]^T$ of dimension M . The M parallel data streams are first independently modulated resulting in the complex vector $X = [X_1, X_2, \dots, X_M]^T$. Note that the modulation constellations may be different on each sub-carrier: due to channel frequency selectivity, the channel gains may be different along the sub-carriers, and thus some streams can carry higher bit-rate than others. The M parallel modulated data symbols S pass then through an IFFT resulting on a set of N complex time-domain samples $\mathbf{x} = [x[0], \dots, x[N-1]]^T$ as any practical OFDM system uses less sub-carriers than the number of processed ones (and then $M \leq N$). The un-used sub-carriers are padded with zeros. The last L_{CP} samples of the IFFT output block are duplicated

and appended at the beginning of \mathbf{x} yielding to the time domain OFDM symbol $[x[N - L_{CP}], \dots, x[N - 1], x[0], \dots, x[N - 1]]^T$. This operation is called Cyclic Prefix (CP) insertion. Figure 1.5 describes the structure of the resulting TX signal. The CP is inserted to eliminate the effect of ISI caused by multi-path propagation. The CP length L_{CP} must be chosen to be longer than the worst case channel length to avoid ISI. The goal of the CP is to convert the aperiodic convolution of the channel into a periodic one which is suitable for DFT processing. This important feature of CP used in OFDM is clarified by the mathematical analysis provided later in this section. The parallel signals are converted back to a serial sequence by using a Parallel to Serial (P/S) device. Finally, the signal is converted to an analog signal and transmitted through the frequency-selective channel.

At the receiver, the reverse procedure is used to demodulate the OFDM signal. Assuming OFDM symbol synchronization is granted, the signal repetition introduced by the CP insertion is removed. The CP removal has in addition the advantage of allowing block processing which can be performed in DSP with very low complexity using the FFT to transform the signal back to frequency domain. Among the N parallel streams returned by the FFT, the used subset of M sub-carriers are selected and further processed by the receiver.

Let $x(t)$ be the signal symbol transmitted a time instant t . The received signal in multi-path environment is then given by

$$y(t) = x(t) * h(t) + z(t) \quad (1.1)$$

$$= \int_{-\infty}^{\infty} h(\tau)x(t - \tau) d\tau + z(t) \quad (1.2)$$

where $h(t)$ is the *continuous-time* impulse response of the channel and $z(t)$ is the additive noise.

Since $x(t)$ is band-limited to $[-W/2, W/2]$, the *continuous-time* signal $x(t)$ can be sampled at sampling rate T_s satisfying Nyquist criterion and obtain

$$y[n] = x[n] * h[n] + z[n] \quad (1.3)$$

where $h[n]$ is the channel response sampled at rate T_s . we have

$$h[n] = \int_{-\infty}^{\infty} h(t)\text{sinc}(t - nT_s) dt \quad (1.4)$$

As a result of the multi-path propagation, several replicas of the transmitted signals arrive at the receiver at different delays. The delayed signals are the result of reflections, refractions and diffractions on surrounding objects referred to as scatterers. In general broad-band systems, one of the main issues is to perform the equalization operation which consists in recovering $x[n]$ from Equation (1.3).

In order to ensure quasi-memoryless behavior, OFDM transmitters insert in a clever manner a cyclic prefix at the beginning of each symbol period, see Figure 1.5.

The discrete time received signal after cyclic prefix removal can be expressed as

$$\begin{bmatrix} y[L_{CP}] \\ y[L_{CP} + 1] \\ \vdots \\ y[N + L_{CP} - 1] \end{bmatrix} = \begin{bmatrix} x[0] & x[N-1] & \cdots & x[N - L_{CP} + 1] \\ x[1] & x[0] & \cdots & x[N - L_{CP}] \\ \vdots & \vdots & \ddots & \vdots \\ x[L_{CP} - 1] & x[L_{CP} - 2] & \cdots & x[0] \end{bmatrix} \begin{bmatrix} h[0] \\ h[1] \\ \vdots \\ h[L_{CP} - 1] \end{bmatrix} + \begin{bmatrix} z[N - L_{CP}] \\ z[N - L_{CP} + 1] \\ \vdots \\ z[N + L_{CP} - 1] \end{bmatrix}$$

This assumes the channel length L is smaller than L_{CP} and therefore some channel taps may be equal to 0. Adding zeros to the channel vector can extend the signal matrix without changing the output vector. This is expressed as

$$\begin{bmatrix} y[N - L_{CP}] \\ y[N - L_{CP} + 1] \\ \vdots \\ y[N + L_{CP} - 1] \end{bmatrix} = \mathbf{A} \begin{bmatrix} h[0] \\ h[1] \\ \vdots \\ h[L_{CP} - 1] \\ 0 \\ \vdots \\ 0 \end{bmatrix} + \begin{bmatrix} z[N - L_{CP}] \\ z[N - L_{CP} + 1] \\ \vdots \\ z[N + L_{CP} - 1] \end{bmatrix}$$

where matrix \mathbf{A} is given by

$$\mathbf{A} = \begin{bmatrix} x[0] & x[N-1] & \cdots & x[N - L_{CP} + 1] & x[N - L_{CP}] & \cdots & x[1] \\ x[1] & x[0] & \cdots & x[N - L_{CP}] & x[N - L_{CP} - 1] & \cdots & x[N - L_{CP}] \\ \vdots & \vdots & \ddots & \vdots & \vdots & \vdots & \vdots \\ x[L_{CP} - 1] & x[L_{CP} - 2] & \cdots & x[0] & x[N - 1] & \cdots & x[L_{CP}] \end{bmatrix}$$

The matrix \mathbf{A} is circular and since any circular matrix is diagonal in the Fourier basis with its eigenvalues given by the FFT of its first row. The equivalent received signal can then be written in matrix notation as

$$\begin{bmatrix} y[N - L_{CP}] \\ y[N - L_{CP} + 1] \\ \vdots \\ y[N + L_{CP} - 1] \end{bmatrix} = \mathbf{F} \begin{bmatrix} X_0 & 0 & 0 & \cdots & 0 \\ 0 & X_1 & 0 & \cdots & 0 \\ \vdots & \vdots & \ddots & \vdots & \vdots \\ 0 & 0 & 0 & \cdots & X_{N-1} \end{bmatrix} \mathbf{F}^H \begin{bmatrix} h[0] \\ h[1] \\ \vdots \\ h[L_{CP} - 1] \\ 0 \\ \vdots \\ 0 \end{bmatrix} + \begin{bmatrix} z[N - L_{CP}] \\ z[N - L_{CP} + 1] \\ \vdots \\ z[N + L_{CP} - 1] \end{bmatrix} \quad (1.5)$$

where \mathbf{F} is the Fourier transform matrix whose elements are $(\mathbf{F})_{n,k} = e^{-j\frac{2\pi}{N}(nk)}/\sqrt{N}$, $0 \leq n \leq N - 1$ and $0 \leq k \leq N - 1$ and N the length of the OFDM symbol. X_i is given by

$$X_k = \sum_{n=1}^N x[n] e^{2j\pi k \frac{n}{N}} \quad (1.6)$$

In the transform domain we can then write

$$\begin{bmatrix} Y_0 \\ \vdots \\ Y_{N-1} \end{bmatrix} = \begin{bmatrix} X_0 & 0 & 0 & \cdots & 0 \\ 0 & X_1 & 0 & \cdots & 0 \\ \vdots & \ddots & \ddots & \ddots & \vdots \\ 0 & 0 & 0 & \cdots & X_{N-1} \end{bmatrix} \begin{bmatrix} H_0 \\ H_1 \\ \vdots \\ H_{N-1} \end{bmatrix} + \begin{bmatrix} Z_0 \\ \vdots \\ Z_{N-1} \end{bmatrix}$$

This shows how OFDM by the use of cyclic prefix turns the linear convolution into a circular one. The circular convolution is very efficiently transformed by the use of FFT into multiplicative operation in the frequency domain. Hence, the transmitted signal over a frequency selective (i.e. multi-path) channel is converted into the transmission over N parallel flat fading channels in the frequency-domain. As a result the equalization is much simpler than for single carrier systems and consists in one complex multiplication per sub-carrier.

1.2.2 PAPR and sensitivity to nonlinearity

A part from the low required complexity receiver to overcome the ISI advantage exposed in previous section, OFDM reveals to have disadvantages and sensitivity to system parameters. The high PAPR of OFDM signal being one of the major drawbacks, this chapter is dedicated to a qualitative analysis of these issues.

The OFDM transmitter can be seen as a linear operation performed over a large block of frequency-domain i.i.d. QAM modulated complex symbols. As a result, due to the central limit theorem, the time-domain OFDM symbol can be very well approximated as a Gaussian waveform. The amplitude variations of the OFDM modulated signal can then be very high. The Power Amplifiers (PA) of RF transmitters work instead in a limited dynamic range. Thus, the high dynamic OFDM signal can likely undergo non-linear effect, namely clipping, resulting in transmitting a distorted OFDM signal. The distortion introduces out-of-band spurious emissions and in-band corruption of the signal. To avoid at most this distortion, power amplifiers are required to operate with large power back-offs. This situation leads to very inefficient amplification or expensive transmitters.

One measure of the high input amplitude dynamic (and thus a measure of the expect degradation) is the Peak to Average Power Ratio (PAPR). PAPR of OFDM increases proportionally with the number of sub-carriers.

In the following we provide a mathematical analysis for PAPR. Let $x[n]$ be the the signal after IFFT as given by equation (1.6). The PAPR of an OFDM symbol is defined as the square of the maximum amplitude divided by the mean power and

is thus given by

$$PAPR = \frac{\max \{|x[n]|^2\}}{E \{|x[n]|^2\}} \quad (1.7)$$

When the number of sub-carriers N is small, a PAPR of N has reasonable chances of occurring. However, if N is large enough a PAPR of N has exceedingly small probability of occurring. The OFDM modulated signal is usually modeled as the sum of independent random variables. According to the central limit theorem if the number of sub-carriers is large, the signal can be approximated as a Gaussian distributed random variable. Thus, the amplitude of $x[n]$ has a Rayleigh distribution, while the power distribution becomes a central chi-square distribution with two degrees of freedom. The cumulative distribution function (CDF) $F_x(\alpha)$ of power is given by

$$F_x(\alpha) = Pr \left(\frac{|x[n]|^2}{E \{|x[n]|^2\}} < \alpha \right) = 1 - e^{-\alpha} \quad (1.8)$$

Without oversampling, the time domain samples are mutually uncorrelated and the probability that the PAPR is below a certain threshold $PAPR_0$ is

$$Pr\{PAPR > PAPR_0\} = 1 - F(PAPR_0)^N = 1 - (1 - e^{-PAPR_0})^N \quad (1.9)$$

Figure 1.6 plots the distribution of the PAPR given by equation (1.9) for different values of the number of sub-carriers N (from left to right 16, 32, 64, 128, 256, 1024).

As can be seen from this curve, high PAPR does not occur very often. However, when it exists, degradation due to non-linearities may be expected. In order to evaluate the impacts of distortion on the OFDM signal reception, we develop in the following an useful framework. Using vector notation, the distortion generated by the non-linear transmitting power amplifier (or any non-linear device present along the transmission chain) for an OFDM signal can be modeled using the Bussgang's theorem [22] as (see also figure 1.7):

$$\tilde{\mathbf{x}} = \alpha \mathbf{x} + \mathbf{d} \quad (1.10)$$

where $\tilde{\mathbf{x}}$ is the distorted OFDM signal by non-linearities, \mathbf{x} is the column vector of the undistorted OFDM symbol, \mathbf{d} is the vector of the equivalent interference term due to distortion uncorrelated to signal \mathbf{x} and α is a complex gain factor accounting for the attenuation and phase rotation. The parameter α can be derived as

$$\alpha = \frac{E\{\tilde{\mathbf{x}}^H \mathbf{x}\}}{E\{\mathbf{x}^H \mathbf{x}\}} \quad (1.11)$$

The covariance matrix of the output signal can therefore be written as

$$\mathbf{C}_{\tilde{\mathbf{x}}\tilde{\mathbf{x}}} = |\alpha|^2 \mathbf{C}_{\mathbf{xx}} + \mathbf{C}_{\mathbf{dd}} \quad (1.12)$$

with $\mathbf{C}_{\mathbf{xx}} = \mathbb{E}\{\mathbf{xx}^H\}$ and $\mathbf{C}_{\mathbf{dd}} = \mathbb{E}\{\mathbf{dd}^H\}$.

The distorted signal $\tilde{\mathbf{x}}$ generated by the RF transmitter is further corrupted by complex white circular Gaussian noise $\mathbf{n} \sim \mathcal{N}(0, \sigma_n^2 \mathbf{I})$ and the signal received by the OFDM receiver is expressed by

$$\mathbf{r} = \tilde{\mathbf{x}} + \mathbf{n} = \alpha \mathbf{x} + \mathbf{d} + \mathbf{n} \quad (1.13)$$

The assumption of AWGN channel is taken for the sake of simplicity but equation (1.13) can be straightforwardly extended to the case of a frequency selective convolutive channel and Cyclic Prefixed OFDM system.

As a result, the signal at the output of the FFT can be written as

$$\mathbf{R} = \alpha \mathbf{F}\mathbf{x} + \mathbf{F}\mathbf{d} + \mathbf{F}\mathbf{n} = \alpha \mathbf{X} + \mathbf{D} + \mathbf{N} \quad (1.14)$$

\mathbf{F} being the Fourier transform matrix.

Consequently, the covariance matrix of the frequency-domain received signal is

$$\mathbf{C}_{\mathbf{RR}} = |\alpha|^2 \mathbf{C}_{\mathbf{XX}} + \mathbf{C}_{\mathbf{DD}} + \mathbf{C}_{\mathbf{NN}} = |\alpha|^2 \mathbf{F}\mathbf{C}_{\mathbf{xx}}\mathbf{F}^H + \mathbf{F}\mathbf{C}_{\mathbf{dd}}\mathbf{F}^H + \sigma_n^2 \mathbf{I} \quad (1.15)$$

Hence this shows how the OFDM received signal distorted by non-linearities can be equivalently expressed as the transmitted signal \mathbf{x} , scaled by a complex gain factor α , corrupted by AWGN and an additional interference term originating in an irreducible error floor for decreasing AWGN σ_n^2 variance.

Assuming OFDM receiver coherent detection, the phase rotation induced by the scaling factor α is not influent as it will be compensated for in the receiver channel estimation. In both coherent and non-coherent OFDM systems, the impact of the magnitude of α translates into a power penalty to the useful signal.

We remand to [5] for a detailed discussion on the derivation of the statistical properties of the distortion as a function of any nonlinear function.

Assuming again FFT processing of large blocks and benefiting of the central limit theorem, the frequency-domain distortion term \mathbf{D} can be well approximated by a complex white circular Gaussian noise $\mathbf{D} \sim \mathcal{N}(0, \sigma_d^2 \mathbf{I})$ and the Signal to Interference and Noise Ratio (SINR) of the distorted received OFDM signal can then be simply expressed as

$$\text{SINR}_d = \frac{|\alpha|^2 \text{tr}\{\mathbf{C}_{\mathbf{XX}}\}}{\text{tr}\{\mathbf{C}_{\mathbf{DD}}\} + \sigma_n^2} = \frac{|\alpha|^2}{\sigma_d^2 + \sigma_n^2} \quad (1.16)$$

assuming a normalized signal \mathbf{X} power.

We finally note that this model is used in setting the performance for LTE and the additive distortion term is commonly included as *transmitter Error Vector Magnitude* (EVM) source. We point at chapter at [61] for a detailed discussion.

PAPR Reduction Techniques

For the sake of completeness, we provide here a short overview of PAPR reduction techniques available in literature. However, 3GPP LTE does not specify any of those leaving to eNodeB manufacturers the burden of handling the increased required RF costs and complexity.

Several algorithms have been proposed to handle the distortion due to the PAPR. At least three concepts for reducing the peak-to-average power ratio have been proposed:

- Clipping and Filtering [7], [8]-[10]: In these techniques, the time domain signal is clipped to a predefined level. This causes significant spectral leak into adjacent channels resulting in a reduction of the spectral efficiency and in-band noise causing degradation of the bit error rate performance. The out-of-band radiation can then be eliminated by filtering. If discrete signals are clipped directly, the resulting clipping noise will all fall in in band and thus can not be reduced using filtering. To avoid this problem, one solution is to oversample the original signal by padding the input signal with zeros and taking a longer IFFT and then use filtering to reduce the out of band clipping noise.
- Selected Mapping: Selected mapping was introduced in [11] for MPSK modulation. In this method, multiple transmit signals which represent the same OFDM data symbol are generated by multiplying the OFDM symbol with different phase vectors. The representation with the lowest PAPR is selected. To recover the phase information, it is of course necessary to transmit to the receiver as side information which phase vector was used.
- Coding techniques: The idea behind these techniques consists in finding the code-words with minimum PAPR from a set of code-words to map the input data [12]-[14]. A look-up table may be used if N is small. It is shown that complementary codes have good properties to combine both peak-to-average power reduction and forward error correction.

Nevertheless, in LTE context, not all of above presented techniques can be applied. For example, Selected Mapping and Coding techniques cannot be supported

in LTE. The first requires additional signaling. The second requires an additional scrambling stage to encoded data symbols.

1.2.3 Sensitivity to carrier frequency offset and time-varying channel

The orthogonality principle of OFDM relies on the condition that transmitter and receiver operate with exactly the same frequency reference. If this is not the case, the perfect sub-carriers orthogonality is destroyed as can be seen from Figure 1.8 causing sub-carriers leakage, also known as Inter-Carrier Interference (ICI). ICI can harm system performance resulting in an increased Bit-Error-Rate (BER) in the decoded signal.

Frequency errors typically arise result from a mismatch between the transmitter and receiver local oscillators reference frequencies. On the receiver side in particular, due to the usually low cost local oscillators drifts in frequency are commonly experienced as function of many parameters such as temperature changes and aging. This difference between the generated reference frequencies is widely referred to as Carrier Frequency Offset (CFO).

The CFO can be several times larger than the sub-carrier spacing. It is usually divided into an integer and fractional part. Thus the frequency error can be written as

$$f_o = (\Gamma + \epsilon) \Delta f \quad (1.17)$$

with Δf being the sub-carriers spacing and Γ is an integer and $\epsilon \in]-1, 1[$. If $\Gamma \neq 0$, then the modulated data are in the wrong positions with respect to the sub-carriers mapping performed at the transmitter. This simply results in a bit-error rate (BER) of 0.5 if the frequency offset is not compensated at the receiver independently of the value of ϵ . In the case of $\Gamma = 0$ and $\epsilon \neq 0$, the perfect sub-carriers orthogonality is destroyed (as can be seen from Figure 1.8) and results in Inter-Carrier Interference (ICI) leakage which might degrade the BER. Only synchronization errors up to a few percents of the carrier spacing are tolerated in OFDM.

Assuming the ideal case where the local oscillators are perfectly aligned, the relative speed between transmitter and receiver generates as well frequency errors. This is well known as Doppler effect.

In case of single-path channel, the UE mobility with constant direction with respect to the angle of arrival α of the electro-magnetic wave-plane front results in a CFO exactly given by Doppler shift f_d is given by

$$f_d = \frac{v f_c}{c} \cos \alpha \quad (1.18)$$

where v is the mobile speed with respect to the transmitter, f_c is the carrier frequency, c is the speed of light ($3 \times 10^8 m/s$).

In most cases, the wireless channel consists of several paths each with index k . Each path angle of arrival may be different due to reach scattering environment. Thus each channel path will introduce its own Doppler frequency shift $f_d^{(k)}$. Hence the overall effect of UE mobility in a multi-path propagation would result from the combination of each component into a spread of the sub-carriers according to a Doppler spectral density $P(f)$. The path delays are irrelevant for the Doppler spread density function, only the angles and path attenuations are determining $P(f)$.

As in [16] and [17], it can be shown that, for both flat and dispersive channels and assuming a transmitted signal power equal to 1, the Inter-Carrier Interference power can be exactly computed in function of the generic Doppler spectral density $P(f)$ by

$$P_{ICI} = \int_0^1 P(f)(1 - \text{sinc}^2(f_{d_{\max}}Tf))df \quad (1.19)$$

where $f_{d_{\max}}$ is the maximum Doppler frequency obtained from Equation (1.18) setting $\alpha = 0$ and T is the OFDM symbol duration.

If the ICI is caused by a mismatch of f_o between the transmitter and receiver oscillators frequencies, it can be seen, using the equivalence with the single path propagation, as

$$P(f) = \delta(f - f_o) \quad (1.20)$$

Hence, substituting (1.20) in (1.19), we straightforwardly find the exact expression of the ICI power in case of deterministic CFO as

$$P_{ICI,CFO} = 1 - \text{sinc}^2(f_oT_s) \quad (1.21)$$

For the classical Jakes model, the expression (1.19) can be written as

$$P_{ICI,Jakes} = 1 - 2 \int_0^1 (1 - |f|)J_0(2\pi f_{d_{\max}}Tf)df \quad (1.22)$$

with J_0 being the zero-th order Bessel function.

When no assumptions on the Doppler spectrum shape can be made, an upper bound on ICI given by equation (1.19) can be found by applying the Cauchy-Schwartz inequality, leading to

$$P_{ICI} \leq \frac{\int_0^1 (1 - \text{sinc}^2(f_dT_s f))^2 df}{\int_0^1 1 - \text{sinc}^2(f_dT_s f) df} \quad (1.23)$$

This upper bound on P_{ICI} is valid only in the case of frequency spread and does not cover the case of deterministic CFO.

Using (1.23), (1.22) and (1.21), we can easily obtain the SIR expression due to ICI as

$$\text{SIR}_{ICI} = \frac{1 - P_{ICI}}{P_{ICI}} \quad (1.24)$$

Figures 1.2.3 and 1.2.3 plot these two quantities for the cases provided. They reveal that the highest ICI is introduced by a constant frequency offset. In case of Doppler spread, instead, the ICI impairment is lower. In addition, figure 1.2.3 shows that, in absence of any other impairment such as interference ($SIR = \infty$), the SNR_{ICI} rapidly decays as function of frequency misalignments. Data transmitted with high order modulations require higher SNR conditions compared to lower orders to be decoded. Thus, the highest is the modulation order the lower is the tolerated maximum frequency offset. According to [15], for SNR shift of 0.5 dB of the BER curve, QPSK modulation can tolerate up to 5% error whereas 64QAM requires at least 1% accuracy.

1.2.4 Timing offset, multi-path channels, and guard interval dimensioning

In case of memoryless channel (i.e. no delay spread), OFDM is insensitive to timing synchronization errors as long as the misalignment remains within the cyclic prefix region. Despite a timing misalignment T_o within the limits of the CP, i.e. $T_o \leq T_{CP}$, orthogonality is maintained thanks to the circulant property of CP. The symbol timing delay would only introduce a constant phase shift from one sub-carrier to another. The received signal at k^{th} sub-carrier is given by

$$Y_k = X_k \exp\left(j2\pi \frac{dk}{N}\right). \quad (1.25)$$

where d is the timing offset in samples.

This phase shift can be safely recovered along with the channel estimation operation. It is worth highlighting that the insensitiveness would not hold for any other kind of guard interval than cyclic prefix such as zero-padding. In such case, depending on the timing misalignment, a portion of the useful signal power would be lost.

In the general case of a channel with delay spread, the maximum tolerated timing offset without degrading the OFDM reception is reduced by an amount exactly equal to the channel length: $T_o \leq T_{CP} - T_L$. For greater timing errors, ISI

and ICI occur either because the decoded signal extends over the next OFDM block boundaries (in addition to a useful signal power loss) either because ISI from previous OFDM symbol is collected. This violation can be assimilated to the condition of an insufficient CP length, as explained in section 1.2.4.

The timing synchronization procedure is hence increasingly critical with the CP occupation by the channel leaving it less error margin.

Initial timing acquisition is normally achieved by the cell-search synchronization procedures (see [61]). For continuous timing-offset tracking, mainly two classes of synchronization approaches exist in the literature: the first class exploiting the cyclic prefix correlation while the second is based on reference symbols (i.e. pilot-based). Combination of the two are also possible possibly combined with data-aided techniques as well. We point the reader to [24] for a comprehensive survey on OFDM synchronization techniques.

Insufficient guard interval

In the assumption of a system designed with a cyclic prefix of length L_{CP} such that $L < L_{CP}$, OFDM benefits from the cyclic periodicity of Fourier transform and come up to an orthogonal multi-carrier system. The condition of a sufficient guard interval is therefore strictly related to the orthogonality property of OFDM. In the unfortunate situation when the channel might be longer than the system designed cyclic prefix length, the orthogonality is destroyed due to the loss of the circularity property, resulting in the introduction of ICI. ISI from previous OFDM symbol is also introduced since not completely absorbed by the CP.

As shown in [20], for an OFDM symbol consisting of $N + L_{CP}$ samples where N is the FFT order and \mathbf{h} the channel vector consisting of L taps, the power of ICI and ISI terms can be computed by

$$P_{ICI} = 2 \sum_{k=L_{CP}}^{N+L_{CP}-1} |h[k]|^2 \frac{N(k - L_{CP}) - (k - L_{CP})^2}{N^2} \quad (1.26)$$

$$P_{ISI} = \sum_{k=L_{CP}}^{N+L_{CP}-1} |h[k]|^2 \frac{(k - L_{CP})^2}{N^2} \quad (1.27)$$

Conversely, the signal power P_S is reduced and can be written as

$$P_S = \sum_{k=0}^{L_{CP}-1} |h(k)|^2 + \sum_{k=L_{CP}}^{N+L_{CP}-1} |h(k)|^2 \frac{(N - k + L_{CP})^2}{N^2} \quad (1.28)$$

The resulting Signal to Interference Ratio due to offened guard interval can then be written as

$$\text{SIR}_{og} = \frac{P_S}{P_{ISI} + P_{ICI}} \quad (1.29)$$

Figures 1.2.4 and 1.2.4 plot Equations (1.27)-(1.29) in the case of *normal* CP LTE OFDM assuming a uniform and normalized PDP channel of length $L < N + L_{CP}$ where the dashed line marks the boundary of the cyclic prefix.

1.3 MIMO and OFDM

The use of multiple antenna at the transmitting and/or receiving side of a wireless link can considerably improve the spectral efficiency and reliability of wireless communications [61]. However, the work in multiple antennas usually only concentrates on narrow band systems. The combination of MIMO and OFDM, i.e. MIMO-OFDM, is thus a particularly attractive technique that gathers the benefits of the two methods in order to offer the high data rates promised by LTE. Figure 1.13 shows a typical MIMO-OFDM transmission/reception scheme. The coded and modulated data are mapped to the different sub-carriers and spatial layers. This mapping is the responsibility of the scheduler. The layers in each sub-carrier can be assigned to a single user (SU-MIMO) or different users (MU-MIMO). The data mapped to each sub-carrier are then spatially precoded over the multiple transmit antennas and the set of sub-carriers belonging to each antenna undergoes an independent OFDM modulation except that the transmissions from the different antennas are synchronous and are using cyclic prefixes of the same length. OFDM, in the same way as for single antenna communications, converts the transmitted signal over a frequency-selective (i.e. multi-path) channel into a transmission over N parallel flat-fading channels in the frequency domain. In each sub-carrier m and OFDM symbol k , the received signal can be expressed as follows:

$$\mathbf{R}_k[m] = \mathbf{H}[m] \cdot \mathbf{X}_k[m] + \mathbf{Z}_k[m] \quad (1.30)$$

where $\mathbf{R}_k[m]$ is the $N_r \times 1$ received vector, $\mathbf{X}_k[m]$ is the $N_t \times 1$ transmitted signal and $\mathbf{H}_k[m]$ is the $N_r \times N_t$ channel matrix between the N_r receiving and the N_t transmitting antennas. This equation is thus the same as for an equivalent narrow band case.

1.4 OFDMA

OFDMA employs OFDM to implement a multi-user communication system. In OFDM systems, only a single user can be scheduled on all sub-carriers at any given time. Straightforward OFDM extensions to support multiple users employ Time or Frequency Division Multiple Access (T/FDMA). OFDMA distributes sub-carriers among users so that all users can be scheduled simultaneously. Each user is assigned to a set of aggregated sub-carriers, in LTE also referred to as Resource Blocks (RB). OFDMA system for mobile communication was first proposed in [25] based on Multi-carrier FDMA, where each user gets assigned to a set of randomly selected sub-channels.

An important characteristic of wide-band systems is frequency diversity, i.e. the channel transfer function in some frequency regions is enhanced whereas it is attenuated in others. Since different users undergo different wireless channels, also known as Multiuser diversity, the probability that all users experience a deep fade in the same sub-channel is very low. Based on feedback information about the channel conditions from each user, adaptive user-to-RB assignment can be performed and enhance considerably the system spectral efficiency compared to single user OFDM systems and multi-users CDMA. Moreover, OFDMA allows the support of differentiated Quality of Service (QoS) or, in other words, to control the data rate and error probability individually for each user. OFDMA can also be used in combination with Time Domain Multiple Access (TDMA), where the resources are partitioned in the time-frequency plane and RBs are assigned along the OFDM symbol index as well as OFDM sub-carrier index. Figure 1.14 depicts such OFDMA/TDMA mixed strategy in use in LTE case.

1.4.1 Parameter Dimensioning

Many parameters, with often conflicting effects, are driving the performance of an OFDMA, as well as for single user OFDM, system. These parameters are to be adequately defined and traded off in order to maximize system spectral efficiency for a given bandwidth while maintaining robustness against propagation impairments. In this section we explain how these parameters are related and how they influence the system performance.

For a given system bandwidth W , an OFDM system is dimensioned mainly taking into account the propagation scenario characteristics, namely the delay spread T_d and the maximum Doppler frequency $f_{d_{max}}$, and in case of cellular systems, the targeted multi-cell deployment cell size.

Preliminarily, it is well known that, given the system bandwidth W , the sam-

pling frequency must satisfy Nyquist theorem and therefore be

$$f_s \geq W \quad (1.31)$$

or, consequently, the sampling period must be

$$T_s \leq \frac{1}{W} \quad (1.32)$$

The propagation channel characteristics impose the constraints on the choice of the CP length and of the sub-carrier spacing.

As, we saw earlier, the CP length should be longer than the channel length to insure the robustness against the ISI. For cellular systems and specially for large cells, users may experience delay spreads longer than those encountered in WLAN for example, eventually implying a much longer CP. On the other hand, a longer CP for a fixed OFDM symbol duration corresponds to a wastage of system resources. This wastage can be expressed in function of CP duration $T_{CP} = L_{CP}T_s$ and the OFDM symbol period T_u as

$$\beta_{wastage} = \frac{N+1}{N} \left(1 + \frac{T_{CP}}{T_u}\right) \quad (1.33)$$

From this equation, it is clear that to maximize spectral efficiency, T_u is to be chosen large enough to be much greater than CP duration but small enough to insure that the channel does not vary within one OFDM symbol. The OFDM symbol duration T_u is related to the the carrier spacing Δf by

$$\Delta f = \frac{1}{T_u} \quad (1.34)$$

Choosing a large T_u leads to a smaller frequency spacing Δf and this has a direct impact on the system performance due to Doppler effect, frequency offset sensitivity, as explained in Section 1.2.3.

This discussion can be summarized in the two following design criteria

$$\frac{f_{dmax}}{\Delta f} \ll 1 \quad (1.35)$$

and

$$T_{CP}\Delta f \ll 1 \quad (1.36)$$

1.4.2 Physical Layer Parameters for LTE

LTE standard aims at covering a large scope of cellular deployment scenarios. It is designed to operate in indoor, urban, sub-urban and rural situations and for both low and high UE mobility conditions (up to 350 Km/h). Cell size spans from home-network pico-cells to few kilometers large cells. LTE also supports a Multimedia Broadcast Mobile Service (MBMS) down-link mode using Macro-diversity (combining from multiple cells) and thus requiring an even increased size of cells to allow overlapping. Regulatory organizations made available a variety of bandwidths ranging from 1.4 to 20 MHz located in spectrum regions around 900 MHz , 2 and 2.6 GHz . All these cases imply different delay spread and Doppler frequencies. LTE OFDMA supports then three different modes to ensure an efficient use of system resources depending on the deployment. Two $\Delta f = 15 \text{ KHz}$ sub-carrier spacing modes with alternative cyclic prefix lengths, namely *normal* and *extended*, of respectively $\approx 5 \mu\text{s}$ and $\approx 16 \mu\text{s}$. The large sub-carrier spacing is intended to be less sensitive to Doppler and therefore allow for higher mobility. The two different cyclic prefix cases cover the heterogeneous cell-size above mentioned: the *normal* CP is suited for small size cells and for indoor and urban propagation conditions while the *extended* CP allows for sub-urban and rural large cells. A $\Delta f = 7.5 \text{ KHz}$ sub-carrier spacing mode with a cyclic-prefix duration of $\approx 33 \mu\text{s}$ is finally defined for MBMS Single Frequency Network (SFN) down-link. The very large cyclic-prefix duration is traded off with a lower sub-carrier spacing for efficiency reasons. This large value allows for large-cell combining although makes this mode more sensitive to Doppler. These modes and corresponding parameters are summarized in figure 1.4.2. It is worth noticing, a specificity of LTE OFDMA, namely an irregular allocation of the cyclic prefix length only for the first symbol of every slot in the normal cyclic prefix case with sub-carrier spacing $\Delta f = 15 \text{ KHz}$. This characteristic feature is due to the need of accommodating an integer number of OFDM symbols, i.e. 7, with FFT block-lengths of 2048.

For backward compatibility with previous 3GPP releases such as UMTS and HSDPA, a sampling frequency multiple of 3.84 MHz is required. In addition, the minimum requirement UE terminal is mandated to support 20 MHz bandwidth. Hence, a sampling frequency of 30.72 MHz is indicated for the maximum system bandwidth of 20 MHz . For this system bandwidth, to enable for efficient implementation, the FFT order is set to 2048. Given this sampling frequency and this system bandwidth, it appears that the ratio between the number of used sub-carriers and the total number of sub-carriers processed by FFT is lower compared to other systems (e.g. DVB, WLAN). This slightly reduces the FFT efficiency. For this 20 MHz maximum bandwidth case, for example only 1200 sub-carriers are used out of 2048 resulting in a ratio of ≈ 0.7 used vs. processed sub-carriers.

Lower sampling frequencies (and proportionally lower FFT orders) are always possible to reduce RF and Base-Band (BB) processors complexity and consumption for narrower bandwidth deployments: for a 5 MHz system bandwidth the FFT order, used sub-carriers and sampling frequency would be respectively scaled down to 512, 300 and $f_s = 7.68\text{MHz}$.

For the sake of further reducing the terminal complexity, the DC sub-carrier is left unused. Figure 1.4.2 graphically depicts the above discussion.

The OFDMA parameters used in the Down-link are defined in the 3GPP Technical Specification 36.211 [21].

1.5 Conclusion

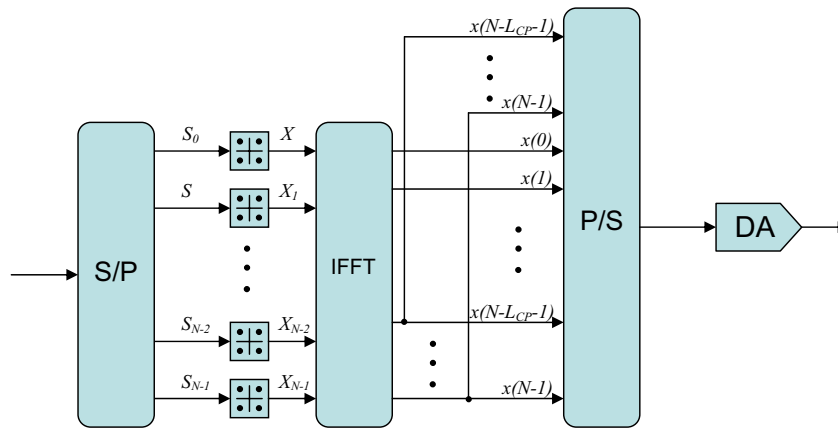
This allows a bit stream with a very high transmission rate to be divided into many bit streams with lower transmission rates. Based on the use of cyclic redundancy, this approach can be made robust against large delay spreads (i.e. against Inter-Symbol Interferences - ISI) while preserving orthogonality in the frequency domain. Furthermore, the clever use of cyclic redundancy at the transmitter reduces the complexity to only FFT processing and to one-tap scalar equalization at the receiver.

This chapter presented results of more than thirty years research and development achievements and understanding. We can sum up the reasons why OFDM has been chosen for LTE down-link in:

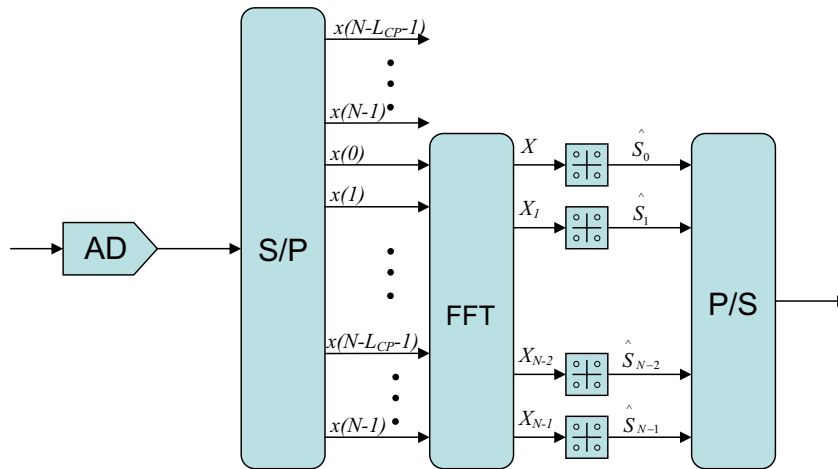
- OFDM is a mature technology.
- It is already widely deployed and is especially suited for broadcast or un-link application because of the low receiver complexity while requiring a high transmitter complexity (expensive Power Amplifier).
- It benefits from efficient implementation by means of the FFT.
- It achieves high transmission rates of broadband transmission, with low receiver complexity.
- It achieves the high transmission rate of broad-band but with the low receiver complexity of narrow-band transmission.
- It makes use of a cyclic-prefix to null Inter-Symbol Interference, enabling block-wise processing.
- It exploits orthogonal sub-carriers to avoid spectrum wastage associated with inter-sub-carrier guard-bands.

- The parametrization allows the system designer to balance tolerance of Doppler and delay-spread depending on the deployment scenario.
- It can be extended to multiple-access scheme, OFDMA, and MIMO in a straightforward manner.

These factors together made OFDMA the technology of choice for the LTE down link.



OFDM Transmitter



OFDM receiver

Figure 1.2: OFDM System Model

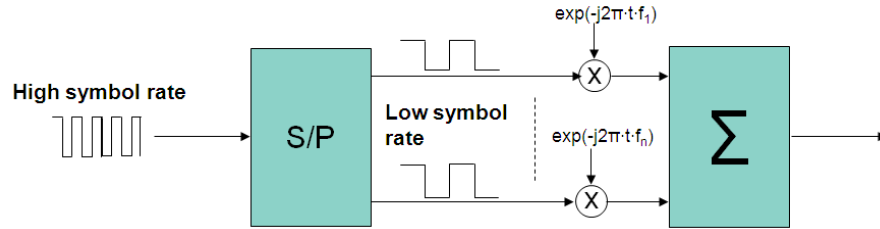


Figure 1.3: Serial-to-parallel conversion operation for OFDM

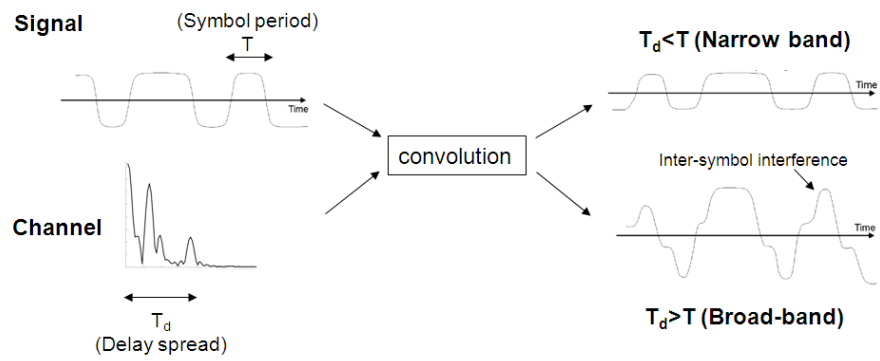


Figure 1.4: Effect of channel on signals with short and long symbol duration

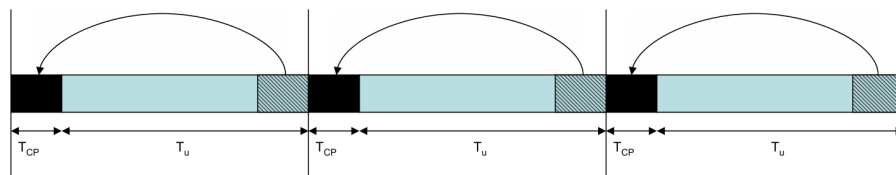


Figure 1.5: OFDM cyclic prefix insertion principle

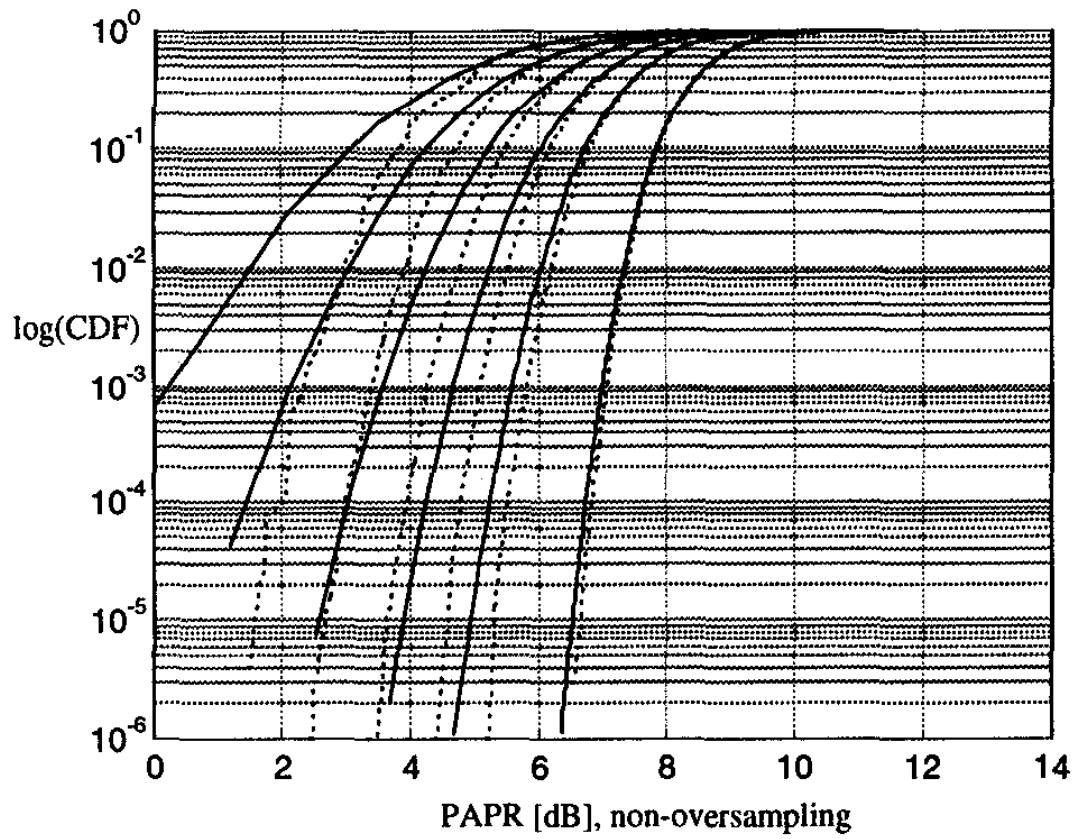


Figure 1.6: PAPR distribution

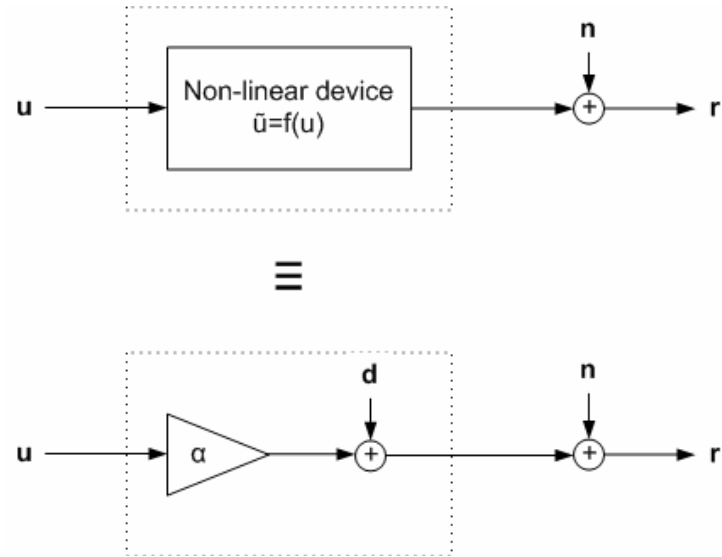


Figure 1.7: Non-linear device equivalent model.

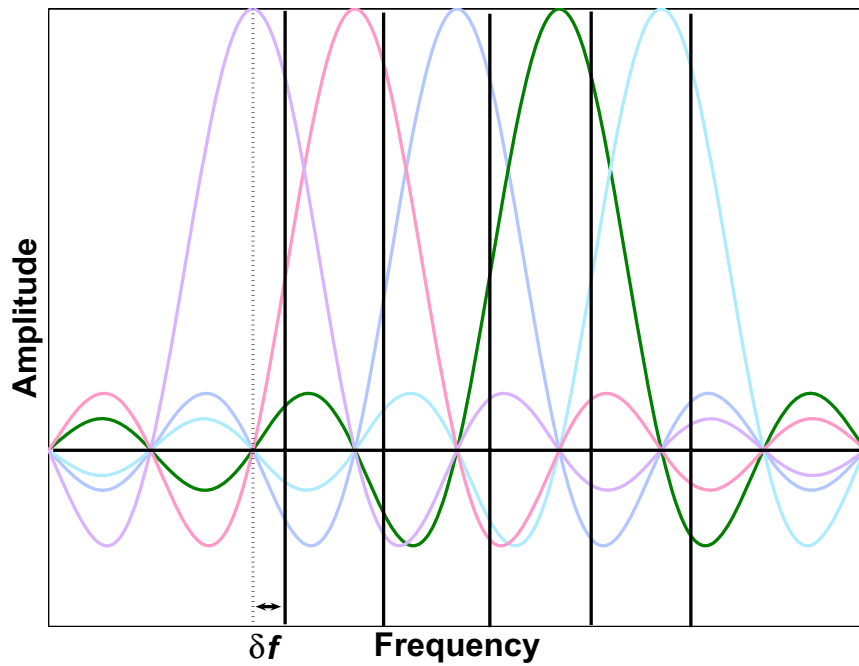


Figure 1.8: OFDM sub-carriers orthogonality loss due to frequency offset

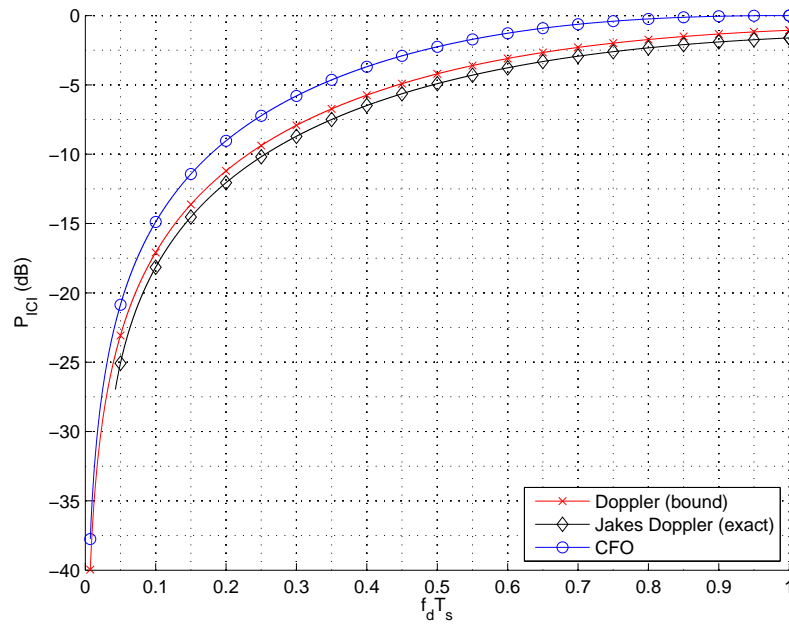


Figure 1.9: P_{ICI} for generic Doppler distribution, Jakes profile and deterministic CFO.

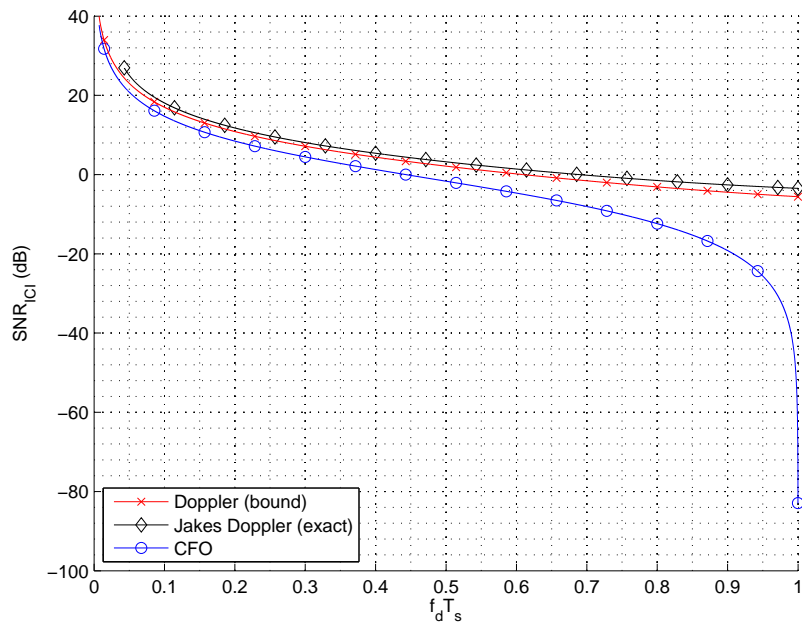


Figure 1.10: SNR_{ICI} for generic Doppler distribution, Jakes profile and deterministic CFO.

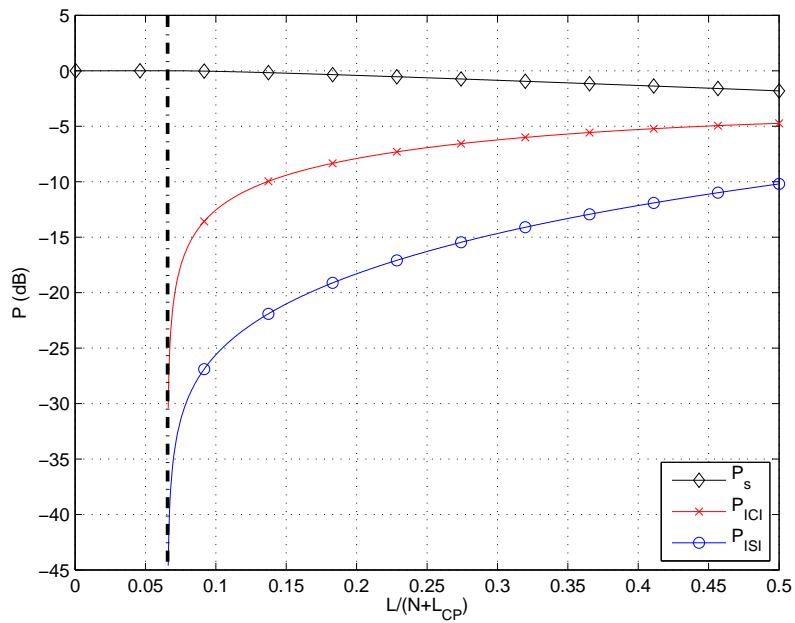


Figure 1.11: Power of signal, ICI and ISI in case of offended guard interval.

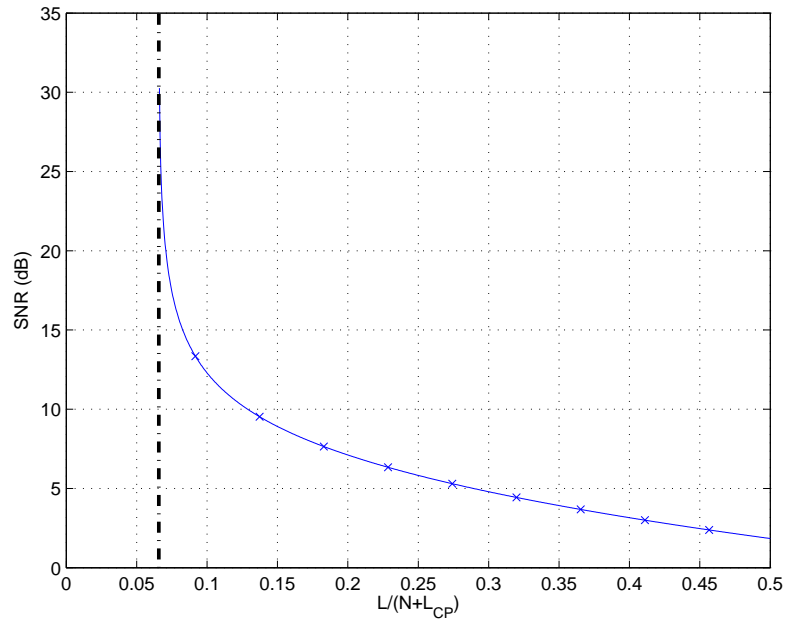


Figure 1.12: SNR in case of offened guard interval.

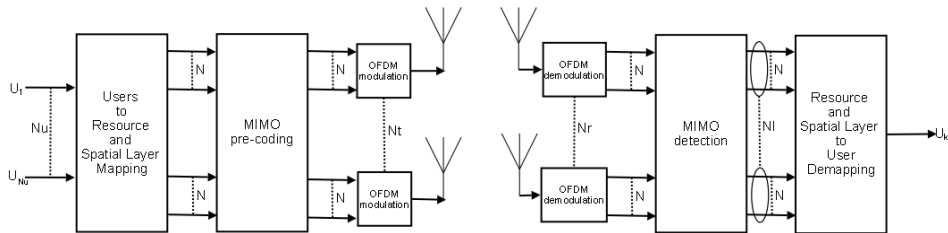


Figure 1.13: General MIMO-OFDM scheme

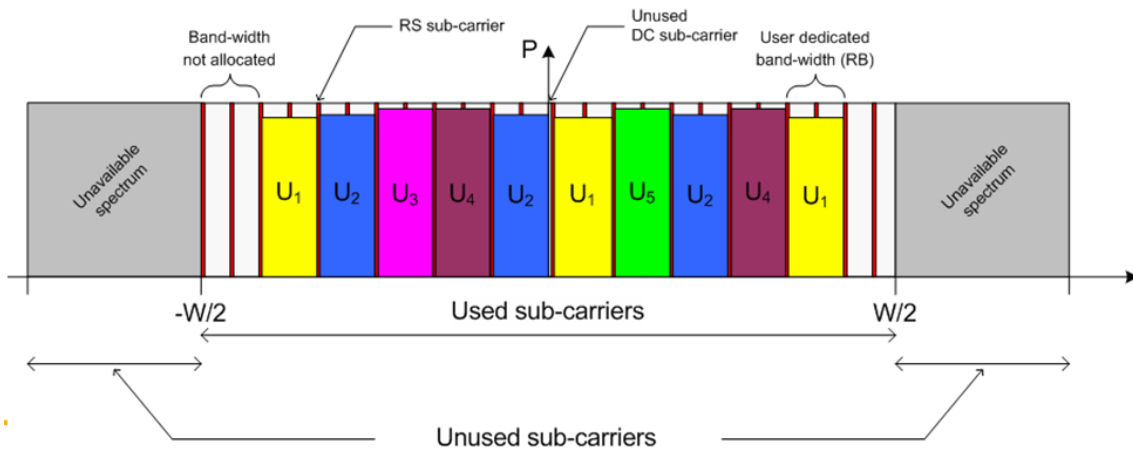


Figure 1.16: LTE OFDMA spectrum allocation.

Chapter 2

Channel Estimation in LTE

2.1 Introduction

A simple communication system can be generally modeled as in Figure 2.1, where the signal \mathbf{x} transmitted by ‘A’ passes through a radio channel \mathbf{H} and suffers additive noise before being received by ‘B’. Mobile radio channels usually exhibit multipath fading, which causes Inter-Symbol Interference (ISI) in the received signal. In order to remove ISI, different kinds of equalization and detection algorithms can be utilized, which may or may not exploit knowledge of the Channel Impulse Response (CIR). Orthogonal Frequency Division Multiple Access (OFDMA) is particularly robust against ISI, thanks to its structure and the use of the Cyclic Prefix (CP) which allows the receiver to perform a low-complexity single-tap scalar equalization in the frequency domain, as described in Section 1.2.1.

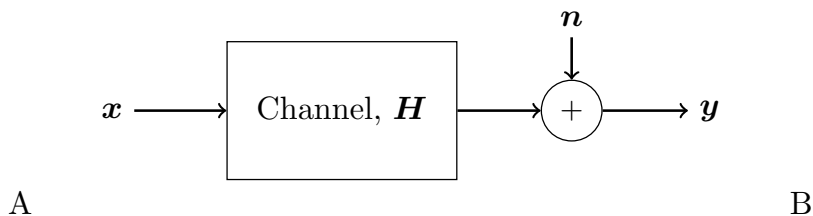


Figure 2.1: A simple transmission model.

When the detection method exploits channel knowledge, it is generally said to be ‘coherent’, while otherwise it is called ‘non-coherent’. Coherent detection can therefore make use of both amplitude and phase information carried by the complex signals, and not of only amplitude information as with non-coherent detection. Optimal reception by coherent detection therefore typically requires accurate esti-

mation of the propagation channel.

The main advantage of coherent detection is the simplicity of the implementation compared to the more complex algorithms required by non-coherent detection for equivalent performance. However, this simplicity comes at a price, namely the overhead needed in order to be able to estimate the channel. A common and simple way to estimate the channel is to exploit known signals which do not carry any data, but which therefore cause a loss in spectral efficiency. In general, it is not an easy task to find the optimal trade-off between minimizing the spectral efficiency loss due to the overhead and providing adequate ability to track variations in the channel.

Other possible techniques for channel estimation include the use of a priori knowledge of a parametric model of the channel, exploiting the correlation properties of the channel, or using blind estimation.

Once synchronization between an eNodeB and a UE has been achieved, the main characteristic of the LTE physical processing architecture (shared with earlier systems such as GSM and UMTS) is that of being a coherent communication system, for which purpose known reference signals are inserted into the transmitted signal structure.

In general, a variety of methods can be used to embed reference signals into a transmitted signal. The reference signals can be multiplexed with the data symbols (which are unknown at the receiver) in either the frequency, time or code domains (the latter being used in the case of the common pilot channel in the UMTS down-link). A special case of time multiplexing, known as preamble-based training, involves transmitting the reference signals at the beginning of each data burst. Multiplexing-based techniques have the advantage of low receiver complexity, as the symbol detection is decoupled from the channel estimation problem. Alternatively, reference symbols may be superimposed on top of unknown data, without the two necessarily being orthogonal. Note that multiplexing reference signals in the code domain is a particular type of superposition with a constraint on orthogonality between known reference signals and the unknown data. A comprehensive analysis of the optimization of reference signal design can be found in [35, 37].

Orthogonal reference signal multiplexing is by far the most common technique. For example, to facilitate channel estimation in the UMTS down-link, two types of orthogonal reference signal are provided. The first is code-multiplexed, available to all users in a cell, and uses a specific spreading code which is orthogonal to the codes used to spread the users' data. The second type is time-multiplexed dedicated reference signals, which may in some situations be inserted into the users' data streams [38].

In the LTE down-link, the OFDM transmission can be described by a two-dimensional lattice in time and frequency. This structure facilitates the multiplexing

of the Reference Signals (RSs), which are mapped to specific Resource Elements (REs) of the two-dimensional lattice in Figure 1.14 according to a pattern explained in Section 2.2.

In order to estimate the channel as accurately as possible, all correlations between channel coefficients in time, frequency and space should be taken into account. Since reference signals are sent only on particular OFDM REs (i.e. on particular OFDM symbols on particular sub-carriers), channel estimates for the REs which do not bear RSs have to be computed via interpolation. The optimal interpolating channel estimator in terms of mean squared error is based on a two-dimensional Wiener filter interpolation [39]. Due to the high complexity of such a filter, a trade-off between complexity and accuracy is achieved by using one-dimensional filters. In Sections 2.4 and 2.5 the problem of channel estimation is approached from a theoretical point of view, and some possible solutions are described.

The work done in the field of channel estimation, and the corresponding literature available, is vast. Nevertheless many challenges still remain, and we refer the interested reader to [37, 40] for a general survey of open issues in this area.

2.2 Design of Reference Signals in LTE

In the Release 8 of LTE down-link, three different types of RSs are provided [41]:

- Cell-specific RSs (often referred to as ‘common’ RSs, as they are available to all UEs in a cell).
- UE-specific RSs, which may be embedded in the data for specific UEs.
- MBSFN-specific RSs, which are only used for Multimedia Broadcast Single Frequency Network (MBSFN) operation [61].

2.2.1 Cell-Specific Reference Signals

References [42, 43] show that in an OFDM-based system an equidistant arrangement of reference symbols in the lattice structure achieves the minimum mean squared error estimate of the channel. Moreover, in the case of a uniform reference symbol grid, a ‘diamond shape’ in the time-frequency plane can be shown to be optimal.

In LTE, the arrangement of the symbols making up the cell-specific RSs in the time-frequency two-dimensional lattice follows these principles. Figure 2.2 illustrates the RS arrangement for the normal CP length.¹

¹In the case of the extended CP, the arrangement of the reference symbols slightly changes, but

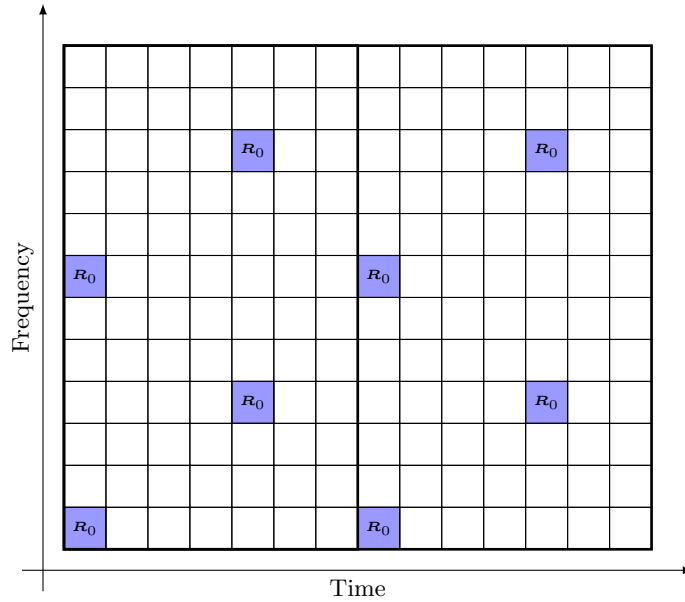


Figure 2.2: Cell-specific reference symbol arrangement in the case of normal CP length for one antenna port.

The LTE system has been conceived to work under high-mobility assumptions, in contrast to WLAN systems which are generally optimized for pedestrian-level mobility. WLAN systems typically use a preamble-based training sequence, the frequency of which governs the degree of mobility they can support.

The required spacing in time between the reference symbols can be obtained by considering the maximum Doppler spread (highest speed) to be supported, which for LTE corresponds to 500 km/h [44]. The Doppler shift is $f_d = (f_c v/c)$ where f_c is the carrier frequency, v is the UE speed in meters per second, and c is the speed of light ($3 \cdot 10^8$ m/s). Considering $f_c = 2$ GHz and $v = 500$ km/h, then the Doppler shift is $f_d \simeq 950$ Hz. According to Nyquist's sampling theorem, the minimum sampling frequency needed in order to reconstruct the channel is therefore given by $T_c = 1/(2f_d) \simeq 0.5$ ms under the above assumptions. This implies that two reference symbols per slot are needed in the time domain in order to estimate the channel correctly.

In the frequency direction there is one reference symbol every six sub-carriers on each OFDM symbols which includes reference symbol, but these are staggered so that within each Resource Block (RB) there is one reference symbol every 3 sub-carriers, as shown in Figure 2.2. This spacing is related to the expected coherence

the explanations in the rest of the chapter are no less valid. The detailed arrangement of reference symbols for the extended CP can be found in [41].

bandwidth of the channel, which is in turn related to the channel delay spread. In particular the 90% and 50% coherence bandwidths² are given respectively by $B_{c,90\%} = 1/50\sigma_\tau$ and $B_{c,50\%} = 1/5\sigma_\tau$ where σ_τ is the r.m.s delay spread. In [45] the maximum r.m.s channel delay spread considered is 991 ns, corresponding to $B_{c,90\%} = 20$ kHz and $B_{c,50\%} = 200$ kHz. In LTE the spacing between two reference symbols in frequency, in one RB, is 45 kHz, thus allowing the expected frequency-domain variations of the channel to be resolved.

The LTE down-link has been specifically designed to work with multiple transmit antennas, as is discussed in detail in Chapter 1.3. RS patterns are therefore defined for multiple ‘antenna ports’ at the eNodeB. An antenna port may in practice be implemented either as a single physical transmit antenna, or as a combination of multiple physical antenna elements. In either case, the signal transmitted from each antenna port is not designed to be further deconstructed by the UE receiver: the transmitted RS corresponding to a given antenna port defines the antenna port from the point of view of the UE, and enables the UE to derive a channel estimate for that antenna port – regardless of whether it represents a single radio channel from one physical antenna or a composite channel from a multiplicity of physical antenna elements together comprising the antenna port.

Up to four cell-specific antenna ports may be used by a LTE eNodeB, thus requiring the UE to derive up to four separate channel estimates.³ For each antenna port, a different RS pattern is designed, with particular attention having been given to the minimization of the intra-cell interference between the multiple transmit antenna ports. In Figure 2.3, 2.4 R_p indicates that the resource element is used for the transmission of an RS on antenna port p . In particular when a resource element is used to transmit an RS on one antenna port, the corresponding resource element on the other antenna ports is set to zero to limit the interference.

From Figure 2.4 it can be noticed that the density of RS for the third and fourth antenna ports is half that of the first two; this is to reduce the overhead in the system. Frequent reference symbols are useful for high-speed conditions as explained above. In cells with a high prevalence of high-speed users, the use of four antenna ports is unlikely, hence for these conditions RSs with lower density can provide sufficient channel estimation accuracy.

All the RSs (cell-specific, UE-specific or MBSFN specific) are QPSK modulated – a constant modulus modulation. This property ensures that the Peak-to-Average Power Ratio (PAPR) of the transmitted waveform is kept low. The signal can be

² $B_{c,x\%}$ is the bandwidth where the autocorrelation of the channel in the frequency domain is equal to $x\%$.

³Any MBSFN and UE-specific RSs, if transmitted, constitute additional independent fifth and sixth antenna ports respectively in the LTE specifications.

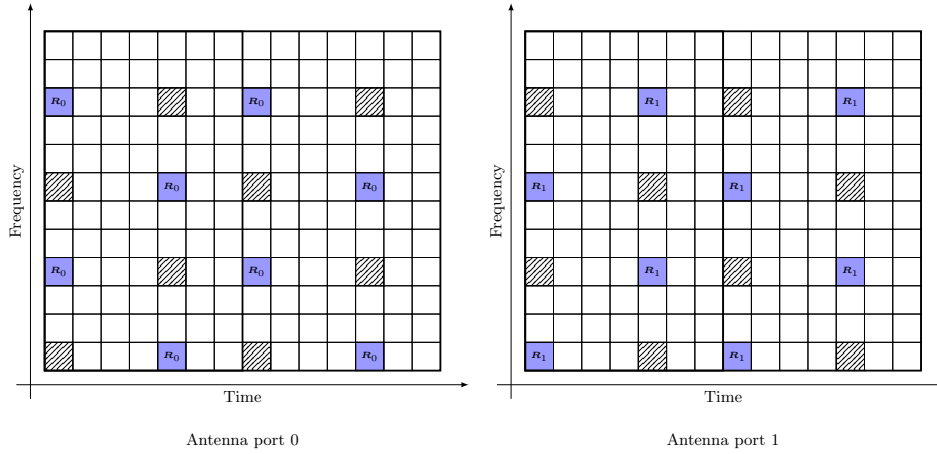


Figure 2.3: Cell-specific RS arrangement in the case of normal CP length for two antenna ports.

written as

$$r_{l,n_s}(m) = \frac{1}{\sqrt{2}}[1 - 2c(2m)] + j\frac{1}{\sqrt{2}}[1 - 2c(2m + 1)] \quad (2.1)$$

where m is the index of the RS, n_s is the slot number within the radio frame and ‘ l ’ is the symbol number within the time slot. The pseudo-random sequence $c(i)$ is comprised of a length-31 Gold sequence [36], with different initialization values depending on the type of RSs.

The RS sequence also carries unambiguously one of the 504 different cell identities, $N_{\text{ID}}^{\text{cell}}$. For the cell-specific RSs, a cell-specific frequency shift is also applied, given by $N_{\text{ID}}^{\text{cell}} \bmod 6$.⁴ This shift can avoid time-frequency collisions between common RS from up to six adjacent cells. Avoidance of collisions is particularly important in cases when the transmission power of the RS is boosted, as is possible in LTE up to a maximum of 6 dB relative to the surrounding data symbols. RS power boosting is designed to improve channel estimation in the cell, but if adjacent cells transmit high-power RS on the same REs the resulting inter-cell interference will prevent the benefit from being realized.

2.2.2 UE-Specific Reference Signals

UE-specific RS may be transmitted in addition to the cell-specific RSs described above. They are embedded only in the RBs to which the PDSCH is mapped for UEs which are specifically configured (by higher-layer RRC signaling) to receive

⁴The mod6 operation is used because RSs are spaced apart by six sub-carriers in the lattice grid.

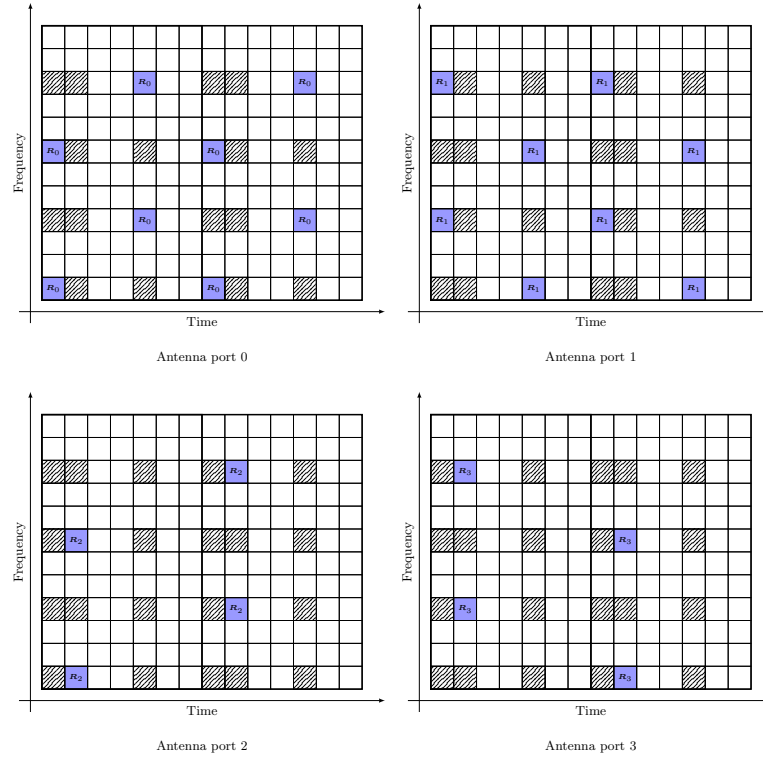


Figure 2.4: Cell-specific RS arrangement in the case of normal CP length for four antenna ports.

their down-link data transmissions in this mode. If UE-specific RSs are used, the UE is expected to use them to derive the channel estimate for demodulating the data in the corresponding PDSCH RBs. Thus the UE-specific RS are treated as being transmitted using a distinct antenna port, with its own channel response from the eNodeB to the UE.

A typical usage of the UE-specific RSs is to enable beam-forming of the data transmissions to specific UEs. For example, rather than using the physical antennas used for transmission of the other (cell-specific) antenna ports, the eNodeB may use a correlated array of physical antenna elements to generate a narrow beam in the direction of a particular UE. Such a beam will experience a different channel response between the eNodeB and UE, thus requiring the use of UE-specific RSs to enable the UE to demodulate the beam-formed data coherently. The use of UE-specific beam-forming is discussed in more detail in [61].

2.3 RS-Aided Channel Modeling and Estimation

The channel estimation problem is related to the channel model assumed, itself determined by the physical propagation characteristics, including the number of transmit and receive antennas, transmission bandwidth, carrier frequency, cell configuration and relative speed between eNodeB and UE receivers. In general,

- The carrier frequencies and system bandwidth mainly determine the scattering nature of the channel.
- The cell deployment governs its multi-path, delay spread and spatial correlation characteristics.
- The relative speed sets the time-varying properties of the channel.

The propagation conditions characterize the channel correlation function in a three-dimensional space comprising frequency, time and spatial domains. In the general case, each MIMO (Multiple-Input Multiple-Output) multi-path channel component can experience different but related spatial scattering conditions leading to a full three-dimensional correlation function across the three domains. Nevertheless, for the sake of simplicity, assuming that the multi-path components of each spatial channel experience the same scattering conditions, the spatial correlation is independent from the other two domains and can be handled separately from the frequency and time domain correlations.

This framework might be suboptimal in general, but is nevertheless useful in mitigating the complexity of channel estimation as it reduces the general three-dimensional joint estimation problem into independent estimation problems.

For a comprehensive survey of MIMO channel estimation the interested reader is referred to [47].

The following two subsections define the channel model and the corresponding correlation properties which are then used as the basis for an overview of channel estimation techniques.

2.3.1 Time-Frequency Domain Correlation: The WSSUS Channel Model

The Wide-Sense Stationary Uncorrelated Scattering (WSSUS) channel model is commonly employed for the multi-path channels experienced in mobile communications.

Neglecting the spatial dimension for the sake of simplicity, let $h(\tau; t)$ denote the time-varying complex baseband impulse response of a multi-path channel realization at time instant t and delay τ .

Considering the channel as a random process in the time direction t , the channel is said to be delay Uncorrelated-Scattered (US) if

$$\mathbb{E}[h(\tau_a; t_1)^* h(\tau_b; t_2)] = \phi_h(\tau_a; t_1, t_2) \delta(\tau_b - \tau_a) \quad (2.2)$$

where $\mathbb{E}[\cdot]$ is the expectation operator. According to the US assumption, two CIR components a and b at relative delays τ_a and τ_b are uncorrelated if $\tau_a \neq \tau_b$.

The channel is Wide-Sense Stationary (WSS)-uncorrelated if

$$\phi_h(\tau; t_1, t_2) = \phi_h(\tau; t_2 - t_1) \quad (2.3)$$

which means that the correlation of each delay component of the CIR is only a function of the *difference* in time between each realization.

Hence, the second-order statistics of this model are completely described by its delay cross-power density $\phi_h(\tau; \Delta t)$ or by its Fourier transform, the scattering function defined as

$$S_h(\tau; f) = \int \phi_h(\tau; \Delta t) e^{-j2\pi f \Delta t} d\Delta t \quad (2.4)$$

with f being the Doppler frequency. Other related functions of interest include the *Power Delay Profile* (PDP)

$$\psi_h(\tau) = \phi_h(\tau; 0) = \int S_h(\tau; f) df$$

the *time-correlation function*

$$\bar{\phi}_h(\Delta t) = \int \phi_h(\tau; \Delta t) d\tau$$

and the *Doppler power spectrum*

$$\bar{S}_h(f) = \int S_h(\tau; f) d\tau$$

A more general exposition of WSSUS models is given in [48]. Classical results were derived by Clarke [49] and Jakes [50] for the case of a mobile terminal communicating with a stationary base station in a two-dimensional propagation geometry.

These well-known results state that

$$\bar{S}_h(f) = \frac{1}{\sqrt{f_d^2 - f^2}} \quad (2.5)$$

for $|f| \leq f_d$ with f_d being the Doppler shift and

$$\bar{\phi}_h(\Delta t) = J_0(2\pi f_d \Delta t) \quad (2.6)$$

where $J_0(\cdot)$ is the zeroth-order Bessel function. Figure 2.5 shows the PSD of the classical Doppler spectrum described by Clarke and Jakes [49, 50]. The Clarke and Jakes derivations are based on the assumption that the physical scattering environment is chaotic and therefore the angle of arrival of the electromagnetic wave at the receiver is a uniformly distributed random variable in the angular domain. As a consequence, the time-correlation function is strictly real-valued, the Doppler spectrum is symmetric and interestingly there is a *delay-temporal separability* property in the general bi-dimensional scattering function $S_h(\tau, \Delta t)$. In other words,

$$S_h(\tau; f) = \psi_h(\tau) \bar{S}_h(f) \quad (2.7)$$

or equivalently

$$\phi_h(\tau; \Delta t) = \psi_h(\tau) \bar{\phi}_h(\Delta t) \quad (2.8)$$

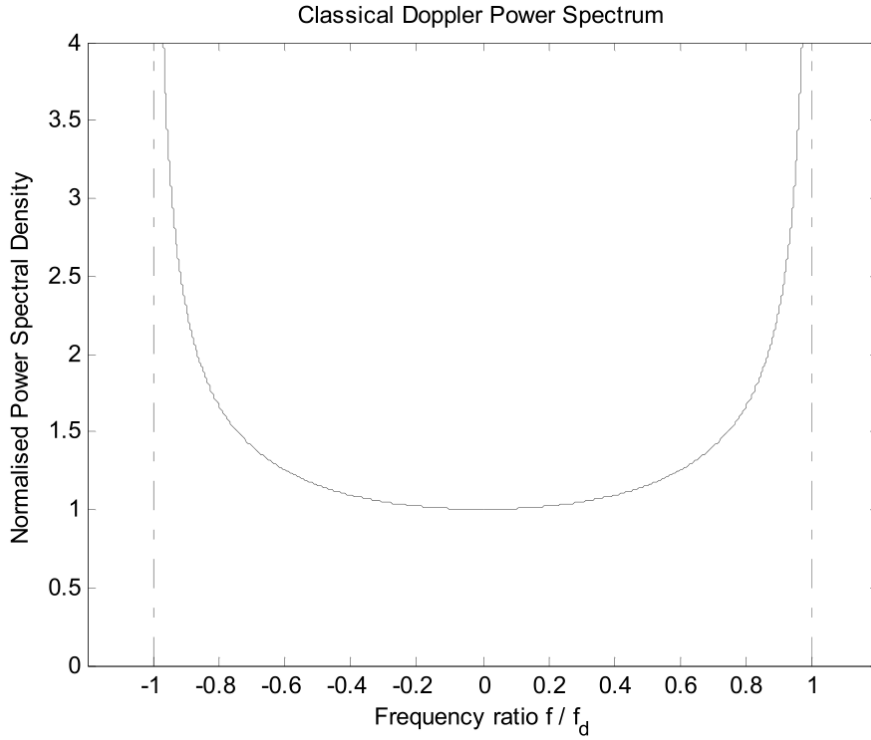


Figure 2.5: Normalized PSD for Clarke's model.

Slot duration [ms]	0.5					
Sub-carrier spacing Δf_{sc} [kHz]	15					
Transmission BW [MHz]	1.25	2.5	5	10	15	20
Sampling frequency [MHz]	1.92	3.84	7.68	15.36	23.04	30.72
FFT size N	128	256	512	1024	1536	2048
Occupied sub-carriers (including DC) K	76	151	301	601	901	1201

Table 2.1: LTE OFDMA parameters.

Separability is a very important assumption for reducing the complexity of channel estimation, allowing the problem to be separated into two one-dimensional operations.

The continuous-time correlation properties of the channel $h(\tau, t)$ discussed above, equivalently apply to the corresponding low-pass sampled discrete-time CIR, i.e. $h[l, k]$ [51], for every l^{th} delay sampled at kT^{th} instant where T is the sampling period. Moreover, these properties are maintained if we assume $h[l, k]$ to be well-approximated by a Finite-Impulse Response (FIR) vector $\mathbf{h}[k] = [h[0, k], \dots, h[L-1, k]]^T$ with a maximum delay spread of L samples. For the sake of notational simplicity and without loss of generality, the index k will be dropped in the sequel.

2.4 Frequency-domain Channel Estimation

Although the general channel estimation problem in case of single antenna transmissions is two-dimensional [26], i.e. is to be carried jointly in the frequency and time domains, it is normally separated into two one-dimensional estimation steps [27] for ease of implementation.

In this context, we deal in particular with the channel estimation problem over one OFDMA symbol (specifically the symbol containing the RS) to exploit the frequency domain characteristics and instead we do not consider its time-varying characteristics due to Doppler effect in the aim of exploiting correlation in time.

In the OFDMA LTE context, as for any comb-distributed pilot OFDM system [52], the Channel Transfer Function (CTF) \mathbf{z} is ML estimated in the frequency domain at the pilot positions by de-correlating the constant modulus Reference Signal pilot sequence. Using matrix notation, it can be modeled as:

$$\hat{\mathbf{z}}_p = \mathbf{z}_p + \tilde{\mathbf{z}}_p = \mathbf{F}_p \mathbf{h} + \tilde{\mathbf{z}}_p \quad (2.9)$$

where

- $P = \lceil K/M \rceil$ is the number of available pilots where K is the number of occupied sub-carriers (including DC).
- \mathbf{h} is the $L \times 1$ Channel Impulse Response (CIR) vector. The effective channel length $L \leq L_{CP}$ is assumed to be known.
- \mathbf{F}_p is the $P \times L$ matrix obtained by selecting the rows corresponding to the pilot positions and the first L columns of the $N \times N$ Discrete Fourier Transform (DFT) matrix whose elements are $(\mathbf{F})_{n,k} = e^{-\frac{j2\pi}{N}(nk)}$ with $0 \leq n \leq N-1$ and $0 \leq k \leq N-1$;
- $\tilde{\mathbf{z}}_p$ is the $P \times 1$ zero-mean complex circular white noise vector whose $L \times L$ covariance matrix is $\mathbf{C}_{\tilde{\mathbf{z}}_p} = \sigma_{\tilde{\mathbf{z}}_p}^2 \mathbf{I}_L$;

2.4.1 Channel Estimation by interpolation

Linear interpolation estimator

The natural approach to estimate the whole CTF is to interpolate the CTF estimate on pilot positions $\hat{\mathbf{z}}_p$. In the general case, let \mathbf{A} be a generic interpolation filter and the interpolated CTF estimate can be written as:

$$\hat{\mathbf{z}}_i = \mathbf{A}\hat{\mathbf{z}}_p \quad (2.10)$$

Substituting (A.1) in (A.2), the error of the interpolated CTF estimate is:

$$\tilde{\mathbf{z}}_i = \mathbf{z} - \hat{\mathbf{z}}_i = (\mathbf{F}_L - \mathbf{A}\mathbf{F}_p) \mathbf{h} - \mathbf{A}\tilde{\mathbf{z}}_p \quad (2.11)$$

where $\mathbf{z} = \mathbf{F}_L \mathbf{h}$ and \mathbf{F}_L is the $N \times L$ matrix obtained taking the first L columns of the Fourier transform matrix.

The error covariance matrix is:

$$\mathbf{C}_{\tilde{\mathbf{z}}_i} = (\mathbf{F}_L - \mathbf{A}\mathbf{F}_p) \mathbf{C}_h (\mathbf{F}_L - \mathbf{A}\mathbf{F}_p)^H + \sigma_{\tilde{\mathbf{z}}_p}^2 \mathbf{A}\mathbf{A}^H \quad (2.12)$$

being $\mathbf{C}_h = \mathbf{E}\mathbf{h}\mathbf{h}^H$ the channel covariance matrix, $\{\cdot\}^H$ and $\mathbf{E}\{\cdot\}$ denoting, respectively, the Hermitian and the expectation operators.

Although pulse-shaping is not mandated in LTE, receiver front-end consists of an anti-aliasing low-pass filtering.

Therefore the channel and its covariance matrix can effectively be modeled as:

$$\mathbf{h} = \mathbf{P}\mathbf{u} \quad \text{and} \quad \mathbf{C}_h = \mathbf{P}\mathbf{C}_u\mathbf{P}^H \quad (2.13)$$

where \mathbf{P} is the matrix of the equivalent pulse-shaping filter, \mathbf{u} is the discrete-time uncorrelated multi-path fading channel vector and

$$\mathbf{C}_{\mathbf{u}} = \mathbf{E}\mathbf{u}\mathbf{u}^H = \text{diag} \left(\sigma_{u_0}^2, \sigma_{u_1}^2, \dots, \sigma_{u_{L_{\text{MP}}-1}}^2 \right)$$

is its diagonal covariance matrix normally assimilated to the channel Power Delay Profile (PDP).

Recalling Equation (A.2), linear interpolation would be the intuitive choice. The filter structure \mathbf{A} is then given by

$$\mathbf{A} = \begin{bmatrix} 0 & 0 & \dots & 0 & 0 \\ 0 & 0 & \dots & 0 & 0 \\ 0 & 0 & \dots & 0 & 0 \\ 1 & 0 & \dots & 0 & 0 \\ \frac{M-1}{M} & \frac{1}{M} & 0 & \dots & 0 \\ \frac{M-2}{M} & \frac{2}{M} & 0 & \dots & 0 \\ \vdots & \vdots & \vdots & \vdots & 0 \\ \frac{1}{M} & \frac{M-1}{M} & 0 & \dots & 0 \\ 0 & \frac{1}{M} & 0 & \dots & 0 \\ 0 & \frac{M-1}{M} & \frac{1}{M} & \dots & 0 \\ 0 & \frac{M-2}{M} & \frac{2}{M} & 0 & 0 \\ 0 & \vdots & \vdots & \vdots & 0 \\ 0 & \frac{1}{M} & \frac{M-1}{M} & 0 & 0 \\ 0 & 0 & 1 & \dots & 0 \\ \vdots & \vdots & \vdots & \vdots & 0 \\ 0 & 0 & \dots & 0 & 0 \\ 0 & 0 & \dots & 0 & 0 \\ 0 & 0 & \dots & 0 & 0 \end{bmatrix} \quad (2.14)$$

This estimator is deterministically biased, but unbiased from the Bayesian viewpoint regardless of the structure of \mathbf{A} .

IFFT estimator

The second natural approach to retrieve the whole CTF estimate is by IFFT interpolation. The *IFFT* CTF estimate interpolated over all sub-carriers can be obtained

by using in (A.2):

$$\mathbf{A} = \frac{1}{P} \mathbf{F}_L \mathbf{F}_p^H \quad (2.15)$$

Hence, the *IFFT* estimator is given by:

$$\hat{\mathbf{z}}_{\text{IFFT}} = \frac{1}{P} \mathbf{F}_L \mathbf{F}_p^H \hat{\mathbf{z}}_p \quad (2.16)$$

The *IFFT* interpolated CTF estimate error and its covariance matrix, applying (A.1) and (A.7) into (A.2), becomes:

$$\tilde{\mathbf{z}}_{\text{IFFT}} = \mathbf{F}_L \left(\mathbf{I}_L - \frac{1}{P} \mathbf{F}_p^H \mathbf{F}_p \right) \mathbf{h} - \frac{1}{P} \mathbf{F}_L \mathbf{F}_p^H \tilde{\mathbf{z}}_p \quad (2.17)$$

$$\mathbf{C}_{\tilde{\mathbf{z}}_{\text{IFFT}}} = \left(\mathbf{F}_L - \frac{1}{P} \mathbf{F}_L \mathbf{F}_p^H \mathbf{F}_p \right) \mathbf{C}_h \left(\mathbf{F}_L - \frac{1}{P} \mathbf{F}_L \mathbf{F}_p^H \mathbf{F}_p \right)^H + \frac{1}{P^2} \sigma_{\tilde{\mathbf{z}}_p}^2 \mathbf{F}_L \mathbf{F}_p^H \mathbf{F}_p \mathbf{F}_L^H \quad (2.18)$$

In the approximation of $\mathbf{I}_L \approx \frac{1}{P} \mathbf{F}_p^H \mathbf{F}_p$, the estimator would be unbiased and its error covariance matrix would reduce to:

$$\mathbf{C}_{\tilde{\mathbf{z}}_{\text{IFFT}}} \approx \frac{1}{P} \sigma_{\tilde{\mathbf{z}}_p}^2 \mathbf{F}_L \mathbf{F}_L^H \quad (2.19)$$

Given the LTE system parameters and the pilot structure, in practice, $\frac{1}{P} \mathbf{F}_p^H \mathbf{F}_p$ is far from being a multiple of an identity matrix: the approximation would be an equality when $K = N, N/M > L$ and N/M being an integer, i.e. the system should be dimensioned without guard-bands and the pilot should be disposed with a spacing which is dividing exactly the FFT order N , namely a power of two. Therefore, according to (A.9), the estimator $\hat{\mathbf{z}}_{\text{IFFT}}$ is biased as for the linear interpolation case if the channel is deterministic and unbiased from the Bayesian point of view.

We remand to the simulation results section of this paper for a comparison of their respective performances.

2.4.2 General approach to linear channel estimation

Compared to the simple approaches presented in the previous section, more elaborated linear estimators derived from both deterministic and statistical viewpoint

proposed in [53], [54] and [55], namely LS, Regularized LS, MMSE and Mismatched MMSE in addition to the novel estimators presented in the following sections, can all be expressed under the general formulation:

$$\hat{\mathbf{z}}_{\text{gen}} = \mathbf{B} (\mathbf{G}^H \mathbf{G} + \mathbf{R})^{-1} \mathbf{G}^H \hat{\mathbf{z}}_p \quad (2.20)$$

Where \mathbf{B} , \mathbf{G} and \mathbf{R} are matrices that vary according to each estimator as detailed in the following. With (A.1) and (A.12), we obtain the error expression:

$$\tilde{\mathbf{z}}_{\text{gen}} = \left(\mathbf{F}_L - \mathbf{B} (\mathbf{G}^H \mathbf{G} + \mathbf{R})^{-1} \mathbf{G}^H \mathbf{F}_p \right) \mathbf{h} - \mathbf{B} (\mathbf{G}^H \mathbf{G} + \mathbf{R})^{-1} \mathbf{G}^H \tilde{\mathbf{z}}_p \quad (2.21)$$

and its covariance matrix:

$$\begin{aligned} \mathbf{C}_{\tilde{\mathbf{z}}_{\text{gen}}} &= \left(\mathbf{F}_L - \mathbf{B} (\mathbf{G}^H \mathbf{G} + \mathbf{R})^{-1} \mathbf{G}^H \mathbf{F}_p \right) \mathbf{C}_h \left(\mathbf{F}_L - \mathbf{B} (\mathbf{G}^H \mathbf{G} + \mathbf{R})^{-1} \mathbf{G}^H \mathbf{F}_p \right)^H + \\ &\quad + \sigma_{\tilde{\mathbf{z}}_p}^2 \mathbf{B} (\mathbf{G}^H \mathbf{G} + \mathbf{R})^{-1} \mathbf{G}^H \mathbf{G} (\mathbf{G}^H \mathbf{G} + \mathbf{R})^{-1} \mathbf{B}^H \end{aligned} \quad (2.22)$$

LS estimator

The LS estimator discussed in [53] can be inferred by choosing:

$$\mathbf{B} = \mathbf{F}_L, \mathbf{G} = \mathbf{F}_p \text{ and } \mathbf{R} = \mathbf{0}_L \quad (2.23)$$

with $\mathbf{0}_L$ being the $L \times L$ matrix containing zeros. And the estimator appears as:

$$\hat{\mathbf{z}}_{\text{LS}} = \mathbf{F}_L (\mathbf{F}_p^H \mathbf{F}_p)^{-1} \mathbf{F}_p^H \hat{\mathbf{z}}_p \quad (2.24)$$

Substituting (A.1) and (A.15) in (A.13) and (A.14), the error reduces to:

$$\tilde{\mathbf{z}}_{\text{LS}} = -\mathbf{F}_L (\mathbf{F}_p^H \mathbf{F}_p)^{-1} \mathbf{F}_p^H \tilde{\mathbf{z}}_p \quad (2.25)$$

showing that the LS estimator, at least theoretically, is unbiased. Thus, compared to the linear interpolation estimator given by (A.2), the LS estimator is considered as the perfect interpolator as it sets to zero the bias term of expression (A.3) with $\mathbf{A} = \mathbf{F}_L (\mathbf{F}_p^H \mathbf{F}_p)^{-1} \mathbf{F}_p^H$. Consequently, the error covariance matrix can be shown to be:

$$\mathbf{C}_{\tilde{\mathbf{z}}_{\text{LS}}} = \sigma_{\tilde{\mathbf{z}}_p}^2 \mathbf{F}_L (\mathbf{F}_p^H \mathbf{F}_p)^{-1} \mathbf{F}_L^H \quad (2.26)$$

Regularized LS estimator

As evidenced in [55], the LTE system parameters make the LS estimator inapplicable: the expression $(\mathbf{F}_p \mathbf{F}_p^H)^{-1}$ is ill-conditioned due to the large unused portion of the spectrum corresponding to the unmodulated sub-carriers.

To counter this problem, the robust *regularized* LS estimator was used to yield a better conditioning of the matrix to be inverted by using the same \mathbf{B} and \mathbf{G} as for the LS estimator but introducing the regularization matrix $\mathbf{R} = \alpha \mathbf{I}_L$ with α being a constant (off-line) chosen to optimize the performance of the estimator in a given Signal-to-Noise Ratio (SNR) working range.

Hence, we can write the estimator as follows:

$$\hat{\mathbf{z}}_{\text{reg,LS}} = \mathbf{F}_L (\mathbf{F}_p^H \mathbf{F}_p + \alpha \mathbf{I}_L)^{-1} \mathbf{F}_p^H \hat{\mathbf{z}}_p \quad (2.27)$$

The expressions for the error and the error covariance matrix of this estimator can be deduced directly from (A.13) and (A.14) by substituting \mathbf{B} , \mathbf{G} and \mathbf{R} with their corresponding expressions.

Down-sampled impulse response LS channel estimation

An alternative solution can be found while investigating the reasons of the ill conditioning problem: the motivation comes from the un-excitation of a large portion of the band which comes from the LTE OFDM symbol structure. Considering for example the case of a symbol size N equal to 1024 from Table A.1, we obtain that the number of modulated sub-carriers is only 600 hence, while the sampling frequency is 15.36 MHz ($N\Delta f_c$), the occupied band-width is only 9 MHz ($N_m\Delta f_c$). It follows that the channel is estimated in the whole 15.36 MHz sampling bandwidth while only the modulated sub-carriers are excited (9 MHz). The channel can indeed be sounded only in the excited band. In order to do this, the *numerical bandwidth*, which is considered to be the ratio between the occupied bandwidth and the sampling frequency, should be increased to somewhat slight smaller than 1. This can be done by decreasing the sampling frequency used for the numerical representation of the channel by a factor 2/3 which ensures the absence of aliasing giving a resulting sampling frequency of 10.24 MHz. Practically, the channel h is not estimated in all the L taps but only in 2 out of 3 taps (obtaining the average down-sampling factor 2/3) and setting to 0 the discarded ones:

$$\bar{\mathbf{h}} = (h_0 \ h_1 \ 0 \ h_3 \ h_4 \ 0 \ \cdots \ h_{L-1})^T \quad (2.28)$$

In fact the channel equalization in the OFDM system is not performed in the time domain but in the frequency domain. Therefore it does not matter to have an exact time domain representation of the channel at the actual sampling frequency. What is only important is the channel transfer function in the band of interest.

$$\begin{aligned} \mathbf{z} &= \mathbf{F}_L \bar{\mathbf{h}} = \\ &= \begin{bmatrix} 1 & 1 & 1 & 1 & 1 \\ 1 & w^1 & w^2 & \cdots & w^{(L-1)} \\ 1 & w^2 & w^3 & \cdots & w^{2(L-1)} \\ 1 & w^3 & w^6 & \cdots & w^{3(L-1)} \\ 1 & w^4 & w^8 & \cdots & w^{4(L-1)} \\ 1 & w^5 & w^{10} & \cdots & w^{5(L-1)} \\ \vdots & \vdots & \vdots & \vdots & \vdots \\ 1 & w^{N-1} & w^{2(N-1)} & \cdots & w^{(L-1)(N-1)} \end{bmatrix} \begin{bmatrix} h_0 \\ h_1 \\ 0 \\ h_3 \\ h_4 \\ 0 \\ \vdots \\ h_{L-1} \end{bmatrix} \end{aligned} \quad (2.29)$$

$$\begin{aligned} \mathbf{z} &= \mathbf{F}_L^{DS} \mathbf{h}^{DS} = \\ &= \begin{bmatrix} 1 & 1 & 1 & 1 & 1 \\ 1 & w^1 & w^3 & \cdots & w^{(L-1)} \\ 1 & w^2 & w^6 & \cdots & w^{2(L-1)} \\ 1 & w^3 & w^9 & \cdots & w^{3(L-1)} \\ 1 & w^4 & w^{12} & \cdots & w^{4(L-1)} \\ 1 & w^5 & w^{15} & \cdots & w^{5(L-1)} \\ \vdots & \vdots & \vdots & \vdots & \vdots \\ 1 & w^{N-1} & w^{3(N-1)} & \cdots & w^{(L-1)(N-1)} \end{bmatrix} \begin{bmatrix} h_0 \\ h_1 \\ h_3 \\ h_4 \\ \vdots \\ h_{L-1} \end{bmatrix} \end{aligned} \quad (2.30)$$

$$w = e^{\frac{j2\pi}{N}} \quad (2.31)$$

As shown by (A.21) and (A.22), this approach turns out to be as if in the received signal representation, the $\frac{L}{3}$ columns of the Fourier matrix \mathbf{F}_L corresponding to the neglected taps are multiplied by 0, so the time domain received signal can be represented as:

$$\mathbf{r} = \mathbf{F}_L^H \mathbf{F}_L^{DS} \mathbf{h}^{DS} + \mathbf{w} \quad (2.32)$$

where \mathbf{h}^{DS} is the down-sampled version of the FIR channel representation with the resulting vector length $\frac{2}{3}L$. Analogously \mathbf{F}_L^{DS} is equal to the Fourier matrix \mathbf{F}_L where the columns corresponding to the removed taps of h are removed.

Again, the LS criterion can be applied to obtain the *down-sampled LS channel estimation* expression:

$$\hat{\mathbf{h}}_{\text{ds}} = (\mathbf{F}_p^{DS,H} \mathbf{F}_p^{DS})^{-1} \mathbf{F}_p^{DS,H} \hat{\mathbf{z}}_p \quad (2.33)$$

Using the Fourier matrix corresponding to the down-sampled channel the ill conditioning problem is solved and furthermore a complexity gain is obtained because the size of the matrix $(\mathbf{F}_p^{DS,H} \mathbf{F}_p^{DS})^{-1} \mathbf{F}_p^{DS,H}$ turns out to be $\frac{2}{3}L \times N$.

MMSE estimator

Using equations (A.12), (A.13) and (A.14), we can formulate the MMSE estimator [53] by denoting:

$$\mathbf{B} = \mathbf{F}_L, \mathbf{G} = \mathbf{F}_p \text{ and } \mathbf{R} = \sigma_{\mathbf{z}_p}^2 \mathbf{C}_h^{-1} \quad (2.34)$$

thus giving

$$\hat{\mathbf{z}}_{\text{MMSE}} = \mathbf{F}_L \left(\mathbf{F}_p^H \mathbf{F}_p + \sigma_{\mathbf{z}_p}^2 \mathbf{C}_h^{-1} \right)^{-1} \mathbf{F}_p^H \hat{\mathbf{z}}_p \quad (2.35)$$

Again, applying (A.1) and (A.26) in (A.13) and (A.14), the error of the MMSE estimator is:

$$\tilde{\mathbf{z}}_{\text{MMSE}} = \mathbf{F}_L \left(\mathbf{I}_L - \left(\mathbf{F}_p^H \mathbf{F}_p + \sigma_{\mathbf{z}_p}^2 \mathbf{C}_h^{-1} \right)^{-1} \mathbf{F}_p^H \mathbf{F}_p \right) \mathbf{h} - \mathbf{F}_L \left(\mathbf{F}_p^H \mathbf{F}_p + \sigma_{\mathbf{z}_p}^2 \mathbf{C}_h^{-1} \right)^{-1} \mathbf{F}_p^H \tilde{\mathbf{z}}_p \quad (2.36)$$

and the error covariance matrix:

$$\begin{aligned} \mathbf{C}_{\tilde{\mathbf{z}}_{\text{MMSE}}} = & \mathbf{F}_L \left(\mathbf{I}_L - \left(\mathbf{F}_p^H \mathbf{F}_p + \sigma_{\mathbf{z}_p}^2 \mathbf{C}_h^{-1} \right)^{-1} \mathbf{F}_p^H \mathbf{F}_p \right) \mathbf{C}_h \\ & \left(\mathbf{I}_L - \left(\mathbf{F}_p^H \mathbf{F}_p + \sigma_{\mathbf{z}_p}^2 \mathbf{C}_h^{-1} \right)^{-1} \mathbf{F}_p^H \mathbf{F}_p \right)^H \mathbf{F}_L^H + \\ & + \sigma_{\mathbf{z}_p}^2 \mathbf{F}_L \left(\mathbf{F}_p^H \mathbf{F}_p + \sigma_{\mathbf{z}_p}^2 \mathbf{C}_h^{-1} \right)^{-1} \mathbf{F}_p^H \mathbf{F}_p \left(\mathbf{F}_p^H \mathbf{F}_p + \sigma_{\mathbf{z}_p}^2 \mathbf{C}_h^{-1} \right)^{-1} \mathbf{F}_L^H \end{aligned} \quad (2.37)$$

Mismatched MMSE estimator

To avoid the estimation of the second order channel statistics \mathbf{C}_h and of the consequent on-line inversion of a $L \times L$ matrix required in the straightforward application of the MMSE of (A.27), the channel PDP can be assumed uniform [54]. Hence, in this *Mismatched*-MMSE formulation, \mathbf{C}_h is imposed to have the structure of an identity matrix.

With reference to the general formulation in (A.12), this scheme consists in taking the same \mathbf{B} and \mathbf{G} of (A.26) but defining $\mathbf{R} = \sigma_{\mathbf{z}_p}^2 / \sigma_{\mathbf{h}}^2 \cdot \mathbf{I}_L$ to give the expression

$$\hat{\mathbf{z}}_{\text{M-MMSE}} = \mathbf{F}_L \left(\mathbf{F}_p^H \mathbf{F}_p + \sigma_{\mathbf{z}_p}^2 / \sigma_{\mathbf{h}}^2 \cdot \mathbf{I}_L \right)^{-1} \mathbf{F}_p^H \hat{\mathbf{z}}_p \quad (2.38)$$

Interestingly, we notice that this estimator is in practice equivalent to *regularized* LS estimator in A.1.2. where the only difference lies in the fact that the ratio $\sigma_{\mathbf{z}_p}^2 / \sigma_{\mathbf{h}}^2$ can be estimated and therefore adapted.

For a given channel length L , to avoid the on-line inversion of the matrix $\left(\mathbf{F}_p^H \mathbf{F}_p + \sigma_{\mathbf{z}_p}^2 / \sigma_{\mathbf{h}}^2 \cdot \mathbf{I}_L \right)$, the practical approach would consist in dividing the SNR working range into sub-ranges and storing different versions of the matrix inverted off-line for each sub-range.

The mismatched MMSE formulation offers the advantage that filtering coefficients can be computed to be real numbers because the uniform PDP is symmetric. Indeed, real filtering coefficients can be used when the OFDM symbol is properly synchronized to span half CP on each side and then strongly reduce complexity. Moreover, since the channel length is small compared to the FFT size, the matrix A_{gen} can be considered to be *low-density* storing only significant coefficients reduce considerably the complexity.

LTE does not implement an exact uniform reference symbols pattern: in particular this is not the case around the d.c. where reference symbols are unevenly spaced. This implies that a larger number of coefficients need to be stored.

Exponential mismatched MMSE estimator

Realistic channel PDP are likely exponentially decaying rather than uniform as assumed by the *mismatched*-MMSE discussed above. We therefore propose an *exponential mismatched*-MMSE estimator that approximates \mathbf{C}_h by a diagonal matrix whose entries are decaying exponentially. This is done by using (A.26) and taking:

$$\mathbf{R} = \frac{\sigma_{\mathbf{z}_p}^2}{\sigma_h^2} \mathbf{C}_{L,\text{exp}}^{-1} \text{ and } \mathbf{C}_{L,\text{exp}} = \gamma \cdot \text{diag} \left(e^{-n \frac{\ln(2L)}{L}} \right) \quad (2.39)$$

with $0 \leq n \leq L - 1$ and $\gamma = 1 / \sum_{n=0}^{L-1} e^{-n \frac{\ln(2L)}{L}}$. Hence, it is represented by:

$$\hat{\mathbf{z}}_{\text{exp-MMSE}} = \mathbf{F}_L \left(\mathbf{F}_p^H \mathbf{F}_p + \frac{\sigma_{\mathbf{z}_p}^2}{\sigma_h^2} \mathbf{C}_{L,\text{exp}}^{-1} \right)^{-1} \mathbf{F}_p^H \hat{\mathbf{z}}_p \quad (2.40)$$

Again, the error and the error covariance matrix can be deduced from (A.13) and (A.14) by substituting \mathbf{B} , \mathbf{G} and \mathbf{R} with their corresponding expressions.

Compared to the uniform channel distribution assumption of *Mismatched*-MMSE, the estimator reveals to be less sensitive to the channel length mis-estimation due to the exponential decaying nature and thus less versions of the inverse of the matrix $\left(\mathbf{F}_p^H \mathbf{F}_p + \frac{\sigma_{\mathbf{z}_p}^2}{\sigma_h^2} \mathbf{C}_{L,\text{exp}}^{-1} \right)$ can be precomputed and stored.

Simplified MMSE estimator

As already mentioned, the direct implementation of the MMSE estimator in (A.27) requires the solution of two problems:

1. The estimation of the variance of the noise and channel second order statistics;
2. The on-line inversion of the large $L \times L$ matrix

$$\mathbf{S}_{\text{MMSE}} = \mathbf{F}_p^H \mathbf{F}_p + \sigma_{\mathbf{z}_p}^2 \mathbf{C}_h^{-1} \quad (2.41)$$

whenever the channel and noise statistics change.

Assuming the required estimations available, we propose here an original solution to overcome in particular the second problem. The idea behind our simplified MMSE estimator lies in separating the problem of the approximation of (A.33) into, first, considering a fixed initialization matrix \mathbf{S}_{init} , as detailed below, and then in enhancing the first approximation by inserting the contribution of a portion of the PDP corresponding to the strongest taps, denoted *captured taps* in the following, on the diagonal of the initialization matrix \mathbf{S}_{init} .

As for previous approximated methods, the dependency from the noise variance can be maintained by quantization of the SNR into sub-ranges and storing a limited set of \mathbf{S}_{init} values.

Let us define:

$$\mathbf{S}_{\text{init}} = \mathbf{F}_p^H \mathbf{F}_p + \sigma_{z_p}^2 \mathbf{C}_{\text{init}}^{-1} \quad (2.42)$$

where $\mathbf{C}_{\text{init}} = \beta \mathbf{I}_L$ and β is a constant carefully chosen to provide sufficiently good performance of the estimator.

The matrix \mathbf{S}_{MMSE} can be approximated by:

$$\mathbf{S}_{\text{SMMSE}} = \mathbf{S}_{\text{init}} + \mathbf{D} \Delta \mathbf{S} \mathbf{D}^H \quad (2.43)$$

where

1. \mathbf{D} is a $L \times M$ selector matrix called after the role it plays in the selection of the positions where the elements of the PDP profile (that correspond to the M captured taps) are going to be located on the diagonal of \mathbf{S}_{init} . The first column of the matrix \mathbf{D} contains one only in the position that corresponds to the index of the first captured tap and zeros everywhere else and the second column contains one only in the position that corresponds to the index of the second captured tap and zeros everywhere else and so on.
2. $\Delta \mathbf{S}$ is a diagonal matrix containing the inverse of the power of the captured taps after removing the effect of initialization, i.e. $\Delta \mathbf{S}_{m,m} = \sigma_{z_p}^2 (\mathbf{C}_{h_m}^{-1} - \beta^{-1})$ where \mathbf{h}_m is a vector contains the M captured taps.

Applying the *Matrix Inversion Lemma*, we can write:

$$\mathbf{S}_{\text{SMMSE}}^{-1} = \mathbf{S}_{\text{init}}^{-1} - \mathbf{S}_{\text{init}}^{-1} \mathbf{D} (\mathbf{D}^H \mathbf{S}_{\text{init}}^{-1} \mathbf{D} + \Delta \mathbf{S}^{-1})^{-1} \mathbf{D}^H \mathbf{S}_{\text{init}}^{-1} \quad (2.44)$$

It is worth mentioning that the number of significant taps in terms of power is usually much less than the overall length of the CIR. Thus, the importance of the proposed estimator stems from the fact that we take advantage of this property to reduce the size of the matrix to be inverted on-line from $L \times L$ to $M \times M$ with $M \ll L$. Knowing that the number of operations required to invert a matrix is proportional to the cube of its size, we infer that our estimator reduces significantly (from L^3 to M^3) the computational power compared to the traditional MMSE estimator in (A.27).

Another important aspect of the proposed estimator is that the accuracy of the approximation is traded-off with the complexity by controlling the number of captured taps. Therefore, the more the number of the captured taps the larger the size of the matrix to be inverted on-line and vice versa.

Finally the estimated CTF is given by:

$$\hat{\mathbf{z}}_{\text{SMMSE}} = \mathbf{F}_L \mathbf{S}_{\text{SMMSE}}^{-1} \hat{\mathbf{z}}_p \quad (2.45)$$

Comparing (A.37) with (A.12), the *Simplified* MMSE consists in choosing:

$$\mathbf{B} = \mathbf{F}_L, \mathbf{G} = \mathbf{F}_p \text{ and } \mathbf{R} = \sigma_{\hat{\mathbf{z}}_p}^2 \mathbf{C}_{\text{init}}^{-1} + \mathbf{D} \Delta \mathbf{S} \mathbf{D}^H \quad (2.46)$$

The estimation error and the error covariance matrix expression of the proposed estimator can then be obtained by substituting (A.38) in (A.13) and (A.14).

2.4.3 Simulation results

We compare the performances of the estimators by mean of *Truncated*-Normalized-Mean-Squared-Error (TNMSE). For each estimator $\hat{\mathbf{z}}$, the TNMSE is computed from its covariance matrix $\mathbf{C}_{\hat{\mathbf{z}}}$ and the true channel $\mathbf{H} = \mathbf{F}_L \mathbf{h}$ using the following:

$$\text{TNMSE}_{\hat{\mathbf{z}}} = \frac{\text{Ttr}(\mathbf{C}_{\hat{\mathbf{z}}})}{\text{Ttr}(\mathbf{F}_L \mathbf{C}_h \mathbf{F}_L^H)} \quad (2.47)$$

where with $\text{Ttr}\{\cdot\}$ we denote the truncated trace operator consisting of the *truncated* covariance matrix considering only the K used sub-carriers.

For the comparison in figure A.2, we used *raised-cosine* pulse-shaping filter with a roll-off factor of $\beta = 0.2$, the SCMA channel and an LTE setup with $N = 1024$ corresponding to the 10 MHz transmission bandwidth case [28]. As for the regularized LS estimator, we use the *regularization* term $\alpha = 0.1$. Connected lines represent the theoretical TNMSE while the dotted points represent the results of simulations. We can first conclude that the *IFFT* and linear interpolation methods yield the lowest performances.

Moreover the *regularized* LS and the *mismatched* MMSE prove to perform exactly equally and the TNMSE curve of the latter is therefore omitted in figure A.2. The *exponential mismatched*-MMSE and the *simplified* MMSE offer a performance gain over all other sub-optimal estimators but the latter proves to be the one approaching the most the MMSE estimator performance particularly in the low SNR region.

To highlight the robustness of our *simplified* MMSE, figure A.3 compares its performance to that of the *mismatched*-MMSE where the MMSE is used as a reference. It should be noted that the simulated *mismatched*-MMSE is further approximated by exploiting a limited number of pilots around the sub-carriers to be estimated in order to reduce complexity. It is evident that the performance of *simplified* MMSE exceeds for any SNR that of *mismatched*-MMSE even though only 11 out of 50 taps are captured.

It can be seen that the IFFT and linear interpolation methods yield the lowest performance. The regularized LS and the mismatched MMSE perform exactly equally and the curve of the latter is therefore omitted. As expected, the optimal MMSE estimator outperforms any other estimator.

The TNMSE computed over all sub-carriers actually hides the behavior of each estimator against a well-known problem of frequency-domain channel estimation techniques: the band-edge effect. This can be represented by the Gibbs [66] phenomenon in a finite-length Fourier series approximation; following this approach, Figure A.1 shows that MMSE-based channel estimation suffers the least band-edge degradation, while all the other methods presented are highly adversely affected.

Figure A.4 compares the performances of the *mismatched*-MMSE and of the *simplified* MMSE in terms of Bit Error Rate with 1/3 Turbo Coding with Block Length = 4992 bits with Maximum Ratio Combining receiver for QPSK modulation. The decoding performance with *simplified* MMSE channel estimation outperforms

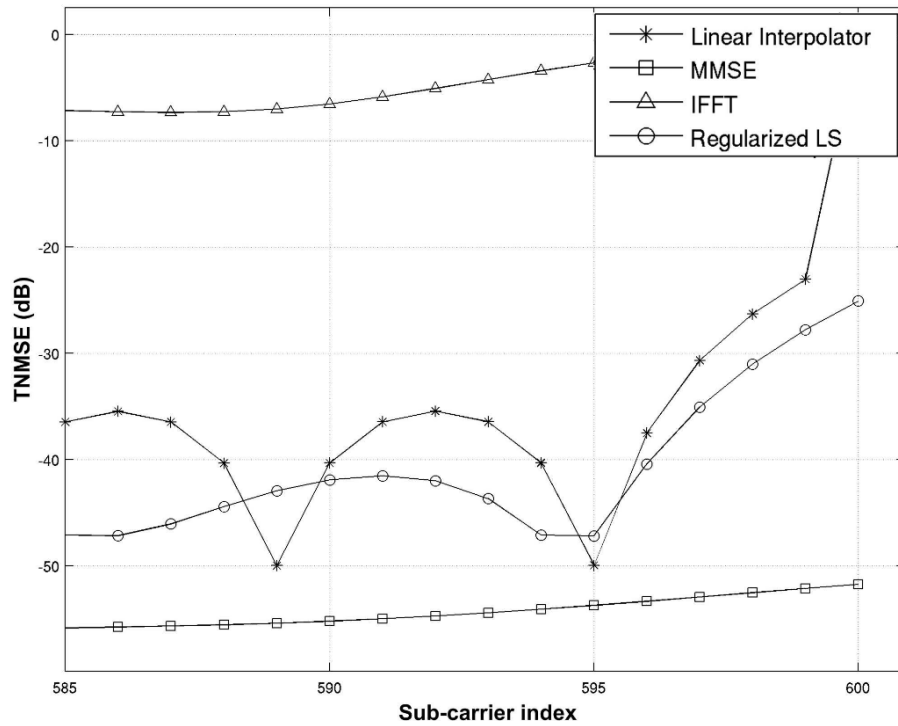


Figure 2.6: Frequency-domain channel estimation performance, band-edge behavior.

that of the *mismatched*-MMSE by 2 dB for BER lower than 10^{-2} .

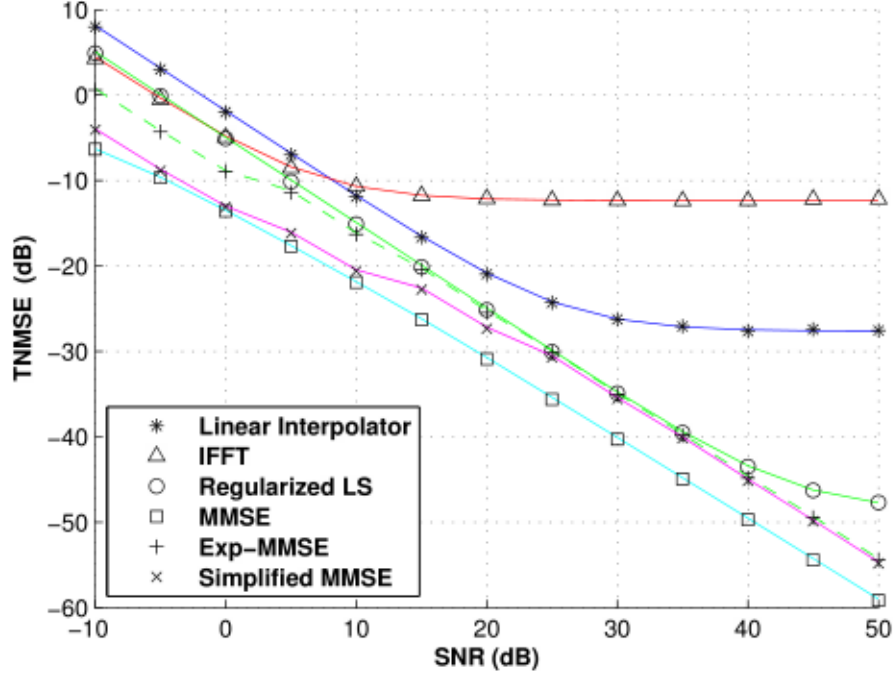


Figure 2.7: CTF TNMSE vs. SNR.

2.4.4 Iterative MMSE Channel Estimation

The MMSE channel estimator (A.27) consists of a linear filter performing jointly an interpolation and a smoothing operation on the ML estimate of the CTF at the pilot positions in order to reconstruct the whole CTF at any sub-carrier position by exploiting the frequency correlation.

The MMSE estimator expression of (A.27) can effectively be separated as the cascade of [64]:

1. a Frequency to Time domain transformation operation to convert the CTF ML estimates on the pilot positions into a raw Channel Impulse Response (CIR) estimate

$$\hat{\mathbf{h}} = \mathbf{F}_p^H \hat{\mathbf{z}}_p \quad (2.48)$$

2. an MMSE CIR estimation operation on the raw CIR estimate

$$\hat{\mathbf{h}}_{\text{MMSE}} = \left(\mathbf{F}_p^H \mathbf{F}_p + \sigma_{\mathbf{w}_p}^2 \mathbf{C}_h^{-1} \right)^{-1} \hat{\mathbf{h}} = \mathbf{U}_{\text{MMSE}}^{-1} \hat{\mathbf{h}} \quad (2.49)$$

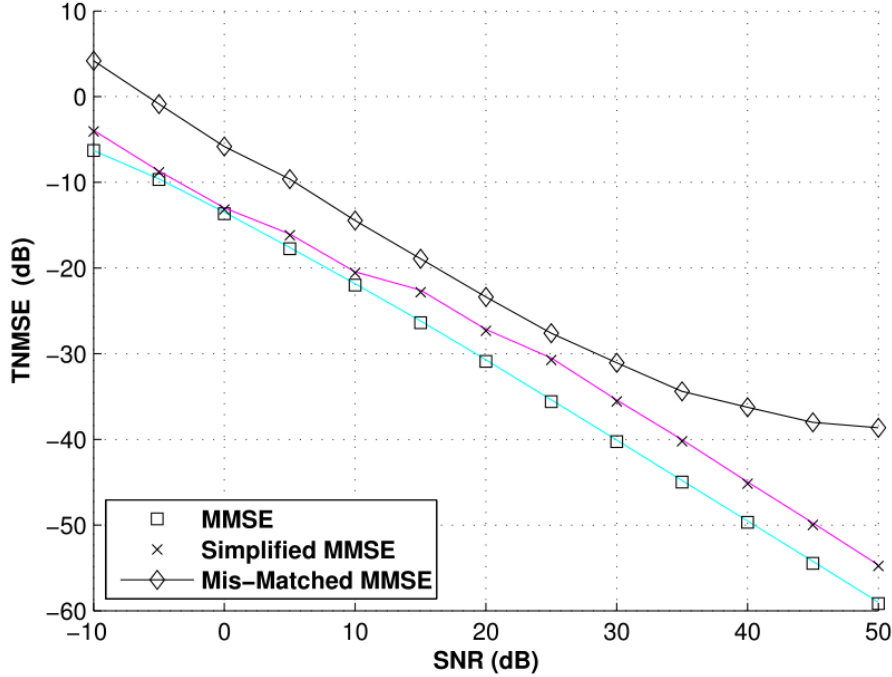


Figure 2.8: CTF TNMSE vs. SNR.

3. a Time to Frequency domain transformation to convert the MMSE CIR estimated vector into the MMSE CTF estimate

$$\hat{\mathbf{z}}_{\text{MMSE}} = \mathbf{F}_L \hat{\mathbf{h}}_{\text{MMSE}} \quad (2.50)$$

The direct application of the MMSE estimator in (2.49) requires on-line inversion of the large $L \times L$ matrix whenever the channel and noise statistics change.

Usual matrix inversion methods such as *Gaussian elimination* [63] entail a complexity proportional to the cube of the size of the matrix to be inverted and in many practical cases this reveals to be costly.

We provide here an iterative approach in order to exploit the structure of the matrix to be inverted and approach the true MMSE channel estimation with complexities proportional to L^2 .

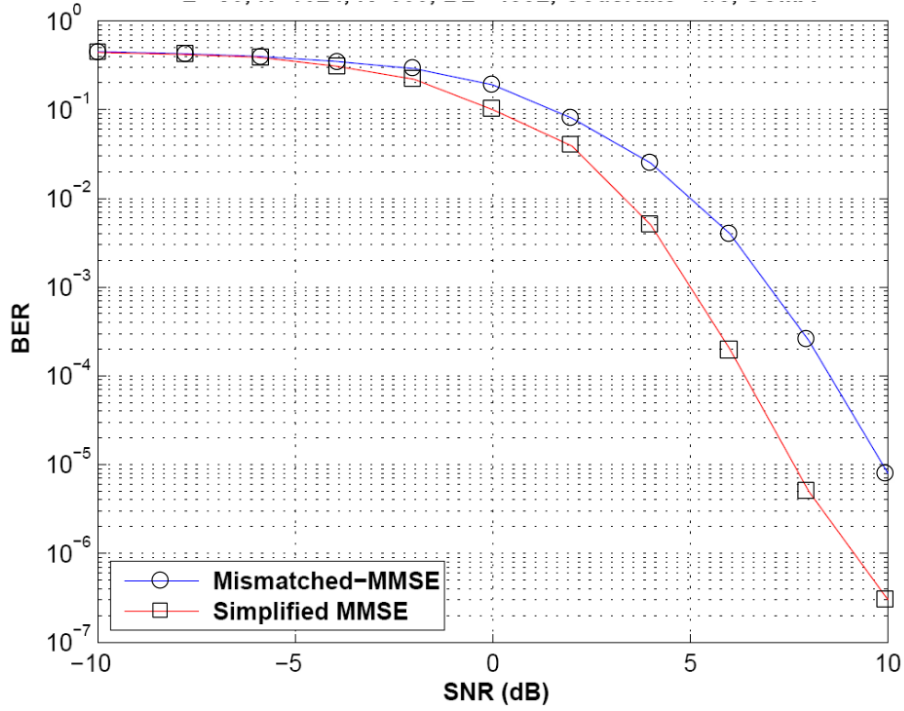


Figure 2.9: BER vs. SNR.

Gauss-Seidel MMSE Channel Estimation

In equation (2.49), note that the matrix inversion operation is not strictly needed as we are only interested in the solution of a system of linear equations. Therefore, we can re-formulate (2.49) to avoid the matrix inversion to directly solve

$$\left(\mathbf{F}_p^H \mathbf{F}_p + \sigma_{w_p}^2 \mathbf{C}_h^{-1}\right) \hat{\mathbf{h}}_{\text{MMSE}} = \mathbf{U}_{\text{MMSE}} \hat{\mathbf{h}}_{\text{MMSE}} = \hat{\mathbf{h}} \quad (2.51)$$

by means of appropriate low complexity techniques such as *successive iterations* algorithm, also known as Gauss-Seidel [63]. Indeed, the $L \times L$ matrix \mathbf{U}_{MMSE} of (2.51) can be decomposed into its strictly lower triangular \mathbf{T}_l , diagonal \mathbf{D} and strictly upper \mathbf{T}_u triangular parts such that $\mathbf{U}_{\text{MMSE}} = \mathbf{T}_l + \mathbf{D} + \mathbf{T}_u$, to give the following iterative process

$$\hat{\mathbf{h}}_{\text{MMSE}}^{(k)} = \mathbf{D}^{-1} \left(\hat{\mathbf{h}} - \mathbf{T}_l \hat{\mathbf{h}}_{\text{MMSE}}^{(k)} - \mathbf{T}_u \hat{\mathbf{h}}_{\text{MMSE}}^{(k-1)} \right) \quad (2.52)$$

where $\hat{\mathbf{h}}_{\text{MMSE}}^{(k)}$ is the MMSE estimate at k -th iteration. This has the advantage of maintaining the result of the iterative estimation process in one vector and it is therefore very well suited for implementation because of its low storage requirements.

The complexity of the algorithm is proportional to $N_{\text{it}}L^2$ where a number of iterations N_{it} is required for the convergence of the algorithm within some needed margins. Interestingly, the number of iterations can be maintained low by exploiting the coherence time of the channel. The iterations can in fact be initialized with the estimate resulting from the previous OFDM symbol containing pilots. Assuming classical Jakes Doppler model [50] for example, the time-correlation at relatively high mobile receiver speed such as 160 km/h allow for a number of iterations $N_{\text{it}} = 5$ to converge to approximately the same performance as MMSE, as shown in section 4.

In case the time correlation cannot be exploited, for example when the estimate from previous OFDM symbol might be out-of-date because of discontinuous reception or excessively high mobile speed, a boot-strap procedure with an increased number of iterations $N_{\text{it}}^{\text{init}} > N_{\text{it}}$ can eventually be employed.

Inspecting the structure of \mathbf{G}_{MMSE} in (2.51), the method requires the storage of one row of the Toeplitz Hermitian matrix $\mathbf{F}_p^H \mathbf{F}_p$ to retrieve all the elements of \mathbf{T}_1 and \mathbf{T}_u matrices. The only coefficients that need to be updated according to the channel and noise statistics are the elements of the diagonal matrix \mathbf{D} and, from (2.52), the coefficients are simply given by

$$(\mathbf{D})_{i,i} = (\mathbf{F}_p^H \mathbf{F}_p)_{i,i} + \sigma_{\mathbf{w}_p}^2 / (\mathbf{C}_h)_{i,i} = P + \gamma_i^{-1} \quad (2.53)$$

where $\gamma_i = \sigma_{h_i}^2 / \sigma_{\mathbf{w}_p}^2$ is the per-path Signal-to-Noise Ratio.

The *diagonal dominance* of the matrix \mathbf{G}_{MMSE} , i.e. $|(\mathbf{G}_{\text{MMSE}})_{i,i}| > \sum_{j \neq i} |(\mathbf{G}_{\text{MMSE}})_{j,i}|$, guarantees the convergence of general successive iterations schemes such as the Jacobi algorithm but it is a rather severe condition that is often not verified in real cases unless for very low SNR. In the case of Gauss-Seidel algorithm instead, the convergence is ensured [62] for any initialization vector if the matrix \mathbf{G}_{MMSE} is *positive definite*: this is easily verified in our case, being both $\mathbf{F}_p^H \mathbf{F}_p$ and $\sigma_{\mathbf{H}_p}^2 \mathbf{C}_h^{-1}$ Hermitian matrices and \mathbf{G}_{MMSE} invertible.

We evaluate the performance of the iterative method in (2.52) to solve (2.49). The iterative method is compared to MMSE channel estimation performed by classical matrix inversion and a robust *regularized* Least-Square (LS) channel estimator of complexity proportional to L^2 .

The performances are expressed in terms of Truncated-Normalized-Mean-Squared-Error (TNMSE) with respect to the true channel CTF $\mathbf{z} = \mathbf{F}_L \mathbf{h}$. The

TNMSE is computed using (2.50) to evaluate $\text{NMSE} = \mathbb{E}[\|\hat{\mathbf{z}}_{\text{MMSE}} - \mathbf{z}\|^2] / \mathbb{E}[\|\mathbf{z}\|^2]$ over Monte-Carlo simulations for OFDM system parameters of 3GPP LTE 10 MHz band-width case. We considered the Extended Typical Urban (ETU) channel PDP for a mobile speed of 160 km/h, a number of iterations $N_{\text{it}} = 5$.

Examining the figure 2.10, we can conclude the method overlaps the performance of the MMSE estimation and outperforms the *regularized* LS estimator of comparable complexity. It has to be noticed though that the complexity of the Gauss-Seidel MMSE estimator is not constant depending on the mobile speed. Even though its complexity cannot be lowered below an order of two of the channel length, it yet provides considerable computational power saving compared to MMSE implementation through direct matrix inversion with negligible loss.

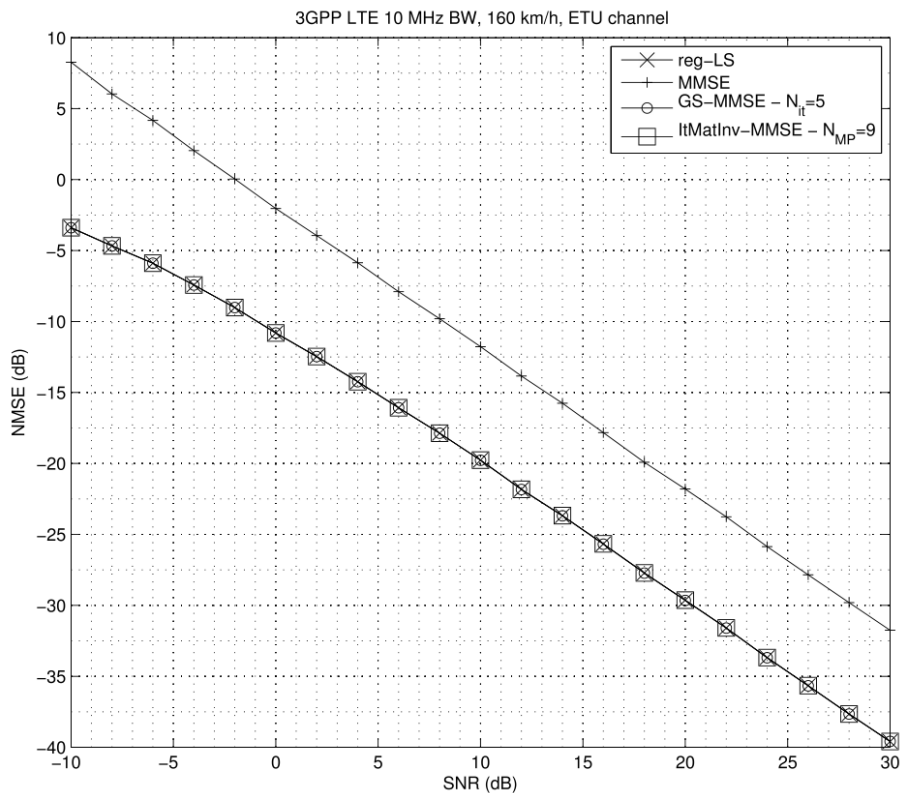


Figure 2.10: Performance of iterative MMSE channel estimation.

2.5 Time-Domain Channel Estimation

The main benefit of Time-Domain (TD) channel estimation is the possibility to enhance the channel estimation of one OFDM symbol containing RS by exploiting its time correlation with the channel at previous OFDM symbols containing RS.

This requires sufficient memory for buffering soft values of data over several OFDM symbols while the channel estimation is carried out.

However, the correlation between consecutive symbols decreases as the UE speed increases, as expressed by Equation (2.6). The fact that the TD correlation is inversely proportional to the UE speed sets a limit on the possibilities for TD filtering in high-mobility conditions.

TD filtering is applied to the CIR estimate, rather than to the CTF estimate in the frequency domain. The use of a number of parallel scalar filters equal to the channel length L does not imply a loss of optimality, because of the WSSUS assumption.

2.5.1 Finite and Infinite Length MMSE

The statistical TD filter which is optimal in terms of Mean Squared Error (MSE) can be approximated in the form of a finite impulse response filter [57]. The channel at the l^{th} tap position and at time instant n is estimated as

$$\hat{h}_{l,n} = \mathbf{w}_l^H \hat{\mathbf{h}}_{l,n}^M \quad (2.54)$$

where \hat{h}_l is the smoothed CIR l^{th} tap estimate which exploits the vector $\hat{\mathbf{h}}_{l,n}^M = [\hat{h}_{l,n}, \dots, \hat{h}_{l,n-M+1}]^T$ of length M of the channel tap h_l across estimates at M time instants.⁵ This is obtained by inverse Fourier transformation of, for example, any frequency-domain technique illustrated in previous section or even a raw estimate obtained by RS decorrelation.

⁵ $h_{l,k}$ is the l^{th} component of the channel vector \mathbf{h}_k at time instant k . $\hat{h}_{l,k}$ is its estimate. Note that for the frequency domain treatment the time index was dropped.

The $M \times 1$ vector of Finite Impulse Response (FIR) filter coefficients \mathbf{w}_l is given by

$$\mathbf{w}_l = (\mathbf{R}_h + \sigma_n^2 \mathbf{I})^{-1} \mathbf{r}_h \quad (2.55)$$

where $\mathbf{R}_h = \mathbf{E}[\mathbf{h}_l^M (\mathbf{h}_l^M)^H]$ is the l^{th} channel tap $M \times M$ correlation matrix, σ_n^2 the additive noise variance and $\mathbf{r}_h = \mathbf{E}[\mathbf{h}_l^M h_{l,n}^*]$ the $M \times 1$ correlation vector between the l^{th} tap of the current channel realization and M previous realizations including the current one.

In practical cases, the FIR filter length M is dimensioned according to a performance-complexity trade-off as a function of UE speed.

By setting M infinite, the upper bound on performance is obtained.

The MSE performance of the finite-length estimator of a channel of length L can be analytically computed as

$$\epsilon^{(M)} = 1 - \frac{1}{\sigma_h^2} \sum_{l=0}^{L-1} \mathbf{w}_l^H \mathbf{r}_h \quad (2.56)$$

The upper bound given by an infinite-length estimator is therefore given by

$$\epsilon^{(\infty)} = \lim_{M \rightarrow \infty} \epsilon^{(M)} \quad (2.57)$$

From Equation (2.55) it can be observed that, unlike Frequency-Domain (FD) MMSE filtering, the size of the matrix to be inverted for a finite-length TD-MMSE estimator is independent of the channel length L but dependent on the chosen FIR order M . Similarly to the FD counterpart, the TD-MMSE estimator requires knowledge of the PDP, the UE speed and the noise variance.

Figure 2.11 shows the performance of TD-MMSE channel estimation as a function of filter length M (Equation (2.56)) for a single-tap channel with a classical Doppler spectrum for low UE speed. The performance bounds derived for an infinite-length filter in each case are also indicated.

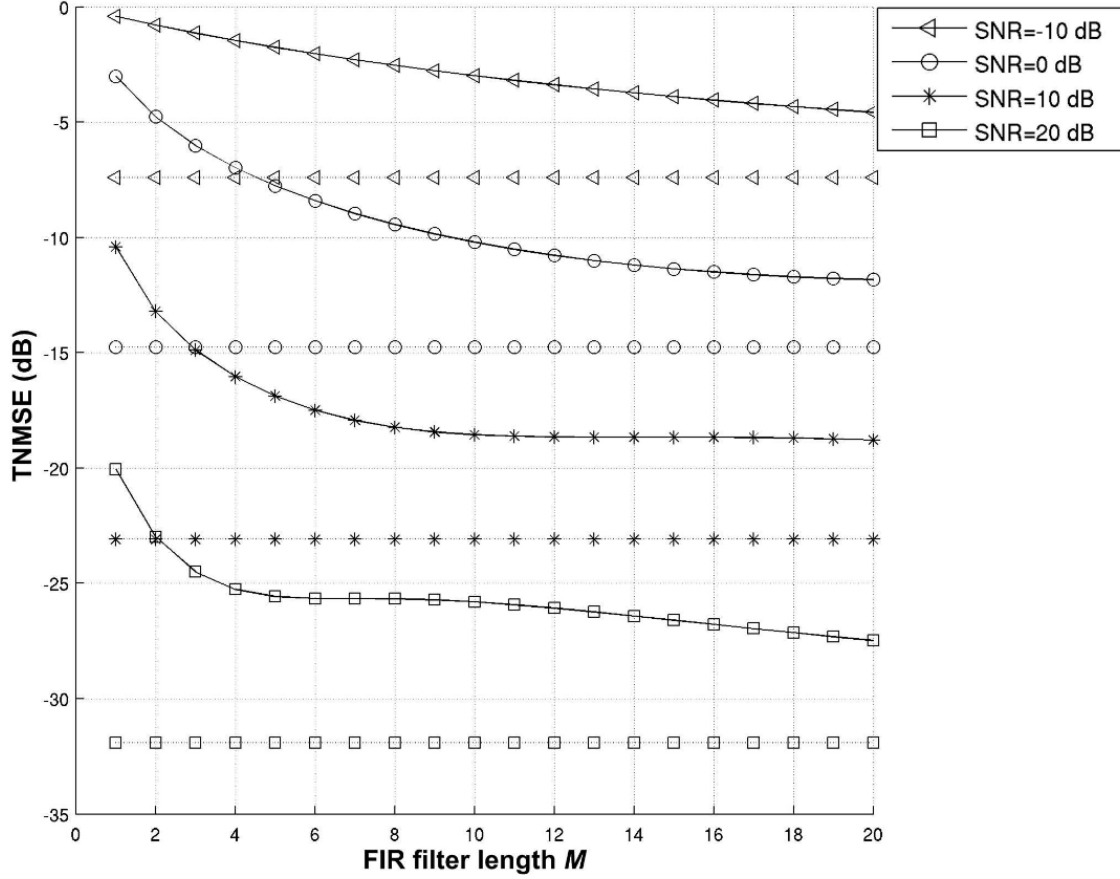


Figure 2.11: Time-domain channel estimation performance.

2.5.2 Normalized Least-Mean-Square

As an alternative to TD-MMSE channel estimation, an adaptive estimation approach can be considered which does not require knowledge of second-order statistics of both channel and noise. A feasible solution is the Normalized Least-Mean-Square (NLMS) estimator.

It can be expressed exactly as in Equation (2.54) but with the $M \times 1$ vector of filter coefficients \mathbf{w} updated according to

$$\mathbf{w}_{l,n} = \mathbf{w}_{l,n-1} + \mathbf{k}_{l,n-1}e_{l,n} \quad (2.58)$$

where M here denotes the NLMS filter order. The $M \times 1$ update gain vector is

computed according to the well-known NLMS adaptation:

$$\mathbf{k}_{l,n} = \frac{\mu}{\|\hat{\mathbf{h}}_{l,n}\|^2} \hat{\mathbf{h}}_{l,n}^M \quad (2.59)$$

where μ is an appropriately-chosen step adaptation, $\hat{\mathbf{h}}_{l,n}^M$ is defined as for Equation (2.54) and

$$e_{l,n} = \hat{h}_{l,n} - \hat{h}_{l,n-1} \quad (2.60)$$

It can be observed that the TD-NLMS estimator requires much lower complexity compared to TD-MMSE as no matrix inversion is required, as well as not requiring any a priori statistical knowledge.

2.5.3 Kalman filter

When the channel \mathbf{h}_k is modeled in a similar manner as previous paragraph, i.e. the channel evolution across time is expressed by the following state-space model

$$\begin{aligned} \mathbf{h}_k &= \lambda \mathbf{h}_{k-1} + \sqrt{1 - \lambda^2} w_k \\ \mathbf{h}'_k &= \mathbf{h}_k + \mathbf{n}_k \end{aligned} \quad (2.61)$$

where $w_k \sim \mathcal{CN}(0, \mathbf{Q})$ is known as the channel innovation term and $\mathbf{n}_k \sim \mathcal{CN}(0, \sigma^2 \mathbf{I}_N)$ is the additive white Gaussian noise on pilot (and data) symbols. It is to be noted that this 1st order auto-regressive model still complies with the statistical assumption on $\mathbf{h}_k \sim \mathcal{CN}(0, \mathbf{Q})$ made so far.

Under these assumptions, one can easily come up with the expression of a channel estimator according to the classical Kalman form [58]. In fact, letting \mathbf{P}_k a diagonal matrix with 1 on those lines where pilots are present and 0 otherwise, this can be written as

$$\begin{cases} \mathbf{M}_k &= \mathbf{F}_L \left(\lambda^2 \mathbf{C}_{k-1} + \frac{1-\lambda^2}{L} \mathbf{I}_L \right) \mathbf{F}_p^H \\ &\times \left(\mathbf{F}_p \left(\lambda^2 \mathbf{C}_{k-1} + \frac{1-\lambda^2}{L} \mathbf{I}_L \right) \mathbf{F}_p^H + \sigma^2 \mathbf{I}_N \right)^{-1} \\ \mathbf{k}_k &= \lambda \mathbf{k}_{k-1} + \mathbf{M}_k \mathbf{P}_k (\mathbf{h}'_k - \lambda \mathbf{k}_{k-1}) \\ \mathbf{C}_k &= (\mathbf{I}_L - \mathbf{M}_k \mathbf{F}_p) \left(\lambda^2 \mathbf{C}_{k-1} + \frac{1-\lambda^2}{L} \mathbf{I}_L \right) \end{cases} \quad (2.62)$$

Notice importantly that the estimation process assumes the knowledge of noise statistics σ^2 and the channel length L . In case the latter is not provided, it would be

necessary to assume L as the largest channel length allowed by the OFDM system parameters in use. Therefore in practice, one should dimension it as $L = \lfloor N/M \rfloor$ [53] in case of imperfect knowledge. In spite of these limitations, the Kalman estimator is often chosen because of the well know robustness against non-stationarity of the signal statistics via the adaptation of the estimate covariance matrix. In order to counter the intrinsic need of parameter knowledge, one could think of using Expectation Maximization in conjunction with Kalman or plain MMSE techniques. Indeed, with an additional complexity cost, any of such channel estimator can be coupled with parameter estimation (speed or channel length) in an iterative fashion. Note that other classical adaptive estimators such as (normalized) least mean squares and recursive least squares, that discard most *a priori* knowledge, perform much less accurately than optimal 2-D MMSE optimal filter [57].

Chapter 3

Detection techniques in selective channels

3.1 OFDM Detection in Rapidly Varying Channels

3.1.1 Introduction

OFDM allows for flexible bandwidth allocation and low-complexity transmitter and receiver architectures. However the performance of classical OFDM low complexity receivers is severely impacted in the presence of time-varying propagation channels by the rising inter-carrier interference (ICI).

Those circumstances occur in the presence of high Doppler spread relative to the OFDM symbol rate due to the mobile receiver velocity. The resulting fast time-varying propagation channel yields to significant ICI. In practice the increased ICI prevents classical OFDM receiver schemes from reliably detecting the desired signal. Hence more advanced receiver equalization techniques are required to mitigate the effect of the ICI.

Optimal linear ICI equalization techniques generally involve complex full chan-

nel matrix inversion. In existing OFDM telecommunication systems, the typical size of the required Discrete Fourier Transform render such a full channel matrix inversion operation prohibitively complex for practical implementation. Hence several approaches have been addressed to reduce the complexity while maintaining acceptable performance. To this end, the use of time-domain windowing of the OFDM received signal has been shown to limit the significant span of the ICI, generating *banded* channel transfer matrices. In addition, iterative equalization and detection techniques have been proposed to further reduce the complexity of the receiver operating in the frequency-domain, see e.g. [65], [67] and references therein, or in the time-domain as in [68], [69].

We introduce a general framework for iterative ICI cancellation. Our analysis of the detection performance, the convergence speed, and the complexity provide guidelines to derive novel fast-converging iterative ICI cancellation algorithms in both time and frequency domains. We show that proper *preconditioning* exploiting the inherent structure of the OFDM signal and the ICI yields to nearly optimal detection performance with very fast-converging and reduced complexity iterative algorithms. Moreover, we interpret windowing techniques under a more general perspective in relation to the Basis Expansion Modeling (BEM) of the time-varying channel [77]. In section A.2.2, we introduce the signal model of the considered OFDM system model including the time-varying channel BEM. Then, we recall known linear equalization techniques and we derive iterative approaches to ICI cancellation in section A.2.4 and A.2.5 respectively. The performance and the complexity of the presented techniques are discussed in section A.2.6 with the support of numerical results.

3.1.2 Signal and System Model

We consider the transmission over a time-varying, frequency-selective fading channel with continuous-time impulse response $h(t, \tau) = \sum_m \alpha_m(t) \psi(\tau - \tau_m)$ assumed to obey the wide sense stationary uncorrelated scattering (WSSUS) model 2.3.1, where $\psi(\tau)$ represents the equivalent transmit-receiver front-end low-pass filter, τ_m represents the p -th path delay, $\alpha_m(t)$ is the time-varying complex channel coefficient associated with the m -th path of the propagation channel respectively. We shall refer to $h[k, l]$ as the corresponding low-pass sampled discrete-time impulse response, and assume $h[k, l]$ to be well-approximated by a finite-impulse response model with a maximum delay spread of L samples. Then we assume a classical OFDM system with cyclic-prefix of duration $N_{cp} \geq L$ to avoid inter-symbol-

interference. By letting N denote the number of sub-carriers the OFDM symbol duration is given by $N_{\text{block}} = N + N_{\text{cp}}$. The frequency-domain k -th OFDM transmit symbol $\mathbf{s}[k] = [s[kN] \dots s[kN - N + 1]]^T$, where $(\cdot)^T$ denotes transpose, comprising the encoded symbols $s[i]$ at the output of channel encoding, interleaving and mapping onto a finite-symbol constellation \mathcal{S} assumed i.i.d. with unit energy, is modulated by an $N \times N$ discrete-Fourier transform unitary matrix \mathbf{F} so as to obtain

$$\mathbf{x}[k] = \mathbf{F}^H \mathbf{s}[k] \quad (3.1)$$

where $(\cdot)^H$ denotes Hermitian transpose. Without accounting for the cyclic-prefix, the n -th received symbol can be written as

$$\mathbf{r}[k] = \mathbf{H}[k] \mathbf{x}[k] + \mathbf{z}[k] \quad (3.2)$$

where $\mathbf{r}[k] = [r[kN] \dots r[kN - N + 1]]^T$, $\mathbf{H}[k]$ represents the $N \times N$ time domain channel convolution matrix, and $\mathbf{z}[k] = [z[kN] \dots z[kN - N + 1]]^T$ represents a circularly symmetric complex additive white Gaussian noise such that $\mathbf{z}[k] \sim \mathcal{N}_C(\mathbf{0}, \sigma_z^2 \mathbf{I})$.

For the sake of the notational simplicity and without loss of generality, we shall drop the time index k in the sequel. Thus equation (A.41) can be rewritten as follows

$$\mathbf{r} = \mathbf{H} \mathbf{F}^H \mathbf{s} + \mathbf{z} \quad (3.3)$$

Since in general $L \ll N$ the channel matrix \mathbf{H} will tend to be *sparse* and *banded*. When the channel is time invariant within an OFDM symbol, \mathbf{H} is circulant and therefore the frequency-domain channel matrix, $\mathbf{F} \mathbf{H} \mathbf{F}^H$, is diagonal.

This characteristic is widely exploited to perform one-tap frequency-domain equalization.

In case of time-varying channel though, \mathbf{H} is no longer circulant and results in a full frequency-domain channel matrix. Thus the classical OFDM equalization approach is highly sub-optimal and more complex equalization is required (see [65], [67] and references therein).

3.1.3 Channel BEM Representation

The channel convolution matrix can be reformulated as

$$\mathbf{H} = \sum_{l=0}^{L-1} \mathbf{Q}_l \text{diag} \{ \mathbf{h}_l \} \quad (3.4)$$

where $\mathbf{h}_l = \mathbf{h}[k, l] = [h[kN, l] \dots h[kN - N + 1, l]]^\top$ comprises the l -th channel tap time-varying values and \mathbf{Q}_l denotes the corresponding $N \times N$ circulant delay matrix with ones in the l -th lower diagonal and zeros elsewhere, i.e. with elements $[\mathbf{Q}_l]_{ij} = 1$ if $j = (i - l)_{\text{mod } N}$ and zero otherwise. The vector corresponding to the time-varying evolution of the l -th channel tap can be expressed according to the BEM as follows

$$\mathbf{h}_l = \mathbf{B} \mathbf{v}_l = \sum_{p=0}^{P-1} v_{l,p} \mathbf{b}_p \quad (3.5)$$

where the $N \times P$ matrix $\mathbf{B} = [\mathbf{b}_0 \mathbf{b}_1 \dots \mathbf{b}_{P-1}]$ denotes the deterministic basis spanned by the P complex vectors \mathbf{b}_p for $p = 0, \dots, P - 1$, and $\mathbf{v}_l = [v_{l,0} \dots v_{l,P-1}]^\top$ the stochastic coefficients describing the l -th channel tap behavior for the given OFDM block on the P basis functions.

Then, by plugging (A.43) in (A.44)

$$\begin{aligned} \mathbf{H} &= \sum_{l=0}^{L-1} \left(\sum_{p=0}^{P-1} v_{l,p} \text{diag} \{ \mathbf{b}_p \} \right) \mathbf{Q}_l \\ &= \sum_{p=0}^{P-1} \text{diag} \{ \mathbf{b}_p \} \sum_{l=0}^{L-1} v_{l,p} \mathbf{Q}_l \end{aligned} \quad (3.6)$$

By defining

$$\mathbf{B}_p = \text{diag} \{ \mathbf{b}_p \}$$

and summing over the L channel taps, it results

$$\mathbf{H} = \sum_{p=0}^{P-1} \mathbf{B}_p \mathbf{F}^H \mathbf{D}_p \mathbf{F} \quad (3.7)$$

Then the received signal \mathbf{r} of (A.42) can be expressed according to the channel BEM as

$$\mathbf{r} = \sum_{p=0}^{P-1} \mathbf{B}_p \mathbf{F}^H \mathbf{D}_p \mathbf{s} + \mathbf{z} \quad (3.8)$$

$\sum_{l=0}^{L-1} v_{l,p} \mathbf{Q}_l$ being a circulant matrix then

$$\mathbf{D}_p = \mathbf{F} \sum_{l=0}^{L-1} v_{l,p} \mathbf{Q}_l \mathbf{F}^H$$

is a diagonal matrix.

Figure A.5 depicts the model of the OFDM received signal in the channel BEM representation.

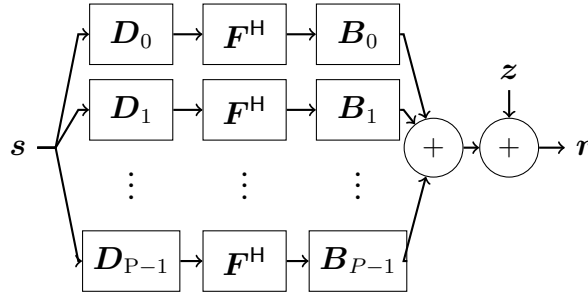


Figure 3.1: BEM representation of OFDM received signal

3.1.4 Linear Equalization

In this section we briefly recall (Linear) Minimum-Mean-Square-Error (L-MMSE), Zero Forcing (ZF), and Matched Filter (MF) equalization.

Letting $\mathcal{H} = \mathbf{H}\mathbf{F}^H$, we have for the estimated OFDM transmitted sequence

$$\hat{\mathbf{s}}_{\text{MMSE}} = (\mathcal{H}^H \mathcal{H} + \sigma_z^2 \mathbf{I})^{-1} \mathcal{H}^H \mathbf{r} \quad (3.9)$$

$$\hat{\mathbf{s}}_{\text{ZF}} = (\mathcal{H}^H \mathcal{H})^{-1} \mathcal{H}^H \mathbf{r} \quad (3.10)$$

$$\hat{\mathbf{s}}_{\text{MF}} = \mathcal{H} \mathbf{r} \quad (3.11)$$

with the MMSE, ZF, and MF linear equalization respectively.

In the assumption of *perfect* knowledge of the channel and of its second order statistics, the MMSE and ZF estimates (A.48) and (A.49) entail the inversion of a full matrix in general requiring $\mathcal{O}(N^3)$ complexity order when classical techniques

are used, e.g. the *Gauss-Jordan elimination* method [76]. In both cases iterative techniques can be adopted to avoid a full matrix inversion thus reducing the receiver equalization complexity as detailed in the following.

3.1.5 Iterative ICI Cancellation

A wide range of iterative techniques have been proposed in the literature to solve linear systems of equation, see e.g. [71].

For a given technique the overall complexity depends on the number of operations per iteration stage times the number of iterations necessary to achieve the estimation accuracy required for the target sequence detection performance. In view of these considerations the speed of convergence is a primary aspect driving the design of an iterative equalization algorithm.

Considering a generic linear system of equations of the form

$$\mathbf{A}\mathbf{x} = \mathbf{b} \quad (3.12)$$

where the vector \mathbf{x} is the sequence to be estimated, \mathbf{b} is the observation vector, and the matrix \mathbf{A} is the input-output transfer matrix, which we assume to be full-rank with dimension $N \times N$ in the scope of our treatment, then for any iterative estimation method, the convergence of the sequence estimates $\hat{\mathbf{x}}^{(k)} \rightarrow \mathbf{x}$ is governed by the spectral properties of the matrix \mathbf{A} . A commonly used metric for those spectral properties is the *condition-number* (CN) $\kappa(\mathbf{A})$, defined as the ratio between the largest and smallest eigen-values of \mathbf{A} , $\kappa(\mathbf{A}) = |\lambda_{\max}(\mathbf{A})/\lambda_{\min}(\mathbf{A})|$ [71]. The closer $\kappa(\mathbf{A})$ is to 1, the faster a given iterative algorithm will converge.

In particular, the equalization problems (A.48) and (A.49) can be expressed in the form of (A.51)

$$(\mathcal{H}^H\mathcal{H} + \sigma_z^2\mathbf{I}) \hat{\mathbf{s}}_{\text{MMSE}} = \mathcal{H}^H\mathbf{r} \quad (3.13)$$

$$\mathcal{H}^H\mathcal{H} \hat{\mathbf{s}}_{\text{ZF}} = \mathcal{H}^H\mathbf{r} \quad (3.14)$$

In light of the above, the convergence of an iterative approach to the solution of both problems will depend on $\kappa(\mathcal{H}^H\mathcal{H}) = \kappa(\mathcal{H})^2$ in the high SNR ($\sigma_z^2 \rightarrow 0$) regimes.

In the case of the OFDM system under analysis the matrix \mathcal{H} is in general full-rank. Then the ZF problem (A.53) can be equivalently expressed as follows

$$\mathcal{H}s_{\text{ZF}} = \mathbf{r} \quad (3.15)$$

whose CN is $\kappa(\mathcal{H})$, and since $\kappa(\mathcal{H}) \leq \kappa(\mathcal{H}^H\mathcal{H})$, an iterative algorithm applied to (A.54) will generally converge faster than if applied (A.52) and (A.53).

We observe that the equalization problem in (A.54) is characterized by the inherent channel matrix properties associated with the OFDM transmission. Conversely, the MMSE and ZF equalization problems of (A.52) and (A.53) are *over-conditioned* in the squared channel matrix domain. In the steady state (number of iterations going to infinity assuming convergence) the ZF solution is generally yield to worse performance than the MMSE solution in terms of detection performance. However when the ZF and MMSE problems are solved by iterative techniques, one should consider the actual detection performance (or estimation accuracy) for a finite, limited number of iterations.

Iterative techniques can greatly take advantage from appropriate *preconditioning* to reduce the CN and to allow faster convergence. The iterative methods is then applied an equivalent *preconditioned* linear system derived from (A.51) into

$$\mathbf{P}\mathbf{A}\mathbf{x} = \mathbf{P}\mathbf{b} \quad (3.16)$$

with \mathbf{P} being the preconditioning matrix and such that $\kappa(\mathbf{A}) \geq \kappa(\mathbf{P}\mathbf{A}) \geq 1$ with $\mathbf{P}\mathbf{A} = \mathbf{I}$ if $\mathbf{P}^{-1} = \mathbf{A}$.

Many preconditioning techniques exist [71]. Among those, a simple, straightforward method is the *Jacobi* preconditioning where \mathbf{P} is chosen to be diagonal and such that $\text{diag}\{\mathbf{P}^{-1}\} = \text{diag}\{\mathbf{A}\}$ if $[\mathbf{A}]_{ii} \neq 0$ for $i = 1, \dots, N$. The *Jacobi* preconditioning suggests that the preconditioning operation consists in approximately solving the problem of inverting matrix \mathbf{A} and transform the original problem into a better conditioned one.

Preconditioned Iterative ZF Equalization

In light of the above, in [68] a relevant approach to the ZF iterative ICI cancellation problem is proposed. Even though the referenced work does not mention

it, the described method consists of a *diagonally pre-conditioned* ZF iterative algorithm. The pre-conditioner is made of a diagonal matrix whose elements are exactly the diagonal matrix of the inverse of the frequency-domain channel matrix $\text{diag}\{\mathbf{P}\} = \text{diag}\left\{(\mathbf{F}\mathbf{H}\mathbf{F}^H)^{-1}\right\}$. Figure A.6 depicts the block diagram of this receiver. Notice that the stage \mathcal{H} is realized using channel BEM as of equation (A.46) and a *polynomial*-basis functions. Interestingly, the complexity of this approach is linear to the OFDM block size N . The performance of the ZF diagonal

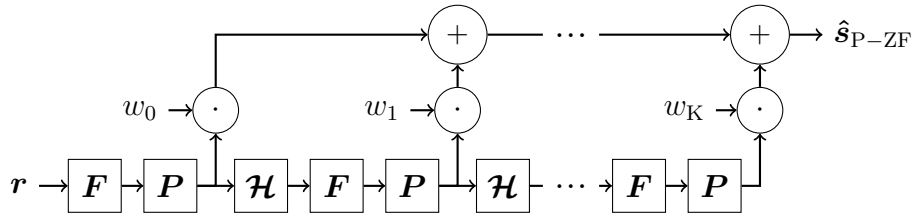


Figure 3.2: Preconditioned iterative ZF receiver

pre-conditioned iterative ICI cancellation method [68] can be improved in several respects. First the diagonal pre-conditioning although low-complexity yields to an increased CN with respect to $\kappa(\mathcal{H})$. Secondly it is inherently sub-optimal with respect to the MMSE since attempting to approximate the global ZF solution.

In the following, we address faster converging iterative ICI techniques approaching the MMSE optimal detection performance for a comparable complexity.

BEM-MMSE Preconditioned Iterative ICI Cancellation

In this section, we approximate the global MMSE optimal solution iterative techniques combining different forms of *local* MMSE pre-conditioning and combining based on BEM structure. As for the method presented in section A.2.5, the channel BEM allows us to derive here expressions for an improved pre-conditioner yet with affordable complexity.

Indeed, the channel BEM can be exploited at the receiver side and interpreted as a *multiple* windowing of the received signal where the windowing functions correspond to the conjugate of the basis \mathbf{B}_p . Let the output of each *windowing*-branch vector be defined as the projection of the received signal onto the p -th basis function

$$\mathbf{y}_p = \mathbf{F}\mathbf{B}_p^H \mathbf{r} \quad (3.17)$$

, then the *expanded* observation vector of the received signal is obtained by stacking each windowing-branch vector in a $PN \times 1$ vector as

$$\mathbf{y} = \begin{bmatrix} \mathbf{y}_0 \\ \mathbf{y}_1 \\ \vdots \\ \mathbf{y}_{P-1} \end{bmatrix} = \begin{bmatrix} \mathbf{F}\mathbf{B}_0^H \\ \mathbf{F}\mathbf{B}_1^H \\ \vdots \\ \mathbf{F}\mathbf{B}_{P-1}^H \end{bmatrix} \mathbf{r} = \mathbf{U}\mathbf{r} \quad (3.18)$$

Given the BEM representation of equation (A.46), we estimate the symbol $s[n]$ at sub-carrier n by adopting *local* MMSE Finite-Impulse-Response (FIR) filter \mathbf{f}_n across tones for all the basis output. Exploiting the particular structure of ICI in the channel BEM representation, one can limit the complexity of a full *per-tone* equalization across all sub-carriers, by properly selecting a subset of the elements of vector \mathbf{y} as $\bar{\mathbf{y}}_n = \mathbf{S}_n\mathbf{y}$ with \mathbf{S}_n being a $L_{\text{FIR}} \times PN$ *selection* matrix obtained by extracting L_{FIR} rows of the identity matrix \mathbf{I}_{PN} optimally exploiting the structure of \mathbf{U} for a given L_{FIR} and sub-carrier n to have

$$\hat{s}[n] = \mathbf{f}_n^T \bar{\mathbf{y}}_n \quad (3.19)$$

Therefore, the *per-tone* MMSE filter coefficients are computed such that

$$\mathbf{f}_n^T = \text{E} \{s[n] \bar{\mathbf{y}}_n^H\} \mathbf{R}_{\bar{\mathbf{y}}_n \bar{\mathbf{y}}_n}^{-1} \quad (3.20)$$

where $\mathbf{R}_{\bar{\mathbf{y}}_n \bar{\mathbf{y}}_n} = \text{E} \{\bar{\mathbf{y}}_n \bar{\mathbf{y}}_n^H\}$ which gives

$$\mathbf{f}_n^T = \mathbf{1}_n \mathcal{H}^H \mathbf{U}^H \mathbf{S}_n^T [\mathbf{S}_n \mathbf{U} (\mathcal{H} \mathcal{H}^H + \sigma_z^2 \mathbf{I}) \mathbf{U}^H \mathbf{S}_n^T]^{-1} \quad (3.21)$$

with $\mathbf{1}_n$ being the $1 \times N$ vector containing 1 in n -th position and 0 elsewhere. It is noteworthy mentioning that the above expression stems from the multiplication of a $1 \times L_{\text{FIR}}$ vector $\text{E} \{s(n) \bar{\mathbf{y}}_n^H\}$ and $L_{\text{FIR}} \times L_{\text{FIR}}$ inverse matrix of $\mathbf{R}_{\bar{\mathbf{y}}_n \bar{\mathbf{y}}_n}$ which varies across sub-carriers.

Nevertheless, the latter can be computed requiring only $(2L - 1) L_{\text{FIR}}^2$ multiplications due to the banded nature of $\mathcal{H} \mathcal{H}^H + \sigma_z^2 \mathbf{I}$ and the L_{FIR} non-zero elements of $\mathbf{S}_n \mathbf{U}$.

Moreover, the computation of the MMSE filtering coefficients can exploit the coherence across sub-carriers and be made by applying a recursive method.

A sufficiently precise approximation of the inverse of the matrix $\mathbf{R}_{\bar{\mathbf{y}}_n \bar{\mathbf{y}}_n}$, i.e. $\|\mathbf{I}_{\text{L}_{\text{FIR}}} - \widehat{\mathbf{R}}_{\bar{\mathbf{y}}_n \bar{\mathbf{y}}_n}^{-1} \mathbf{R}_{\bar{\mathbf{y}}_n \bar{\mathbf{y}}_n}\| \leq \epsilon$ with ϵ as small as desired, can be computed using the approximation of the inverse on sub-carrier $n - 1$ as initialization and applying the following iterative formula:

$$\begin{cases} \widehat{\mathbf{R}}_{\bar{\mathbf{y}}_n \bar{\mathbf{y}}_n}^{-1(0)} = \widehat{\mathbf{R}}_{\bar{\mathbf{y}}_{n-1} \bar{\mathbf{y}}_{n-1}}^{-1} \\ \widehat{\mathbf{R}}_{\bar{\mathbf{y}}_n \bar{\mathbf{y}}_n}^{-1(i)} = 2\widehat{\mathbf{R}}_{\bar{\mathbf{y}}_n \bar{\mathbf{y}}_n}^{-1(i-1)} - \widehat{\mathbf{R}}_{\bar{\mathbf{y}}_n \bar{\mathbf{y}}_n}^{-1(i-1)} \mathbf{R}_{\bar{\mathbf{y}}_n \bar{\mathbf{y}}_n} \widehat{\mathbf{R}}_{\bar{\mathbf{y}}_n \bar{\mathbf{y}}_n}^{-1(i-1)} \end{cases} \quad (3.22)$$

to be used in (A.73) to compute the filtering coefficients.

All the filters coefficients can be stacked in a *sparse* filter matrix

$$\mathbf{G} = \begin{bmatrix} \mathbf{f}_0^\top \mathbf{S}_0 \\ \mathbf{f}_1^\top \mathbf{S}_1 \\ \vdots \\ \mathbf{f}_{N-1}^\top \mathbf{S}_{N-1} \end{bmatrix} \quad (3.23)$$

The matrix resulting from the product of $\mathbf{G}\mathbf{U}$ can therefore be seen a *improved* BEM-MMSE pre-conditioner of \mathcal{H} . Moreover, the complexity associated to the filtering operation is proportional to $P(N + N \log_2 N)$.

Indeed, this approach achieves considerably better preconditioning than the one previously presented relying on *diagonal* preconditioning. Its effectiveness is shown in Figure A.7 where the Cumulative-Distribution-Function (CDF) of the CN for BEM-MMSE preconditioning is compared to both the diagonal preconditioning explained above and to the channel without preconditioning.

This novel approach can be directly plugged into the method described in section A.2.5 to give the *stationary* polynomial iterative receiver depicted in figure A.8 whose performance are considerably improved, as shown in the simulation results of section A.2.6, but yet of affordable complexity as the original method.

Non-stationary BEM-MMSE-Preconditioned Iterative ICI Cancellation

The same scheme scheme can be iteratively applied in the time domain to improve the ICI cancellation performance according to the scheme in figure A.9.

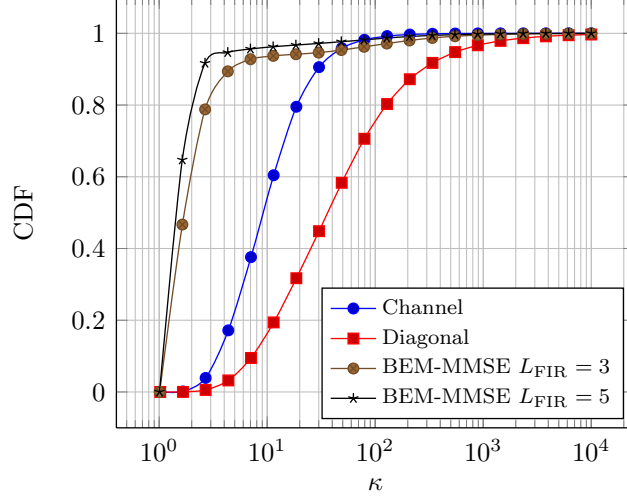


Figure 3.3: Condition number for diagonal and BEM-MMSE preconditioning

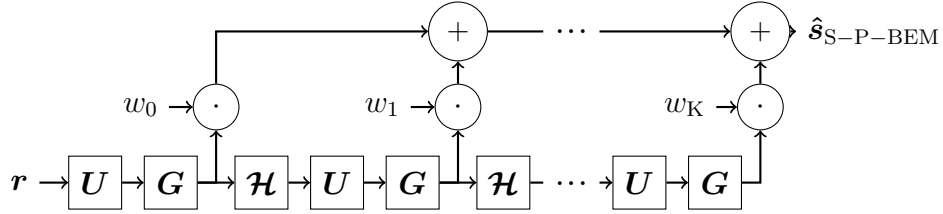


Figure 3.4: Stationary polynomial BEM-MMSE preconditioned iterative receiver

In this case the MMSE filter matrix \mathbf{G} is optimized at each stage.

Taking the first iteration resulting signal:

$$\mathbf{y}_1 = \mathbf{U} (\mathbf{r} - \mathcal{H} \hat{\mathbf{s}}_0) \quad (3.24)$$

and $\hat{\mathbf{s}}_0$ computed as in (20), we then get

$$\begin{aligned} \mathbf{y}_1 &= \mathbf{U} (\mathbf{r} - \mathcal{H} \mathbf{G}_0 \mathbf{y}_0) \\ &= (\mathbf{I} - \mathbf{U} \mathcal{H} \mathbf{G}_0) \mathbf{U} \mathbf{r} \end{aligned} \quad (3.25)$$

and, by setting $\mathbf{U}_1 = (\mathbf{I} - \mathbf{U} \mathcal{H} \mathbf{G}_0) \mathbf{U}$, we can re-use expression (18) to find the *per-tone* MMSE coefficients of first iteration. It is easy to verify that at second iteration we would have

$$\begin{aligned} \mathbf{U}_2 &= (\mathbf{I} - \mathbf{U} \mathcal{H} \mathbf{G}_1 + \mathbf{U} \mathcal{H} \mathbf{G}_1 \mathbf{U} \mathcal{H} \mathbf{G}_0) \mathbf{U} \\ &= [\mathbf{I} - \mathbf{U} \mathcal{H} \mathbf{G}_1 (\mathbf{I} - \mathbf{U} \mathcal{H} \mathbf{G}_0)] \mathbf{U} \end{aligned} \quad (3.26)$$

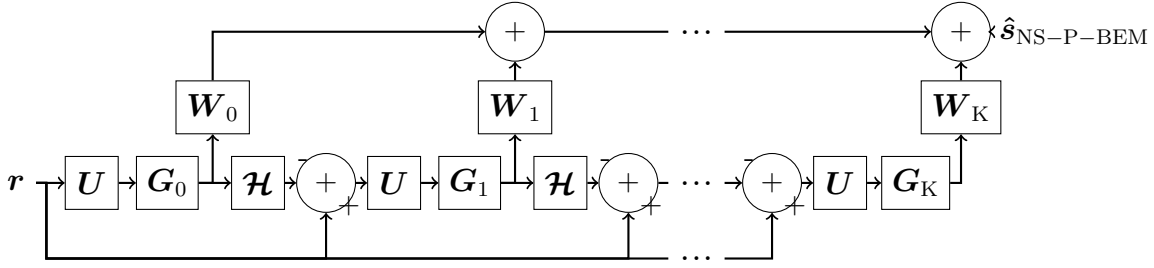


Figure 3.5: Non-stationary BEM-MMSE preconditioned iterative receiver

At the generic stage k , the coefficients can then be computed by

$$\mathbf{f}_n^{\text{T}(k)} = \mathbf{1}_n \mathcal{H}^H \mathbf{U}_k^H \mathbf{S}_n^T [\mathbf{S}_n \mathbf{U}_k (\mathcal{H} \mathcal{H}^H + \sigma_z^2 \mathbf{I}) \mathbf{U}_k^H \mathbf{S}_n^T]^{-1} \quad (3.27)$$

and get \mathbf{G}_k as in (A.74).

The overall signal estimate after K iterations can then be obtained by MMSE combining of the estimates at each stage. Let

$$\mathbf{X} = \begin{bmatrix} \mathbf{G}_0 \mathbf{U}_0 \\ \mathbf{G}_1 \mathbf{U}_1 \\ \vdots \\ \mathbf{G}_{K-1} \mathbf{U}_{K-1} \end{bmatrix} \quad (3.28)$$

then, the $K \times 1$ coefficient vector for n -th sub-carrier \mathbf{c}_n^{T} can be computed by

$$\mathbf{c}_n^{\text{T}} = \mathbf{1}_n \mathcal{H}^H \mathbf{X}^H \mathbf{S}_n^T [\mathbf{S}_n \mathbf{X} (\mathcal{H} \mathcal{H}^H + \sigma_z^2 \mathbf{I}) \mathbf{X}^H \mathbf{S}_n^T]^{-1} \quad (3.29)$$

With \mathbf{S}_n being in this case the $K \times KN$ matrix selecting the sub-carrier n on all the iterations stage output.

We then obtain the whole $N \times K$ weighting matrix as

$$\mathbf{W} = \begin{bmatrix} \mathbf{c}_0^{\text{T}} \\ \mathbf{c}_1^{\text{T}} \\ \vdots \\ \mathbf{c}_{N-1}^{\text{T}} \end{bmatrix} \quad (3.30)$$

and derive the per-stage weighting matrices by taking the columns of $\mathbf{W} = [\mathbf{w}_0 \cdots \mathbf{w}_{K-1}]$ to obtain the overall estimate

$$\begin{aligned} \hat{\mathbf{s}}_{\text{NS-P-BEM}} &= \text{diag}\{\mathbf{w}_0\} \hat{\mathbf{s}}_0 + \cdots + \text{diag}\{\mathbf{w}_{K-1}\} \hat{\mathbf{s}}_{K-1} \\ &= \mathbf{W}_0 \hat{\mathbf{s}}_0 + \cdots + \mathbf{W}_{K-1} \hat{\mathbf{s}}_{K-1} \end{aligned} \quad (3.31)$$

BEM-MMSE Parallel Interference Cancellation

One could think of performing time-domain PIC detection and figure A.10 shows the block diagram of the PIC receiver using *hard-decisions* as non-linear decision criterion.

By setting $\mathcal{H}_p = \mathbf{B}_p \mathbf{F}^H \mathbf{D}_p$ and $\mathcal{H} = \sum_{k=0}^{P-1} \mathcal{H}_k = \mathbf{H} \mathbf{F}^H$, let

$$\mathcal{H}_{\bar{0}} = \mathcal{H} - \mathcal{H}_0 \quad (3.32)$$

represent the *time-varying* part of the channel matrix assuming an orthogonal-polynomial basis, the coefficients of the PIC filtering matrix $\dot{\mathbf{G}}$ are computed according to a modified formula assuming perfect cancellation of the ICI

$$\begin{aligned} \dot{\mathbf{G}} &= \mathcal{H}_0^H \mathbf{U}_0^H [\mathbf{U}_0 (\mathcal{H}_0 \mathcal{H}_0^H + \sigma_z^2 \mathbf{I}) \mathbf{U}_0^H]^{-1} \\ &= \mathcal{H}_0^H [\mathbf{U}_0 (\mathcal{H}_0 \mathcal{H}_0^H + \sigma_z^2 \mathbf{I})]^{-1} \end{aligned} \quad (3.33)$$

where $\dot{\mathbf{G}}$ is a diagonal matrix.

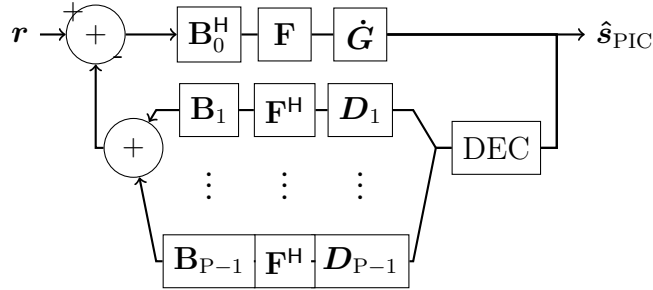


Figure 3.6: Time-domain PIC iterative decoder

Preconditioned Conjugate Gradient MMSE Receiver

For the sake of completeness and comparison, it is worth deriving iterative ICI cancellation techniques operating in the squared channel matrix domain and solving the steady state MMSE problem as given in expression (A.52). Although not attractive because of the inherent additional complexity required and reduced convergence properties, they are still relevant to demonstrate the statements provided in section A.2.5.

Noticing that the left hand-side of the linear system of MMSE detection in (A.52) is Hermitian, the well known Conjugate Gradient (CG) algorithm can be applied.

A *banded* preconditioning computed with similar development as for BEM-MMSE can be derived for a *Preconditioned* CG iterative receiver [71], whose algorithm is presented in figure A.11. Letting

```

INPUT:  $\mathcal{H}$ ,  $\check{\mathbf{G}}$ ,  $\sigma_z^2$ ,  $\mathbf{r}$ ,  $K$ 
OUTPUT:  $\mathbf{s}_K$ 
# Initialize parameters
 $\mathbf{r}_0 = \mathcal{H}^H \mathbf{r}$ 
 $\mathbf{z}_0 = \check{\mathbf{G}} \mathbf{r}_0$ 
 $\mathbf{d}_0 = \mathbf{z}_0$ 
 $\mathbf{s}_0 = \mathbf{0}_N$ 
# Main loop
for  $k = 0$  to  $K - 1$  do
   $\alpha_k = \frac{\mathbf{r}_k^H \mathbf{z}_k}{\mathbf{d}_k^H (\mathcal{H}^H \mathcal{H} + \sigma_z^2 \mathbf{I}) \mathbf{d}_k}$ 
   $\mathbf{s}_{k+1} = \mathbf{s}_k + \alpha_k \mathbf{d}_k$ 
   $\mathbf{r}_{k+1} = \mathbf{r}_k - \alpha_k (\mathcal{H}^H \mathcal{H} + \sigma_z^2 \mathbf{I}) \mathbf{d}_k$ 
   $\mathbf{z}_{k+1} = \check{\mathbf{G}} \mathbf{r}_{k+1}$ 
   $\beta_k = \frac{\mathbf{r}_{k+1}^H \mathbf{z}_{k+1}}{\mathbf{r}_k^H \mathbf{z}_k}$ 
   $\mathbf{d}_{k+1} = \mathbf{z}_{k+1} + \beta_k \mathbf{d}_k$ 
end for

```

Figure 3.7: Preconditioned Conjugate Gradient algorithm

$$\mathbf{f}_n^T = \mathbf{1}_n \mathcal{H}^H \mathcal{H} \mathbf{S}_n^T [\mathbf{S}_n \mathcal{H}^H (\mathcal{H} \mathcal{H}^H + \sigma_z^2 \mathbf{I}) \mathcal{H} \mathbf{S}_n^T]^{-1} \quad (3.34)$$

and

$$\check{\mathbf{G}} = \begin{bmatrix} \mathbf{f}_0^T \mathbf{S}_0 \\ \mathbf{f}_1^T \mathbf{S}_1 \\ \vdots \\ \mathbf{f}_{N-1}^T \mathbf{S}_{N-1} \end{bmatrix} \quad (3.35)$$

for an appropriate choice of the selection matrix \mathbf{S}_n and filter length L_{FIR} .

3.1.6 Simulation results

We compare the methods proposed in this paper by means of Monte Carlo simulations assuming a cyclic prefixed OFDM setup with $N = 128$ sub-carriers, a multi-path channel with $L = 4$ with uniform power delay profile and Jakes Doppler spectrum with normalized Doppler frequency of 0.1 with respect to the sub-carrier spacing. We assume a first order orthogonal-polynomial BEM channel with $P = 2$. The performance are measured in terms of bit-error-rate of uncoded QPSK modulated transmitted sequences. The SNR is defined as the ratio $1/\sigma_z^2$. The methods presented in the paper are evaluated for BEM-MMSE preconditioning filtering lengths of $L_{\text{FIR}} = 3$ and $L_{\text{FIR}} = 5$. A number of iterations $K = 1$ and $K = 3$ are tried to allow fair comparison with the method of [68]. For all simulation results presented in figures A.12–A.15, the Non Stationary BEM-MMSE Preconditioned iterative ICI cancellation technique (NS-P-BEM) provides always the overall best performances compared to the reference full-blown matrix inversion MMSE method (labeled MMSE in the plots). The Preconditioned CG method (P-CG), instead, always provides the worst performance for the same number of iteration and MMSE filter lengths. The Preconditioned ZF Iterative (P-ZF) of [68] is drastically improved by the use of Stationary BEM-MMSE preconditioning (S-P-BEM) and the PIC iterative receiver provides a good trade-off in terms of performance and complexity.

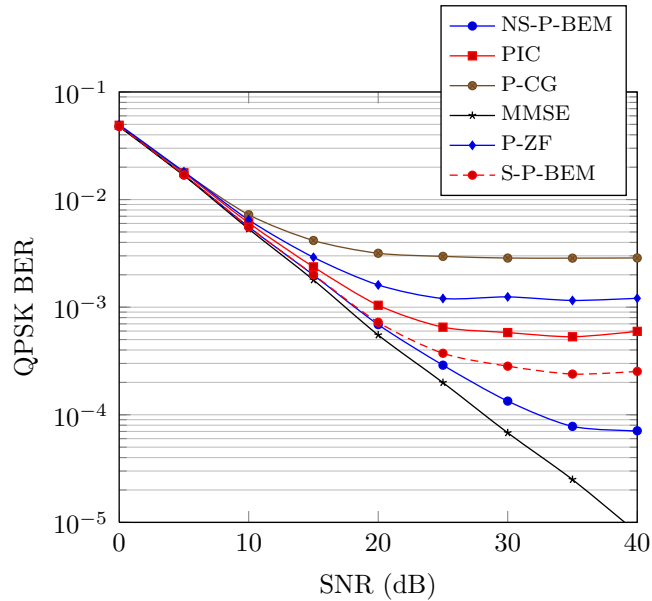


Figure 3.8: Performance comparison of iterative methods with 1 iterations, $L_{\text{FIR}} = 5$

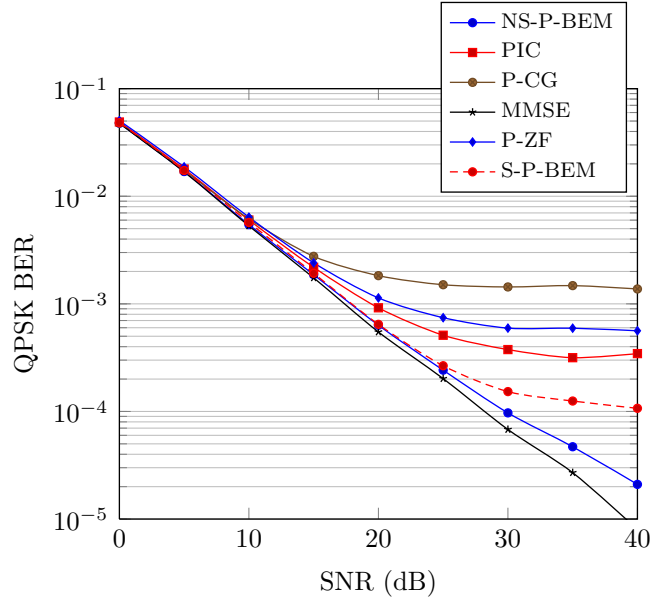


Figure 3.9: Performance comparison of iterative methods with 3 iterations, $L_{\text{FIR}} = 5$

3.2 Analysis of Preconditioned Iterative IC

3.2.1 Preconditioned Iterative Reception

For the sake of the convenience for our analysis we shall start from classical linear Zero-Forcing (ZF) equalization problem, where an estimate of the transmitted signal \mathbf{s} is computed from the received signal \mathbf{r} of (A.42) as

$$\hat{\mathbf{s}}_{\text{ZF}} = (\mathbf{H}^H \mathbf{H})^{-1} \mathbf{H}^H \mathbf{r} \quad (3.36)$$

Typically, Equation (3.36) is solved by first performing the Matched Filter (MF) operation on the received signal \mathbf{r} and then by applying classical iterative techniques to approximate the inversion of $\mathbf{H}^H \mathbf{H}$ based on its *Hermitian* structure. This approach has been widely adopted in a large number of works, especially for Code Division Multiple Access (CDMA) multi-user Minimum Mean Square Error (MMSE) linear equalization (for example in [72] – [73] and references therein).

When \mathbf{H} is full-rank as in OFDM, Equation (3.36) reduces to

$$\hat{\mathbf{s}}_{\text{ZF}} = \mathbf{H}^{-1} \mathbf{r} \quad (3.37)$$

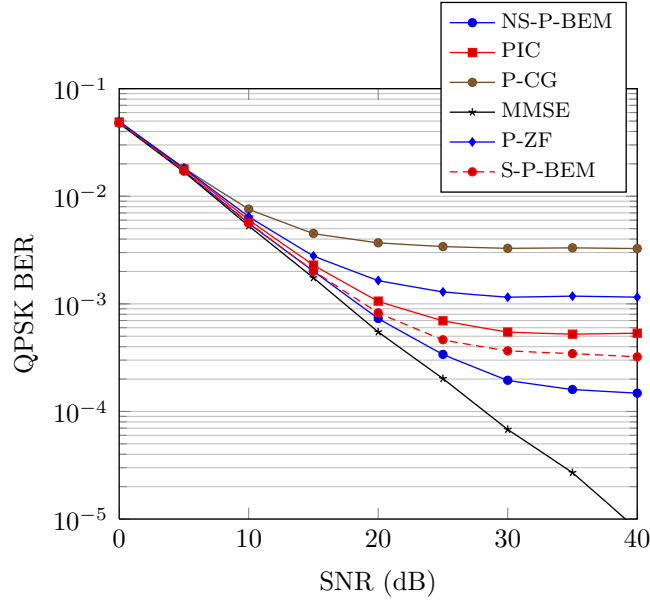


Figure 3.10: Performance comparison of iterative methods with 1 iterations, $L_{\text{FIR}} = 3$

Following this formulation, it is straightforward to show that the problem of approximating the inverse of \mathbf{H} is inherently better conditioned than the one of inverting $\mathbf{H}^H\mathbf{H}$ by observing the relation of their respective condition numbers (CN): $\kappa(\mathbf{H}) \leq \kappa(\mathbf{H}^H\mathbf{H})$ where $\kappa(\mathbf{X}) = \|\mathbf{X}\| \|\mathbf{X}^{-1}\|$. As it is well-known from the literature the smaller the CN, the faster an iterative algorithm will converge.

We therefore shall concentrate on iterative solution of the linear system of Equation (3.37). The most common iterative procedure, used throughout this discussion, can be derived by the *Taylor* expansion of matrix \mathbf{H}^{-1} to give an *iterative* ZF (IT-ZF) receiver expressed by

$$\hat{\mathbf{s}}_{\text{IT-ZF}} = \left(\sum_{k=0}^{K-1} (\mathbf{I} - \mathbf{H})^k \right) \mathbf{r} \quad (3.38)$$

Obviously, $\hat{\mathbf{s}}_{\text{IT-ZF}} = \hat{\mathbf{s}}_{\text{ZF}}$ for $K \rightarrow \infty$ if and only if $\rho(\mathbf{I} - \mathbf{H}) < 1$, where $\rho(\mathbf{X})$ denotes the *spectral radius* of matrix \mathbf{X} .

For finite (and low) number of iterations, the IT-ZF receiver of equation (3.38) can be interpreted as a *polynomial expansion* receiver since it can be formulated as

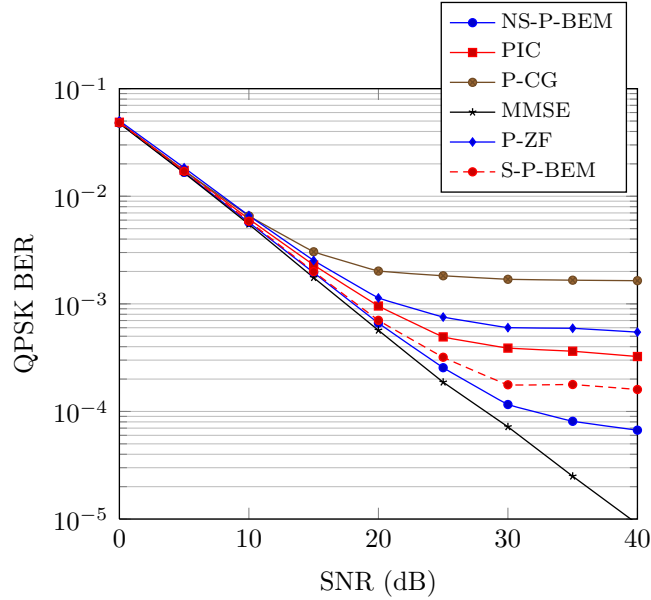


Figure 3.11: Performance comparison of iterative methods with 3 iterations, $L_{\text{FIR}} = 3$

$(K - 1)$ -th order polynomial in \mathbf{H} as $\sum_{k=0}^{K-1} (\mathbf{I} - \mathbf{H})^k = \sum_{k=0}^{K-1} w_k \mathbf{H}^k$ with $w_k = (-1)^k \binom{K}{k+1}$. Polynomial expansion receivers have been extensively studied [74] [75], in particular for the CDMA case, as an effective mean of approximating ZF or MMSE linear equalizers. Relying in particular on Cayley-Hamilton theorem [76], these techniques aim at optimizing combining coefficients w_k for a reduced number of iterations (i.e. polynomial order) than N , the dimension of the linear system to be solved.

Alternatively to polynomial expansion receivers and the problem of finding optimized combining coefficients w_k , we instead focus on *preconditioning* as an advantageous mean to improve performance of iterative interference cancellation (IC) and signal detection by reducing the CN of the linear system to be solved and allow for faster convergence. For this purpose, the linear system

$$\hat{\mathbf{s}}_{\text{ZF}} = (\mathbf{P}\mathbf{H})^{-1} \mathbf{P}\mathbf{r} \quad (3.39)$$

easily proves being exactly equivalent to (3.37). Using the same derivation of (3.38) from (3.37), we can therefore approximate (3.37) by a *preconditioned* iterative ZF (P-IT-ZF) receiver such as

$$\hat{\mathbf{s}}_{\text{P-IT-ZF}} = \left(\sum_{k=0}^{K-1} (\mathbf{I} - \mathbf{P}\mathbf{H})^k \right) \mathbf{P}\mathbf{r} \quad (3.40)$$

if and only if $\rho(\mathbf{I} - \mathbf{PH}) < 1$ and where \mathbf{P} is a suitable non-singular preconditioning matrix such that $\kappa(\mathbf{H}) \geq \kappa(\mathbf{PH}) \geq 1$. The equality holds in the trivial case where $\mathbf{P}^{-1} = \mathbf{H}$ and the linear system in (3.39) is solved in one iteration.

It is worth noting that the ZF signal detection problem as formulated in (3.36) is a particular case of the preconditioned system (3.40) with $\mathbf{P} = \mathbf{H}^H$, but where the CN is increased instead.

The asymptotic convergence in the receiver order K of the P-IT-ZF receiver of (3.40) to the ZF solution is independent of the choice of \mathbf{P} . For lower iteration orders instead, its convergence and performance behavior strongly depend on the chosen preconditioning.

In the absence of noise, i.e. $\sigma_z^2 \rightarrow 0$, the error of the $(K - 1)$ -th order P-IT-ZF receiver $\tilde{\mathbf{s}}_{\text{P-IT-ZF}} = \mathbf{s} - \hat{\mathbf{s}}_{\text{P-IT-ZF}}$ is

$$\tilde{\mathbf{s}}_{\text{P-IT-ZF}} = \left(\sum_{k=0}^{K-1} (-1)^k \binom{K-1}{k} (\mathbf{PH})^k \right) \mathbf{s} = (\mathbf{I} - \mathbf{PH})^{K-1} \mathbf{s}$$

For the P-IT-ZF receiver, by defining

$$\tilde{\mathbf{G}} = (\mathbf{I} - \mathbf{PH})^{K-1}, \quad (3.41)$$

the error norm is $\|\tilde{\mathbf{s}}\| = \|\tilde{\mathbf{G}}\mathbf{s}\| \leq \|\tilde{\mathbf{G}}\| \|\mathbf{s}\|$. $\|\tilde{\mathbf{G}}\|$ and $\rho(\mathbf{I} - \mathbf{PH}) = \lim_{K \rightarrow \infty} \|\tilde{\mathbf{G}}\|^{\frac{1}{K}}$ are the $(K - 1)$ -th order and *asymptotic* convergence-factors of the iterative receiver, respectively.

3.2.2 Iteration-Dependent Preconditioned Iterative Reception

The P-IT-ZF receiver of Equation (3.40) is based on a constant preconditioning over iterations. By construction, this receiver is intrinsically sub-optimal because, as $K \rightarrow \infty$, it degenerates to the ZF solution independently of the choice of the preconditioner.

The approach can be generalized and improved to give an *Iteration-Dependent*

Preconditioned Iterative (ID-P-IT) receiver as follows

$$\hat{\mathbf{s}}_{\text{ID-P-IT}} = \left(\left(\sum_{k=1}^{K-1} \prod_{j=1}^k (\mathbf{I} - \mathbf{P}_j \mathbf{H}) \right) + \mathbf{I} \right) \mathbf{P}_0 \mathbf{r} \quad (3.42)$$

where the preconditioning matrix \mathbf{P} is optimized at each iteration forming the set $\mathcal{P}_K = \{\mathbf{P}_0, \mathbf{P}_1, \dots, \mathbf{P}_{K-1}\}$.

This generalization introduces new degrees of freedom to our receiver that can be exploited to achieve better performances than those achievable with \mathbf{P} constant.

The block diagram of the ID-P-IT receiver is depicted in Figure A.9, the P-IT-ZF receiver of Equation (3.40) can be obtained imposing the same preconditioning matrix \mathbf{P} for all stages.

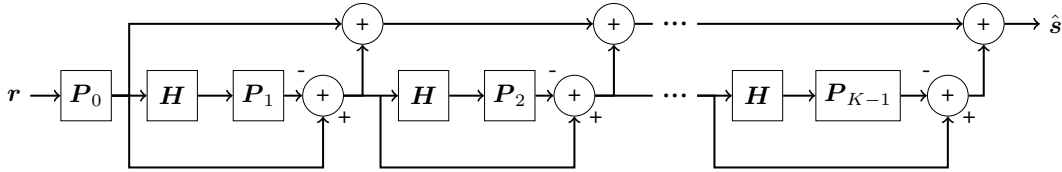


Figure 3.12: Iteration-Dependent Iterative ICI cancellation receiver

Similarly as for the P-IT-ZF in (3.41), in case of the ID-P-IT receiver we can define

$$\tilde{\mathbf{G}} = \prod_{k=0}^K \tilde{\mathbf{G}}_k = \prod_{k=0}^K (\mathbf{I} - \mathbf{P}_k \mathbf{H}) \quad (3.43)$$

Then, by denoting $\tilde{\mathbf{T}}_{K-1} = \prod_{k=0}^{K-1} \tilde{\mathbf{G}}_k$, the error of the ID-P-IT receiver of the $(K-1)$ -th order can be written as

$$\begin{aligned} \tilde{\mathbf{s}} &= \tilde{\mathbf{G}} (\mathbf{s} + \mathbf{H}^{-1} \mathbf{z}) - \mathbf{H}^{-1} \mathbf{z} = \\ &= \tilde{\mathbf{G}}_K \tilde{\mathbf{T}}_{K-1} \mathbf{s} + \left(\tilde{\mathbf{G}}_K \tilde{\mathbf{T}}_{K-1} - \mathbf{I} \right) \mathbf{H}^{-1} \mathbf{z} \end{aligned} \quad (3.44)$$

and its *mean square error* (MSE) as

$$\begin{aligned} \mathbb{E} \|\tilde{\mathbf{s}}\|^2 &= \text{tr} \left\{ \sigma_s^2 \tilde{\mathbf{G}}_K \tilde{\mathbf{T}}_{K-1} \tilde{\mathbf{T}}_{K-1}^H \tilde{\mathbf{G}}_K^H \right\} + \\ &+ \text{tr} \left\{ \sigma_z^2 \left(\tilde{\mathbf{G}}_K \tilde{\mathbf{T}}_{K-1} - \mathbf{I} \right) \mathbf{R}^{-1} \left(\tilde{\mathbf{G}}_K \tilde{\mathbf{T}}_{K-1} - \mathbf{I} \right)^H \right\} \end{aligned} \quad (3.45)$$

where $\mathbb{E}\{\cdot\}$ denotes the expectation operator and $\mathbf{R} = \mathbf{H}^H \mathbf{H}$.

3.2.3 Sparse Preconditioning Derivation

The optimal preconditioning matrix \mathbf{P}_K for K -th iteration can be found minimizing the MSE of Equation (3.45), that is

$$\begin{aligned} \mathbf{P}_K = \arg \min_{\mathbf{P}_K \in \mathcal{P}_K} \mathbb{E} \|\tilde{\mathbf{s}}\|^2 &= \left(\sigma_s^2 \tilde{\mathbf{T}}_{K-1} + \sigma_z^2 (\tilde{\mathbf{T}}_{K-1} - \mathbf{I}) \mathbf{R}^{-1} \right) \cdot \\ &\cdot \tilde{\mathbf{T}}_{K-1}^H \mathbf{H}^H \left(\mathbf{H} \tilde{\mathbf{T}}_{K-1} (\sigma_s^2 \mathbf{I} + \sigma_z^2 \mathbf{R}^{-1}) \tilde{\mathbf{T}}_{K-1}^H \mathbf{H}^H \right)^{-1} \end{aligned} \quad (3.46)$$

Nevertheless, as we can see for the first iteration, i.e. $\mathbf{T}_{K-1} = \mathbf{I}$, Equation (3.46) gives

$$\mathbf{P}_0 = \sigma_s^2 \mathbf{H}^H (\sigma_s^2 \mathbf{H} \mathbf{H}^H + \sigma_z^2 \mathbf{I})^{-1} \quad (3.47)$$

which is the trivial solution corresponding to MMSE receiver. In this case, such preconditioning coefficients would allow any preconditioned receiver to converge to the optimal solution in the MMSE sense in one iteration but at the cost of unaffordable complexity entailing the inversion of a $N \times N$ matrix. In general, this operation requires complexity orders of $\mathcal{O}(N^3)$ or $\mathcal{O}(N^2)$ order when classical techniques are used, such as *Gauss-Jordan elimination* or *Cholesky decomposition* (exploiting the Hermitian nature of $\mathcal{H}^H \mathcal{H}$) respectively [76].

In order to avoid the trivial and extremely complex solution, we therefore need to add a complexity-limitation constraint to the minimization problem in (3.46).

The optimal *constrained* MMSE preconditioning matrix can be obtained by estimating the transmitted symbol $s(n)$ at sub-carrier n by adopting *sparse* MMSE Finite-Impulse-Response (FIR) preconditioning filter $\bar{\mathbf{p}}_n$ across L_{FIR} (neighboring) tones to limit the complexity of a full *per-tone* equalization across all N sub-carriers.

Considering for example the first iteration case, this corresponds to selecting a subset of the elements of vector \mathbf{r} as $\bar{\mathbf{r}}_n = \mathbf{S}_n \mathbf{r}$ with \mathbf{S}_n being a $L_{\text{FIR}} \times N$ *selection* matrix obtained by extracting L_{FIR} rows of the identity matrix \mathbf{I}_N for a given filter-length L_{FIR} and sub-carrier n to have

$$\hat{s}(n) = \bar{\mathbf{p}}_n^H \bar{\mathbf{r}}_n = \bar{\mathbf{p}}_n^H \mathbf{S}_n \mathbf{r} = \mathbf{p}_n^H \mathbf{r} \quad (3.48)$$

with $\mathbf{p}_n^H = [\mathbf{P}_0]_{i=n; j=1, \dots, N}$.

Therefore, the *sparse* MMSE filtering coefficients are computed such that $\bar{\mathbf{p}}_n^H = \mathbf{E}\{s(n)\bar{\mathbf{r}}_n^H\} (\mathbf{E}\{\bar{\mathbf{r}}_n\bar{\mathbf{r}}_n^H\})^{-1}$ to give

$$\bar{\mathbf{p}}_n^H = \mathbf{1}_n \mathbf{H}^H \mathbf{S}_n^H [\mathbf{S}_n (\mathbf{H}\mathbf{H}^H + \gamma^{-1}\mathbf{I}) \mathbf{S}_n^H]^{-1} \quad (3.49)$$

with $\mathbf{1}_n$ being the $1 \times N$ vector containing 1 at n -th position and 0 elsewhere. It is noteworthy mentioning that the above expression stems from the multiplication of a $1 \times L_{\text{FIR}}$ vector $\mathbf{E}\{s(n)\bar{\mathbf{r}}_n^H\}$ and $L_{\text{FIR}} \times L_{\text{FIR}}$ inverse matrix of $\mathbf{E}\{\bar{\mathbf{r}}_n\bar{\mathbf{r}}_n^H\}$ which varies across sub-carriers.

By limiting the complexity and determining preconditioning coefficients subject to this constraint, we are instead able to reduce the computational requirements to $\mathcal{O}(L_{\text{FIR}}^3)$ at the expense of an increased number of iterations depending on the target performance.

The trade-off between the complexity for computing the preconditioning matrix elements and the number of iterations shall be considered in light of the fact that, even in time-varying channel OFDM reception, each iterative stage can be efficiently implemented with $\mathcal{O}(N \log_2 N)$ complexity, as shown in [3], using the using channel Polynomial Basis Expansion Modeling (Poly-BEM) approximation [77].

Similarly to (A.73), we can therefore derive the *constrained* MMSE preconditioning matrix elements at n -th sub-carrier for the $(K + 1)$ -th iteration stage, provided the set $\mathcal{P}_{K-1} = \{\mathbf{P}_0, \mathbf{P}_1, \dots, \mathbf{P}_{K-1}\}$ and subject to the limited-complexity constraint \mathbf{S}_n , as

$$\begin{aligned} [\mathbf{P}_K]_{i=n, j=1, \dots, N} &= \\ &= \mathbf{1}_n \left(\sigma_s^2 \tilde{\mathbf{T}}_{K-1} + \sigma_z^2 (\tilde{\mathbf{T}}_{K-1} - \mathbf{I}) \mathbf{R}^{-1} \right) \tilde{\mathbf{T}}_{K-1}^H \mathbf{H}^H \mathbf{S}_n^H \cdot \\ &\cdot \left[\mathbf{S}_n \left(\mathbf{H} \tilde{\mathbf{T}}_{K-1} (\sigma_s^2 \mathbf{I} + \sigma_z^2 \mathbf{R}^{-1}) \tilde{\mathbf{T}}_{K-1}^H \mathbf{H}^H \right) \mathbf{S}_n^H \right]^{-1} \mathbf{S}_n \end{aligned} \quad (3.50)$$

The ID-P-IT receiver of Equation (3.42) making use of preconditioning matrices computed according to Equation (3.50) is optimal by construction subject to the aforementioned limited-complexity constraint.

As a result of this analysis, it is evident how the optimality allowing the method to achieve the best possible MSE performance along iterations relates to the fastest possible convergence property in the Euclidean norm sense for the given complexity

constraint. For this reason, as $K \rightarrow \infty$, and contrarily to the P-IT-ZF receiver of Equation (3.40), does not show degeneration to ZF despite the initial derivation.

Nevertheless, the ID-P-IT receiver appears to be considerably more complex than the P-IT-ZF making use of constant MMSE preconditioning as of Equation (A.73) because the preconditioning coefficients are optimized at each iteration.

Quickly time-varying and frequency-selective channels, also known as doubly-selective channels, show different ICI level depending on the sub-carrier index. This suggests that the limited-complexity constraint can be made varying depending on the sub-carrier and its corresponding ICI level. Larger L_{FIR} filters can be used on those sub-carriers severely impacted by ICI, while minimum preconditioning filtering effort ($L_{\text{FIR}} = 1$) can be dedicated to the others.

Strong complexity reduction for all above mentioned schemes can then be easily achieved by first estimating the ICI level then selecting only a subset of sub-carriers for which the ICI level is above a given acceptance threshold or, using a *fixed-complexity* (FC) principle, deciding for a fixed amount of indexes corresponding to those sub-carriers mostly impacted by ICI. The ICI level on each sub-carrier can be estimated effortlessly by considering that, in the OFDM case under examination, the full channel matrix can be decomposed into *time-invariant* and *time-varying* terms such as $\mathbf{H} = \mathbf{H}_{\text{TI}} + \mathbf{H}_{\text{TV}}$ where \mathbf{H}_{TI} is diagonal. By taking $\tilde{\mathbf{G}}_{\text{J}} = \mathbf{H}_{\text{TI}}^{-1} \mathbf{H}_{\text{TV}}$, the Signal-to-Interference Ratio (SIR) can be estimated by $\text{SIR}(n) = 1 / \|\tilde{\mathbf{g}}_{\text{J},n}\|^2$ with $\tilde{\mathbf{g}}_{\text{J},n}^{\text{H}} = \left[\tilde{\mathbf{G}}_{\text{J}} \right]_{i=n; j=1, \dots, N}$.

3.2.4 Performance evaluation

In the previous sections, we derived general expressions for the MSE. Here we will provide other significant performance metrics such SINR and mutual information. For both P-IT-ZF and ID-P-IT receivers of Equations (3.40) and (3.42), the transmitted sequence estimate can be written as

$$\hat{\mathbf{s}}_{\text{P-IT-ZF}} = \mathbf{G}\mathbf{s} + \mathbf{G}\mathbf{H}^{-1}\mathbf{z} \quad (3.51)$$

where $\mathbf{G} = \mathbf{I} - \tilde{\mathbf{G}}$ denotes the cascade of the channel and of the iterative receiver computed by plugging respective expressions for $\tilde{\mathbf{G}}$ from (3.41) and (3.43). Additionally, we consider the MMSE receiver as of Equation (3.47) as reference for performance evaluation.

The error term can be expressed as $\tilde{\mathbf{s}} = \mathbf{s} - \mathbf{G}\mathbf{s} - \mathbf{W}\mathbf{z}$ with $\mathbf{W} = \mathbf{G}\mathbf{H}^{-1}$ being the receiver transfer-function.

Letting $\mathbf{g}_n^H = [\mathbf{G}]_{i=n;j=1,\dots,N}$ and $\mathbf{w}_n^H = [\mathbf{W}]_{i=n;j=1,\dots,N}$ be the n -th row of \mathbf{G} and \mathbf{W} respectively, the expected value of the n -th sub-carrier symbol estimate power is

$$\mathbb{E}|\hat{s}(n)|^2 = \underbrace{\sigma_s^2 |g_n(n)|^2}_{\text{useful signal}} + \underbrace{\|\mathbf{g}_n\|^2 - |g_n(n)|^2}_{\text{ICI}} + \underbrace{\sigma_z^2 \|\mathbf{w}_n\|^2}_{\text{noise}}$$

Thus, we find the general error expression of the SINR at n -th sub-carrier to be

$$\text{SINR}(n) = \frac{|g_n(n)|^2}{\|\mathbf{g}_n\|^2 - |g_n(n)|^2 + \gamma^{-1} \|\mathbf{w}_n\|^2} \quad (3.52)$$

with $\gamma = \sigma_s^2/\sigma_z^2$.

Finally, as a convenient performance metric for our discussion, we evaluate the average *mutual information*, using

$$\mathcal{I}(\text{SINR}) = \frac{1}{N} \sum_{n=1}^N \log_2(1 + \text{SINR}(n)) \quad (3.53)$$

assuming independent per sub-carrier symbol detection of transmitted sequence.

3.2.5 Simulation results

We compare the methods proposed in this paper by evaluation of the analytical expressions as described in Section 3.2.4. Monte Carlo simulations were conducted on an equivalent OFDM setup with $N = 128$ sub-carriers for a sufficient number of realizations of uniform power-delay-profile multi-path channel of length $L = 4$. The channel is time-varying within an OFDM symbol according to Jakes Doppler spectrum with normalized Doppler frequency of 0.256 with respect to the sub-carriers spacing. The performances are measured in terms of average mutual information (bits/sub-carrier) assuming perfect channel and noise statistics knowledge. The receiver uses $P = 2$ orthonormal Poly-BEM channel. In figures 1 – 3, the methods presented are evaluated for MMSE preconditioning filtering lengths of $L_{\text{FIR}} = 3$.

As a general behavior, all methods show to achieve the MMSE capacity for decoding full-rate QPSK (2 bits/sub-carrier) with 1 iteration, 16QAM (4 bits/sub-carrier) with 2 iterations and 64QAM (6 bits/sub-carrier) with 3 iterations. As expected by optimal analytical construction, the ID-P-IT receiver shows the best approximation to the full-blown MMSE solution compared to any other method for the same number of iterations. Interestingly, the P-IT-ZF using MMSE preconditioning approaches MMSE performances very well for a very limited number of iterations and short length of MMSE preconditioning filter. Moreover, the complexity reduction techniques proposed provide negligible performance loss with respect to P-IT-ZF receiver with full complexity MMSE preconditioning for QPSK and 16 QAM and 1 dB loss for 64 QAM compared to MMSE. In particular, the FC reduction method realizes a complexity reduction of a factor 10 but still provides similar performance to the full complexity P-IT-ZF for QPSK and 16QAM. Hence, in practical applications, the P-IT-ZF with MMSE preconditioning and FC reduction appears to be very attractive.

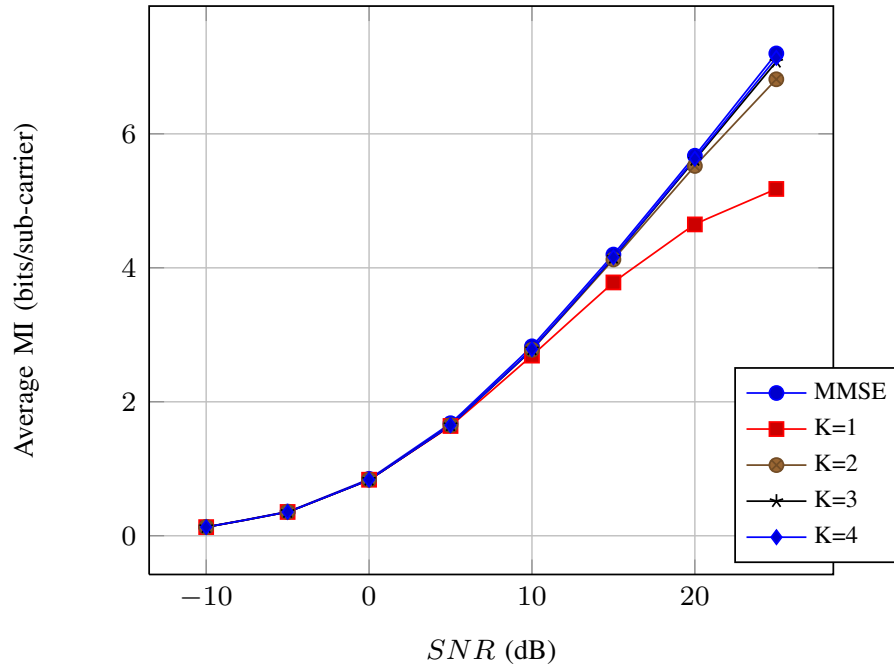
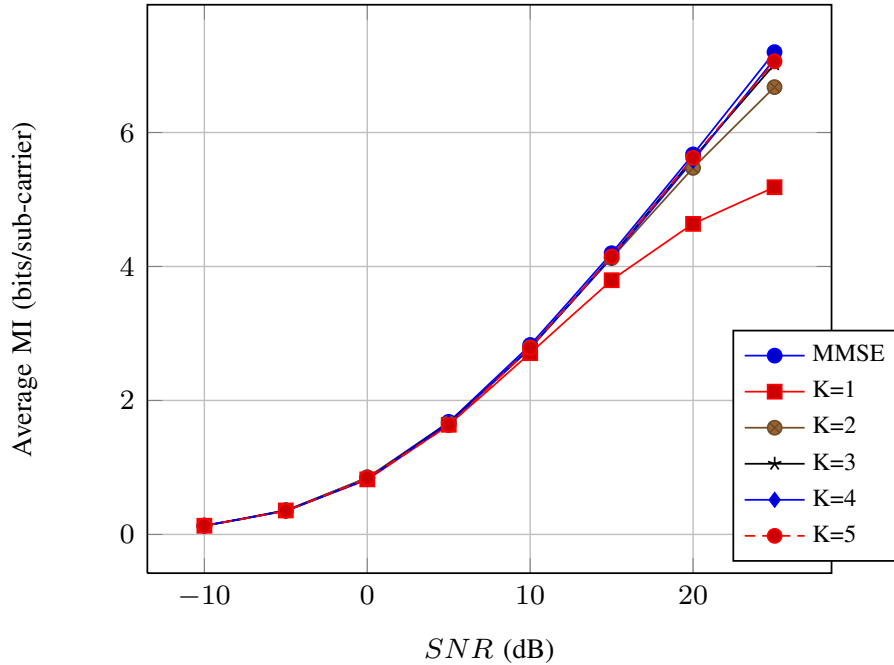


Figure 3.13: Performances of ID-P-IT receiver with $L_{\text{FIR}} = 3$

Figure 3.14: Performances of P-IT-ZF receiver with $L_{\text{FIR}} = 3$

3.3 Alamouti Detection Over Selective Channels

Over the last decade, multi-antenna transmissions imposed as the effective mean to improve wireless communications over fading channels. The fundamental multiplexing-diversity trade-off [78] offers the clear insight that multi-antenna communications can enjoy the added spatial dimension as a degree of freedom for increasing the data-rate or enhancing the link quality. While modern wireless systems such as Wireless-Local Access Network (WLAN) and 3GPP Long Term Evolution are starting to support spatial-multiplexing, the multi-antenna diversity is already widely employed in existing standards such as 3GPP UMTS W-CDMA. In particular, the well known Alamouti scheme [79] revealed to be extremely efficient in allowing wireless and cellular systems to increase link reliability. Its efficiency proves because of the extremely simple encoding technique at the transmitter and more importantly in the low complexity linear and optimal decoding which can also easily be extended to multiple receiving antenna case. This scheme is well known and deeply analyzed [80]. Nevertheless, the efficiency of this block-code is based on the assumption of static conditions over the two periods or channel uses spanning its transmission. The static channel assumption is actually never verified in practice and remains ideal. In OFDM, for example, the channel is selective because of the

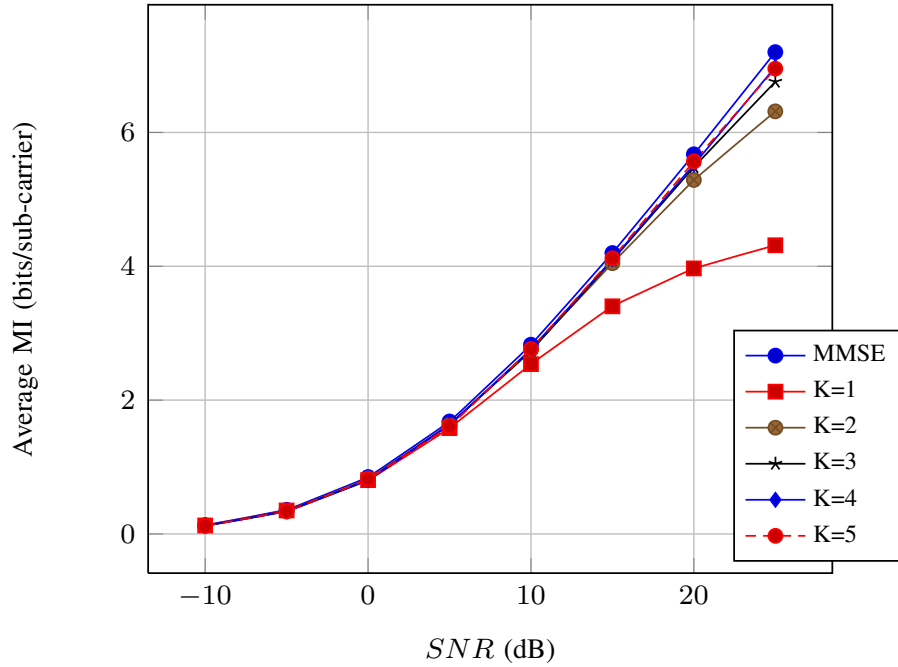


Figure 3.15: Performances of P-IT-ZF receiver with $L_{\text{FIR}} = 3$ and FC mechanism

time-varying or frequency selective nature of the terminal mobility and the rich scattering of the wireless environment. Receiving equipments must therefore cope with these non-idealities and the need for efficient receiving techniques to do so motivated this work beyond previous contributions [81][82]. In this paper, the signal model employed along the study is introduced in section 3.3.1, the diversity analysis of the Maximum-Likelihood detection is carried out in section 3.3.2, modified and improved Decision-Feedback (DF) based schemes are discussed in 3.3.3, extension to Space-Frequency Block-Codes (SFBC) and Space-Time Block-Codes (STBC) for OFDM are given in section 3.3.5 and, finally, simulation results are presented in section 3.3.6.

3.3.1 Signal model definition

We consider a communication system between a transmitter with two antennas and a receiver with one receiving antenna. Despite this simplification, the results presented are general and can be straightforwardly extended to multiple receiving antennas case.

The transmitter employing Alamouti transmit-diversity scheme requires two signaling periods or two parallel channels to convey a pair of finite-alphabet complex symbols x_1 and x_2 : during the first symbol period, the first antenna sends x_1 and the second antenna sends x_2 ; in the second period, the symbols $-x_2^*$ and x_1^* are respectively transmitted by first and second antenna.

Denote h_1 and h_2 the complex flat-fading channel coefficients between the two transmit antennas and the receiving antenna during the first period while \tilde{h}_1 and \tilde{h}_2 are the channel coefficients of the second symbol period.

It is easy to show that the received symbol vector can be conveniently written in matrix form as

$$\begin{bmatrix} y_1 \\ y_2^* \end{bmatrix} = \begin{bmatrix} h_1 & h_2 \\ -\tilde{h}_2^* & \tilde{h}_1^* \end{bmatrix} \begin{bmatrix} x_1 \\ x_2 \end{bmatrix} + \begin{bmatrix} n_1 \\ n_2^* \end{bmatrix} \quad (3.54)$$

with $*$ being the complex conjugate. The same expression can be written even more compactly as

$$\mathbf{y} = \mathbf{H}\mathbf{x} + \mathbf{n} \quad (3.55)$$

where

- \mathbf{n} is the zero-mean circularly symmetric complex Gaussian noise vector whose covariance matrix is equal to \mathbf{I} .
- Rayleigh fading channel coefficients such that h_1, h_2, \tilde{h}_1 and \tilde{h}_2 are zero-mean circularly symmetric complex Gaussian random variables each with variance equal to σ_h^2 , i.e. $E[|h_1|^2] = E[|h_2|^2] = \sigma_h^2$ with $E[\cdot]$ denoting the expectation operator.
- Uncorrelated transmitting antennas such that h_1 and h_2 are independent, i.e. $E[h_1 h_2^*] = 0$.
- Correlated channel coefficients between the two symbol periods such that $E[h_1 \tilde{h}_1^*] = E[h_2 \tilde{h}_2^*] = \rho$ where ρ is the *complex* correlation factor with $|\rho|^2 \leq 1$. We stress the fact about ρ being complex as this is the general case as it will be shown in section 3.3.5. The correlated processes are generated using a first-order auto-regressive model as $\tilde{h}_i = \rho h_i + \sqrt{1 - \rho^2} w_i$ with w_i being again a zero-mean circularly symmetric complex Gaussian random variable with variance equal to σ_h^2 .
- \mathbf{x} a vector of Binary Phase-Shift Keying (BPSK) symbols with $x_i \in \{\pm 1\}$.

3.3.2 Diversity analysis of Maximum Likelihood detection

We are interested in determining the detection performances in case of selective channel by means of bit error probability. In this section we will, in particular, handle the case of ML detection using diversity analysis.

We assume the ML detector using the minimum vector norm

$$\mathbf{z}_{\text{ML}} = \arg \min_{\mathbf{x}} \|\mathbf{y} - \mathbf{H}\mathbf{x}\|^2 \quad (3.56)$$

As introduced in section 3.3, in the static case, i.e. $\rho = 1$ the optimal detection is obtained by the Matched Filter detector

$$\mathbf{z}_{\text{MF}} = \mathbf{H}^H \mathbf{y} \quad (3.57)$$

and applying hard decisions on each component on the output vector, namely $\hat{x}_i = \text{sign}(\hat{x}_i)$ where the *sign* operation is performed on the *real* component of x_i for BPSK case.

In the non-static case, i.e. with $\rho \neq 1$, it was shown in [81] that the MF detector is not optimal anymore while the ML detector is the only method which can optimally benefit of the diversity offered by the Alamouti code. Nevertheless, only simulations results were provided as a proof.

A more formal proof of the optimality of the ML detector without constraints on the correlation factor ρ can be made by computing upper and lower bounds on bit-error probability of ML detection. Although an exact ML bit-error probability would be definitive, we can come to the same conclusion by showing that upper and lower bounds still get all the diversity order especially in the asymptotic high Signal-to-Noise Ratio (SNR) regime.

ML detection upper bound

The Union Bound (UB) upper bounds the ML detection of equation (3.56) bit-error probability and corresponds to the sum of the *Pairwise* Error Probability (PEP) of

the error events:

$$P_b(e) \leq \sum_{\check{\mathbf{x}} \neq \mathbf{x}} \bar{P}(\mathbf{x} \rightarrow \check{\mathbf{x}}) \quad (3.58)$$

Note that the bit-error probability of (3.58) does not need to be averaged over all the possible transmitted vectors \mathbf{x} belonging to the constellation because of the symmetry of bit-error probabilities for BPSK. We can therefore compute the UB assuming a fixed transmitted symbol, $\mathbf{x} = [1 \ 1]^T$ for example, for the three only possible error events – $\check{\mathbf{x}}_1 = [1 \ 0]^T$, $\check{\mathbf{x}}_2 = [0 \ 1]^T$ and $\check{\mathbf{x}}_3 = [1 \ 1]^T$ – to give

$$P_b(e) \leq \bar{P}(\mathbf{x} \rightarrow \check{\mathbf{x}}_1) + \bar{P}(\mathbf{x} \rightarrow \check{\mathbf{x}}_2) + \bar{P}(\mathbf{x} \rightarrow \check{\mathbf{x}}_3) \quad (3.59)$$

By similar derivation as in [83], the PEP for a given channel realization \mathbf{H} can be found applying the Chernoff bound

$$P(\mathbf{x} \rightarrow \check{\mathbf{x}}_i) \leq e^{-\frac{\|\mathbf{H}(\mathbf{x} - \check{\mathbf{x}}_i)\|^2}{\sigma^2}} \quad (3.60)$$

Taking the expectation of (3.60) over the channel statistics, we obtain the following bound on the average PEP

$$\bar{P}(\mathbf{x} \rightarrow \check{\mathbf{x}}_i) = \mathbb{E}[P(\mathbf{x} \rightarrow \check{\mathbf{x}}_i)] \leq \frac{1}{\det(\mathbf{I} + \frac{1}{\sigma^2} \mathbf{R}_{\mathbf{w}_i \mathbf{w}_i})} \quad (3.61)$$

with $\mathbf{R}_{\mathbf{w}_i \mathbf{w}_i} = \mathbb{E}[\mathbf{w}_i \mathbf{w}_i^H]$ being the covariance matrix of $\mathbf{w}_i = \mathbf{H}(\mathbf{x} - \check{\mathbf{x}}_i)$.

In Alamouti case, the covariance matrices turn out to be as

$$\begin{aligned} \mathbf{R}_{\mathbf{w}_1 \mathbf{w}_1} &= \mathbf{R}_{\mathbf{w}_2 \mathbf{w}_2} = 4\sigma_h^2 \mathbf{I} \\ &\text{and} \\ \mathbf{R}_{\mathbf{w}_3 \mathbf{w}_3} &= 8\sigma_h^2 \mathbf{I} \end{aligned} \quad (3.62)$$

and, interestingly, independent of ρ .

Finally, substituting (3.62) in (3.61) and (3.59), an upper bound on the ML detection can be found to be

$$P_b(e) \leq P_b(e)^{UB} = \frac{2}{(1 + 2\gamma)^2} + \frac{1}{(1 + 4\gamma)^2} \quad (3.63)$$

where $\gamma = 2\sigma_h^2$ is the SNR.

From equation (3.63), the asymptotic bit-error probability [84] of the ML detector is derived as

$$P_b(e) \leq P_b(e)^{UB} \leq P_b(e)^{UB\infty} = \lim_{\gamma \rightarrow \infty} P_b^{UB}(e) = \frac{9}{16} \frac{1}{\gamma^2} \quad (3.64)$$

Asymptotic ML detection lower bound

An asymptotic lower bound for ML detection can be taken considering that

$$P_b(e) \geq \mathbb{E}[\max_i (P(\mathbf{x} \rightarrow \check{\mathbf{x}}_i))] \geq \max_i (\mathbb{E}[P(\mathbf{x} \rightarrow \check{\mathbf{x}}_i)]) \quad (3.65)$$

From equation the (3.63) and (3.65), the maximum PEP is clearly associated to the error events $\check{\mathbf{x}}_1$ and $\check{\mathbf{x}}_2$. An asymptotic lower bound for the ML detection can then be inferred as

$$P_b(e)^\infty = \lim_{\gamma \rightarrow \infty} P_b(e) \geq P_b(e)^{LB\infty} = \frac{1}{4} \frac{1}{\gamma^2} \quad (3.66)$$

Concluding remarks

The result of equation (3.64) are sufficient alone to prove that the ML detector is asymptotically optimal as the maximum diversity order available is 2 and the upper bound retrieve it and that a correlation factor $\rho \neq 1$ has no asymptotic impact on the ML detection.

Note that this result is general and not limited to the simplistic BPSK assumption taken here. That is because, for any constellation, an error event of the form $\mathbf{x} - \check{\mathbf{x}}_i = [a \ b]^T$ would always originate a covariance matrix $\mathbf{R}_{\mathbf{w}_i \mathbf{w}_i}$ being a multiple of an identity as

$$\begin{aligned} (\mathbf{R}_{\mathbf{w}\mathbf{w}})_{i,i} &= \sigma_h^2 (|a|^2 + |b|^2) \\ (\mathbf{R}_{\mathbf{w}\mathbf{w}})_{1,2} &= (\mathbf{R}_{\mathbf{w}\mathbf{w}})_{2,1} = \\ &= \mathbb{E}[(ah_1 + bh_2)(a\tilde{h}_2 - a\tilde{h}_1)] = 0 \end{aligned} \quad (3.67)$$

3.3.3 Decision-Feedback detection

The DF detection schemes are non-linear detectors that were shown to be sub-optimal in case of selectivity of channel [81] capable of only one order of diversity. Nevertheless, they are in general less complex than ML detector and in some cases could be preferred.

The studies on the effect of ordering on DF schemes in other fields such as MIMO detection [85] motivated us to verify the gain offered by ordering.

By applying the Whitening-Matched Filter to the received signal

$$\mathbf{z}_{WMF} = \mathbf{G}\mathbf{y} \quad (3.68)$$

where the WMF matrix is obtained by

$$\mathbf{G} = \mathbf{C}^{-H}\mathbf{H}^H \quad (3.69)$$

and \mathbf{C} is the Cholesky factor such that

$$\mathbf{C}^H\mathbf{C} = \mathbf{H}^H\mathbf{H} \quad (3.70)$$

Using (3.55), (3.69) and (3.68)

$$\mathbf{z}_{WMF} = \mathbf{C}\mathbf{x} + \mathbf{n}' \quad (3.71)$$

where \mathbf{n}' is a zero-mean circularly symmetric complex Gaussian noise vector distributed as \mathbf{n} .

Supposing \mathbf{C} upper triangular, the DF detection is performed by solving

$$\begin{aligned} \hat{x}_1 &= \text{sign}(z_1) \\ \hat{x}_2 &= \text{sign}\left(z_2 - (C)_{1,2}\hat{x}_1\right) \end{aligned} \quad (3.72)$$

since the diagonal elements of \mathbf{C} have the nice property of being *real* and *positive*.

It is worth noticing that the Cholesky factor corresponds exactly to the triangular matrix of the QR decomposition of the channel \mathbf{H} .

Actually two possible factorizations exist: an upper \mathbf{C}_U and a lower \mathbf{C}_L triangular matrices satisfying the expression (3.70). The straightforward derivation of the two factorizations from the 2×2 channel matrix \mathbf{H} is omitted.

The two factorizations can then be used to improve the classical DF scheme that blindly chooses one among the two possibilities.

The easiest option is to define an *ordered* DF (ODF) scheme exactly equivalent to (3.72) but where:

1. choose $\mathbf{C} = \mathbf{C}_U$ if $(\mathbf{C}_U)_{2,2} \geq (\mathbf{C}_L)_{1,1}$, otherwise choose $\mathbf{C} = \mathbf{C}_L$;
2. apply the classical DF scheme, permuting indexes in (3.72) if case \mathbf{C} is lower triangular.

Another option, at the expense of doubling the complexity, is to define a *parallel* DF (PDF) detector where two parallel DF detections according to (3.72) are executed for both \mathbf{C}_U and \mathbf{C}_L and the final estimate is constructed using as

$$\begin{aligned} \hat{x}_1 &= \hat{x}_1^L \\ \hat{x}_2 &= \hat{x}_2^U \end{aligned} \tag{3.73}$$

where $\hat{\mathbf{x}}^L$ and $\hat{\mathbf{x}}^U$ denote the estimated transmitted vectors obtained by lower and upper Cholesky DF respectively.

The reader is pointed at section 3.3.6 for a comparison in terms of performance of the two schemes with respect to classical DF detection. Nevertheless, it is worth mentioning that in *any* case these two modified DF schemes would be able to retrieve the bit-error probability sub-optimality in terms of diversity order but eventually in terms of coding gain (SNR offset) [84].

3.3.4 Lattice-Reduction Near-ML detection

The direct implementation to retrieve the maximum-likelihood estimate of Equation (3.56) is practically unfeasible due to the size of the search for large constellations and numbers of dimensions. A number of rather efficient near-ML algorithms, i.e.



Figure 3.16: Undisturbed received signals and decision regions of: (a) Maximum-Likelihood, (b) Linear ZF, (c) Decision-Feedback, (d) Lattice-Reduction aided ZF and (e) Lattice-Reduction aided Decision-Feedback detection.

Sphere Decoders, have been proposed in the context of MIMO detection [88] [89]. We instead choose a conceptually simpler approach based on Lattice Reduction (LR) solving any critical dependency on a parameter like the search radius. The noiseless received points in the communication scenario correspond to points of the *integer* lattice which depend on the chosen constellation and on the channel \mathbf{H} . Complex Lattice (basis) reduction [90] [91] optimizes the generating matrix of the lattice to obtain a *nicer* description of the lattice. The result is

$$\mathbf{H}_{red} = \mathbf{H}\mathbf{T} \quad (3.74)$$

where \mathbf{T} is a *unimodular* matrix, i.e. whose determinant is $|\det(\mathbf{T})| = 1$ and whose entries are integer complex values (and so is for \mathbf{T}^{-1} , too). As the basis change does not change the lattice, we can now interpret the noiseless received signal points as points in the lattice described by \mathbf{H}_{red} . Denoting $\mathbf{H} = [\mathbf{b}_1 \mathbf{b}_2]$, the algorithm to obtain \mathbf{H}_{red} is summarized in 3.17. It is worth noticing that the chosen algorithm is the *complex* extension of the well known LLL algorithm [86]. Moreover, in the Alamouti case (2×2 channel matrix case), it is totally equivalent to the Korkine-Zolotareff optimal method [87].

Figure 3.3.4 depicts the decision regions of noiseless received signal for classical ML, Linear ZF and LR aided method. Since the matrix \mathbf{H}_{red} has much *nicer* than \mathbf{H} , for instance with respect to inversion, it is easier to detect the transmitted symbol in this lattice when noise is present using a simple low-complexity detector. Having found these estimates, we can reverse the lattice basis change to obtain an estimate in the original lattice. Using the reduction of \mathbf{H} given in (3.74), we can write $\mathbf{H}_{red}^{-1} = \mathbf{T}^{-1}\mathbf{H}^{-1}$ to perform a linear Zero Forcing equalization aided by Lattice Reduction (LR-ZF). If we apply this matrix to the received signal of equation 3.55, we get

$$\mathbf{y}' = \mathbf{H}_{red}^{-1}\mathbf{y} = \mathbf{T}^{-1}\mathbf{x} + \mathbf{H}_{red}^{-1}\mathbf{n} \quad (3.75)$$

We see that the signal \mathbf{y}' contains the desired signal \mathbf{x} plus a noise term $\mathbf{H}_{red}^{-1}\mathbf{n}$.

```

INPUT:  $\mathbf{b}_1, \mathbf{b}_2$ 
OUTPUT:  $\mathbf{H}_{red}$ 
while  $ok = 0$  do
   $c = \mathbf{b}_1^H \mathbf{b}_2$ 
   $m = \mathbf{b}_1^H \mathbf{b}_1$ 
  if  $|\text{Re}(c)| > 0.5m$  OR  $|\text{Im}(c)| > 0.5m$  then
    # Reduce basis
     $\mathbf{b}_2 = \mathbf{b}_2 - \lfloor c/m \rfloor \mathbf{b}_1$ 
  end if
  if  $\mathbf{b}_2^H \mathbf{b}_2 > \mathbf{b}_1^H \mathbf{b}_1$  then
    # H is reduced
     $ok = 1$ 
  else
    # Swap basis
     $\mathbf{t} = \mathbf{b}_1$ 
     $\mathbf{b}_1 = \mathbf{b}_2$ 
     $\mathbf{b}_2 = \mathbf{t}$ 
  end if
end while
 $\mathbf{H}_{red} = [\mathbf{b}_1 \ \mathbf{b}_2]$ 

```

Figure 3.17: Complex Lattice Reduction LLL algorithm

Being the columns of \mathbf{H}_{red} are *rather* orthogonal, only relatively small noise enhancement and coloring is present.

Since $\mathbf{T}^{-1}\mathbf{1}$ contains only integer entries, the noiseless signal points $\mathbf{T}^{-1}\mathbf{x}$ lie on a distorted and scaled version of the original constellation. We can then quantize \mathbf{y}' to the constellation lattice. Finally, the estimates corresponding to the original signal points can be obtained by

$$\hat{\mathbf{x}} = \mathbf{T} \mathcal{Q}(\mathbf{y}') \quad (3.76)$$

where $\mathcal{Q}(\cdot)$ denotes the quantization operation to complex integer lattice values. This operation corresponds to the generalization for any constellation of $\text{sign}(\cdot)$ operator for BPSK case. As this quantization does not regard the boundary region of the constellation used for \mathbf{x} , the points obtained in $\hat{\mathbf{x}}$ stem from an *extended* version of the original constellation, and, in a final step, points that happen to lie outside the boundary region of the original constellation have to be assigned to the nearest point within the boundary region.

Note that instead of LR-ZF, decision-feedback equalization of $\mathbf{H}_{red}^{-1}\mathbf{n}$ is also possible. Hence, LR aided extension of methods introduced in 3.3.3 can be easily obtained by operating on \mathbf{H}_{red} rather than on \mathbf{H} to expect gain in error propagation. In the following, we shall then refer to Lattice-Reduction aided Decision-Feedback (LR-DF) to the method obtained by substituting \mathbf{H}_{red} in Equations (3.70),(3.69), (3.68) and, finally, (3.72). Similarly, we then indicate Lattice-Reduction aided Parallel Decision-Feedback (LR-PDF) to the method obtained from Equation (3.73) applying the substitution of \mathbf{H} into \mathbf{H}_{red} .

3.3.5 OFDM SFBC and STBC extension

As introduced in section 3.3, Alamouti block-codes naturally fit OFDM context because of the availability of orthogonal frequency flat channels with quasi-static properties and are well known to as SFBC and STBC. They are distinguished depending if the quasi-static channel property is assumed in *frequency* or *time* respectively.

Considering the OFDM SFBC case, the Channel Transfer Function (CTF) discretized into parallel channels at each sub-carrier is characterized in terms of correlation-bandwidth which is roughly proportional to the inverse of the Channel Impulse Response (CIR) length.

Hence, in case of sufficiently *short* CIR with respect to the cyclic prefix, the CTF over adjacent sub-carriers is strongly correlated and can then be used to convey Alamouti block-codes. The two symbol periods used for the block transmission are then transferred into pairs of neighboring sub-carriers to exploit the local quasi-static channel conditions.

While the correlation factor ρ is widely assumed as a *real* coefficient, it is easy to prove that in SFBC case the factor ρ is instead a complex value and can be obtained by the Power Delay Profile (PDP) \mathbf{p} of the tapped delay line of length L representing the channel as

$$\rho = \sum_{i=1}^L p_i e^{j2\pi \frac{i}{N}} \quad (3.77)$$

where N is the FFT order of the OFDM system in use.

In STBC case instead, the symbol periods to be used for Alamouti block-codes transmission are spanning the same sub-carrier over two neighboring OFDM symbols. The time-correlation of the time-varying channel in case of low relative speed between transmitter and receiver is exploited in this case.

In the assumption of classical Jakes Doppler spectrum the correlation factor ρ is *real* and given by

$$\rho = J_0(2\pi f_d T_s) \quad (3.78)$$

where $f_d = f_c v/c$ is the maximum Doppler frequency of a mobile unit with relative speed v for an OFDM system modulated around f_c carrier frequency, c is the speed of light constant and T_s is the OFDM symbol duration of the system (including the cyclic prefix).

3.3.6 Simulation results

The performances of the ML detector, the ML upper and lower bounds, the proposed modified DF schemes together with linear detectors such as MF and Zero-Forcing (ZF) and classical DF are plotted in Figure 3.18 for a correlation coefficient $\rho = 0$, in Figure 3.19 for a correlation coefficient $\rho = 0.5$ and in Figure 3.20 for a correlation coefficient $\rho = 0.9$.

We can first conclude that the upper and lower bounds confine the simulated

ML performances and confirm the analytical derivation. Furthermore, the optimality of the ML detector over all other classes of linear and non-linear estimators presented in the paper in case of selective channel appears evident: the ML detector being the only offering a bit-error probability curve whose slope decays by a factor of two, all other detectors suffer from a diversity penalty and can only enjoy of an order of one.

The proposed modified DF schemes outperform the classical DF detector and the gain offered by the *ordered*-DF and the *parallel*-DF can be evaluated in 3 dB and 5 dB respectively.

In Figure 3.21, we instead compare ML, Linear and DF schemes to Lattice-Reduction aided methods proposed (LR-ZF, LR-DF and LR-PDF) in terms of raw BER performance for 16-QAM modulation case and $\rho = 0.9$. We can notice that LR aided gather the full diversity and their performance stands close to ML. In this case DF methods do not show the the same coding gain improvement as for linear based methods and their performance differs of few points of dB. Nevertheless, the LR-PDF method outperforms all other methods proposed as expected.

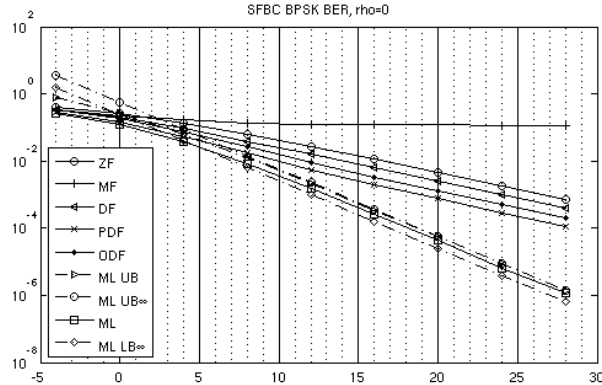


Figure 3.18: Performance of SFBC detectors in selective Rayleigh channel ($\rho = 0$).

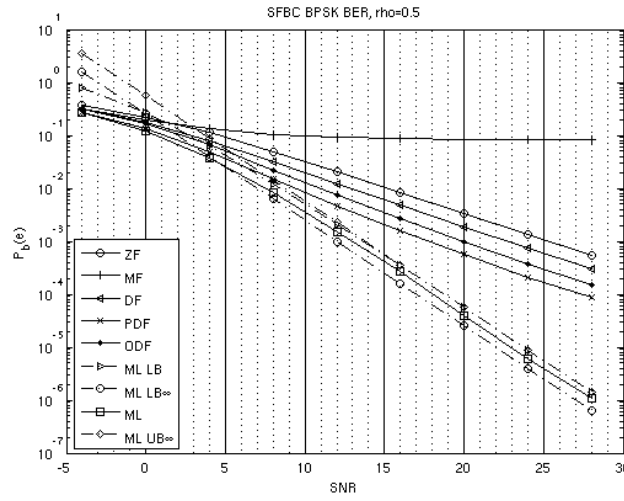


Figure 3.19: Performance of SFBC detectors in selective Rayleigh channel ($\rho = 0.5$).

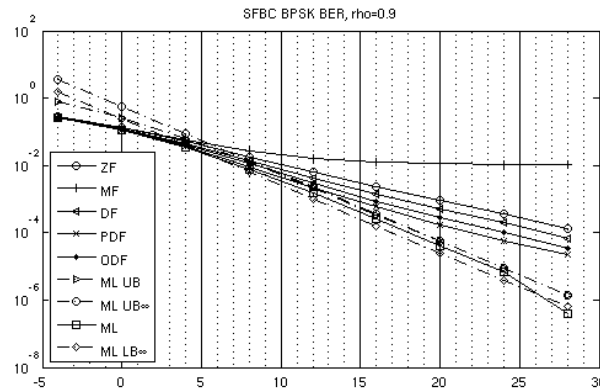


Figure 3.20: Performance of SFBC detectors in selective Rayleigh channel ($\rho = 0.9$).

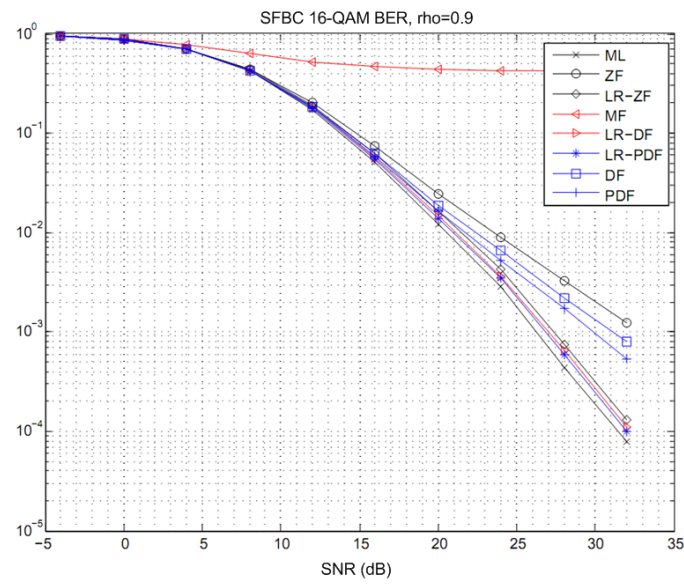


Figure 3.21: Performance of SFBC detectors in selective Rayleigh channel ($\rho = 0.9$).

Appendix A

Résumé de thèse

Slot duration [ms]	0.5					
Sub-carrier spacing Δf_{sc} [kHz]	15					
Transmission BW [MHz]	1.25	2.5	5	10	15	20
Sampling frequency [MHz]	1.92	3.84	7.68	15.36	23.04	30.72
FFT size N	128	256	512	1024	1536	2048
Occupied sub-carriers (including DC) K	76	151	301	601	901	1201

Table A.1: Paramètres de OFDMA en LTE.

A.1 Estimation de canal en LTE

Bien que le problème général d'estimation de canal en cas de transmissions à une seule antenne est bidimensionnel [26], c'est à dire qu'il doit être effectué en commun dans les domaines des fréquence et du temps, il est normalement divisé en deux étapes d'estimation unidimensionnels [27] pour la facilité de mise en oeuvre.

Dans ce contexte, nous nous intéressons en particulier au problème d'estimation de canal sur un symbole OFDMA (plus précisément le symbole contenant la RS) à fin d'exploiter les caractéristiques du domaine de la fréquence sans considérer ses caractéristiques de temps-variance en raison de l'effet Doppler.

Dans le contexte de l'OFDMA pour LTE, comme pour tout système OFDM avec pilotes distribués en peigne [52], la fonction de transfert du canal (CTF) \mathbf{z} est estimé par Maximum de Vraisemblance dans le domaine des fréquences sur les sous-porteuses des pilotes par décorrélation de la suite-pilote du signal de référence à module constant. Utilisant la notation matricielle, il peut être modélisé comme:

$$\hat{\mathbf{z}}_p = \mathbf{z}_p + \tilde{\mathbf{z}}_p = \mathbf{F}_p \mathbf{h} + \tilde{\mathbf{z}}_p \quad (\text{A.1})$$

where

- $P = \lceil K/M \rceil$ est le nombre de pilotes disponibles où K est le nombre de sous-porteuses occupées (y compris DC).
- \mathbf{h} est le vecteur $L \times 1$ de la réponse impulsionnelle du canal (CIR). La longueur du canal effectif $L \leq L_{CP}$ est supposée connue.
- \mathbf{F}_p est la matrice $P \times L$ obtenue en selectionnant les lignes correspondant aux positions des pilotes and les premières L colonnes de la matrice $N \times N$ de la transformée discrète de Fourier (DFT). La matrice dont les éléments sont $(\mathbf{F})_{n,k} = e^{-\frac{j2\pi}{N}(nk)}$ avec $0 \leq n \leq N - 1$ et $0 \leq k \leq N - 1$;

- $\tilde{\mathbf{z}}_p$ est le vecteur $P \times 1$ du bruit blanc complexe circulairement symétrique à moyenne zero dont la matrice $L \times L$ de covariance est $\mathbf{C}_{\tilde{\mathbf{z}}_p} = \sigma_{\tilde{\mathbf{z}}_p}^2 \mathbf{I}_L$;

A.1.1 Estimation de canal par interpolation

Estimateur par interpolation linéaire L'approche naturelle pour estimer l'ensemble de la CTF est d'interpoler l'estimation du CTF sur les positions des pilotes $\hat{\mathbf{Z}}_p$. Dans le cas général, \mathbf{A} est un filtre d'interpolation générique et l'estimation interpolée de la CTF peut être écrite comme:

$$\hat{\mathbf{z}}_i = \mathbf{A}\hat{\mathbf{z}}_p \quad (\text{A.2})$$

En substituant (A.1) in (A.2), l'erreur de l'estimation interpolée du CTF est:

$$\tilde{\mathbf{z}}_i = \mathbf{z} - \hat{\mathbf{z}}_i = (\mathbf{F}_L - \mathbf{A}\mathbf{F}_p) \mathbf{h} - \mathbf{A}\tilde{\mathbf{z}}_p \quad (\text{A.3})$$

où $\mathbf{z} = \mathbf{F}_L \mathbf{h}$ et \mathbf{F}_L est la matrice $N \times L$ obtenue en prenant les premières L colonnes de la matrice de la transformée de Fourier.

La matrice de covariance de l'erreur est:

$$\mathbf{C}_{\tilde{\mathbf{z}}_i} = (\mathbf{F}_L - \mathbf{A}\mathbf{F}_p) \mathbf{C}_h (\mathbf{F}_L - \mathbf{A}\mathbf{F}_p)^H + \sigma_{\tilde{\mathbf{z}}_p}^2 \mathbf{A}\mathbf{A}^H \quad (\text{A.4})$$

étant $\mathbf{C}_h = \mathbf{E}\mathbf{h}\mathbf{h}^H$ la matrice de covariance du canal, $\{\cdot\}^H$ and $\mathbf{E}\{\cdot\}$ désignant respectivement l'opérateur Hermitien et l'opérateur de l'attente.

Bien que un filtre de mise en forme de l'impulsion n'est pas obligatoire dans LTE, la première opération du récepteur est constituée d'un filtrage passe-bas d'anti-crénelage.

Par conséquent, le canal et sa matrice de covariance peuvent effectivement être modélisés comme:

$$\mathbf{h} = \mathbf{P}\mathbf{u} \quad \text{and} \quad \mathbf{C}_h = \mathbf{P}\mathbf{C}_u\mathbf{P}^H \quad (\text{A.5})$$

où \mathbf{P} est la matrice de filtrage de la forme d'impulsion, \mathbf{u} est le vecteur du canal multi-trajet et

$$\mathbf{C}_u = \mathbf{E}\mathbf{u}\mathbf{u}^H = \text{diag} \left(\sigma_{u_0}^2, \sigma_{u_1}^2, \dots, \sigma_{u_{L_{MP}-1}}^2 \right)$$

est la matrice de covariance diagonale normalement assimilée au profil de retard de puissance du canal (PDP).

Rappelant l'équation (A.2), l'interpolation linéaire serait le choix intuitif. La structure du filtre \mathbf{A} est alors donnée par

$$\mathbf{A} = \begin{bmatrix} 0 & 0 & \cdots & 0 & 0 \\ 0 & 0 & \cdots & 0 & 0 \\ 0 & 0 & \cdots & 0 & 0 \\ 1 & 0 & \cdots & 0 & 0 \\ \frac{M-1}{M} & \frac{1}{M} & 0 & \cdots & 0 \\ \frac{M-2}{M} & \frac{2}{M} & 0 & \cdots & 0 \\ \vdots & \vdots & \vdots & \vdots & 0 \\ \frac{1}{M} & \frac{M-1}{M} & 0 & \cdots & 0 \\ 0 & 1 & 0 & \cdots & 0 \\ 0 & \frac{M-1}{M} & \frac{1}{M} & \cdots & 0 \\ 0 & \frac{M-2}{M} & \frac{2}{M} & 0 & 0 \\ 0 & \vdots & \vdots & \vdots & 0 \\ 0 & \frac{1}{M} & \frac{M-1}{M} & 0 & 0 \\ 0 & 0 & 1 & \cdots & 0 \\ \vdots & \vdots & \vdots & \vdots & 0 \\ 0 & 0 & \cdots & 0 & 0 \\ 0 & 0 & \cdots & 0 & 0 \\ 0 & 0 & \cdots & 0 & 0 \end{bmatrix} \quad (\text{A.6})$$

Cet estimateur est déterministiquement biaisé, mais non biaisée du point de vue bayésien indépendamment de la structure de \mathbf{A} .

IFFT estimator La deuxième approche naturelle pour récupérer l'ensemble estimation FCT est par IFFT interpolation. L'estimation du CTF par interpolation *IFFT* sur toutes les sous-porteuses peut être obtenu en utilisant dans (A.2):

$$\mathbf{A} = \frac{1}{P} \mathbf{F}_L \mathbf{F}_P^H \quad (\text{A.7})$$

Ainsi, l'estimateur par *IFFT* est donné par:

$$\hat{\mathbf{z}}_{\text{IFFT}} = \frac{1}{P} \mathbf{F}_L \mathbf{F}_p^H \hat{\mathbf{z}}_p \quad (\text{A.8})$$

L'erreur de l'estimé par interpolation *IFFT* et sa matrice de covariance, appliquant (A.1) etnd (A.7) into (A.2), deviennent:

$$\tilde{\mathbf{z}}_{\text{IFFT}} = \mathbf{F}_L \left(\mathbf{I}_L - \frac{1}{P} \mathbf{F}_p^H \mathbf{F}_p \right) \mathbf{h} - \frac{1}{P} \mathbf{F}_L \mathbf{F}_p^H \tilde{\mathbf{z}}_p \quad (\text{A.9})$$

$$\mathbf{C}_{\tilde{\mathbf{z}}_{\text{IFFT}}} = \left(\mathbf{F}_L - \frac{1}{P} \mathbf{F}_L \mathbf{F}_p^H \mathbf{F}_p \right) \mathbf{C}_h \left(\mathbf{F}_L - \frac{1}{P} \mathbf{F}_L \mathbf{F}_p^H \mathbf{F}_p \right)^H + \frac{1}{P^2} \sigma_{\tilde{\mathbf{z}}_p}^2 \mathbf{F}_L \mathbf{F}_p^H \mathbf{F}_p \mathbf{F}_L^H \quad (\text{A.10})$$

Dans l'approximation de $\mathbf{I}_L \approx \frac{1}{P} \mathbf{F}_p^H \mathbf{F}_p$, estimateur serait biaisé et sa matrice de covariance d'erreur réduirait à:

$$\mathbf{C}_{\tilde{\mathbf{z}}_{\text{IFFT}}} \approx \frac{1}{P} \sigma_{\tilde{\mathbf{z}}_p}^2 \mathbf{F}_L \mathbf{F}_L^H \quad (\text{A.11})$$

Compte tenu des paramètres du système LTE et la structure pilote, dans la pratique, $\frac{1}{P} \mathbf{F}_p^H \mathbf{F}_p$ est loin d'être un multiple d'une matrice identité: le rapprochement serait une égalité lorsque $K = N, N/M > L$ et N/M étant un nombre entier: autrement dit, le système doit être dimensionné sans garde-bandes et les pilotes doivent être disposé avec un espacement qui est divisant exactement l'ordre de la FFT N , notamment une puissance de deux. Donc, en accordance avec (A.9), l'estimateur $\hat{\mathbf{z}}_{\text{IFFT}}$ est biaisé comme dans le cas de l'interpolation linéaire Si le canal est déterministe et non biaisé du point de vue bayésien. Nous renvoyons à la section des résultats de simulation de ce document pour une comparaison de leurs performances respectives.

A.1.2 Une approche général à l'estimation linéaire de canal

Par rapport aux approches simples présentés dans la section précédente, les estimateurs linéaires plus élaborés dérivés à la fois du point de vue déterministe et du

point de vue statistique proposée dans [53], [54] et [55], à savoir LS, LS régularisée, MMSE MMSE, en plus des nouveaux estimateurs présentés dans les sections suivantes, peuvent tous être exprimés sous la formulation générale:

$$\hat{\mathbf{z}}_{\text{gen}} = \mathbf{B} (\mathbf{G}^H \mathbf{G} + \mathbf{R})^{-1} \mathbf{G}^H \hat{\mathbf{z}}_{\text{p}} \quad (\text{A.12})$$

où \mathbf{B} , \mathbf{G} et \mathbf{R} sont des matrices qui varient en fonction de chaque estimateur tel que décrit ci-après. Avec (A.1) et (A.12), on obtient l'expression d'erreur:

$$\tilde{\mathbf{z}}_{\text{gen}} = \left(\mathbf{F}_L - \mathbf{B} (\mathbf{G}^H \mathbf{G} + \mathbf{R})^{-1} \mathbf{G}^H \mathbf{F}_p \right) \mathbf{h} - \mathbf{B} (\mathbf{G}^H \mathbf{G} + \mathbf{R})^{-1} \mathbf{G}^H \tilde{\mathbf{z}}_{\text{p}} \quad (\text{A.13})$$

et sa matrice de covariance:

$$\begin{aligned} \mathbf{C}_{\tilde{\mathbf{z}}_{\text{gen}}} &= \left(\mathbf{F}_L - \mathbf{B} (\mathbf{G}^H \mathbf{G} + \mathbf{R})^{-1} \mathbf{G}^H \mathbf{F}_p \right) \mathbf{C}_h \left(\mathbf{F}_L - \mathbf{B} (\mathbf{G}^H \mathbf{G} + \mathbf{R})^{-1} \mathbf{G}^H \mathbf{F}_p \right)^H + \\ &\quad + \sigma_{\tilde{\mathbf{z}}_{\text{p}}}^2 \mathbf{B} (\mathbf{G}^H \mathbf{G} + \mathbf{R})^{-1} \mathbf{G}^H \mathbf{G} (\mathbf{G}^H \mathbf{G} + \mathbf{R}^H)^{-1} \mathbf{B}^H \end{aligned} \quad (\text{A.14})$$

LS estimator L'estimateur LS discuté dans [53] peut être déduit en choisissant:

$$\mathbf{B} = \mathbf{F}_L, \mathbf{G} = \mathbf{F}_p \text{ and } \mathbf{R} = \mathbf{0}_L \quad (\text{A.15})$$

avec $\mathbf{0}_L$ étant la matrice $L \times L$ contenant zeros. Et l'estimateur apparait comme:

$$\hat{\mathbf{z}}_{\text{LS}} = \mathbf{F}_L (\mathbf{F}_p^H \mathbf{F}_p)^{-1} \mathbf{F}_p^H \hat{\mathbf{z}}_{\text{p}} \quad (\text{A.16})$$

En substituant (A.1) et (A.15) en (A.13) et (A.14), l'erreur se réduit à:

$$\tilde{\mathbf{z}}_{\text{LS}} = -\mathbf{F}_L (\mathbf{F}_p^H \mathbf{F}_p)^{-1} \mathbf{F}_p^H \tilde{\mathbf{z}}_{\text{p}} \quad (\text{A.17})$$

montrant que l'estimateur LS, au moins théoriquement, est non biaisé. Ainsi, par rapport à l'estimateur d'interpolation linéaire donné par (A.2), l'estimateur LS est considéré comme l'interpolateur idéal car il remet à zéro le terme de biais de l'expression (A.3) avec $\mathbf{A} = \mathbf{F}_L (\mathbf{F}_p^H \mathbf{F}_p)^{-1} \mathbf{F}_p^H$. Par conséquent, la matrice de covariance d'erreur peut être démontré:

$$\mathbf{C}_{\tilde{\mathbf{z}}_{\text{LS}}} = \sigma_{\tilde{\mathbf{z}}_{\text{p}}}^2 \mathbf{F}_L (\mathbf{F}_p^H \mathbf{F}_p)^{-1} \mathbf{F}_L^H \quad (\text{A.18})$$

Estimateur LS Regularisé Comme en témoigne [55], les paramètres du système LTE font l'estimateur LS inapplicable: l'expression $(\mathbf{F}_p \mathbf{F}_p^H)^{-1}$ est mal conditionné en raison de la grande partie inutilisée du spectre correspondant aux sous-porteuses non modulées. Pour contrer ce problème, le robuste estimateur LS *régularisé* a été utilisée pour obtenir un meilleur conditionnement de la matrice à inverser en utilisant la même \mathbf{B} et \mathbf{G} que pour l'estimateur LS mais en introduisant la matrice de régularisation $\mathbf{R} = \alpha \mathbf{I}_L$ avec α une constante choisie (offline) pour optimiser la performance de l'estimateur dans une plage de rapport signal-bruit (SNR) donné. Par conséquent, nous pouvons écrire l'estimateur comme suit:

$$\hat{\mathbf{z}}_{\text{reg,LS}} = \mathbf{F}_L (\mathbf{F}_p^H \mathbf{F}_p + \alpha \mathbf{I}_L)^{-1} \mathbf{F}_p^H \hat{\mathbf{z}}_p \quad (\text{A.19})$$

Les expressions de l'erreur et de la matrice de covariance d'erreur de cet estimateur peuvent être déduites directement à partir de (A.13) et (A.14) en remplaçant \mathbf{B} , \mathbf{G} et \mathbf{R} avec leurs expressions correspondantes.

Estimation LS par sous-échantillonnage de la réponse impulsionnelle du canal Une autre solution peut être trouvée lors de l'enquête les raisons du problème de conditionnement malade: la motivation vient de la non-excitation d'une grande partie de la bande qui vient de la structure de symbole OFDM LTE. Considérant par exemple le cas d'un A.1, taille du symbole N égal à 1024 du tableau, on obtient que le nombre de sous-porteuses modulées est de seulement 600. Ainsi, alors que la fréquence d'échantillonnage est de 15,36 MHz ($N\Delta f_c$), la bande passante occupée est à seulement 9 MHz ($N_m\Delta f_c$). il s'ensuit que le canal est estimé dans l'ensemble 15,36 MHz échantillonnage bande passante alors que seuls les sous-porteuses modulées sont excités (9 MHz). Le canal peut en effet être sonné uniquement dans le excité bande. Pour ce faire, la *bande passante numérique*, ce qui est considéré comme étant le rapport entre la largeur de bande occupée et l' la fréquence d'échantillonnage, doit être portée à un peu moins que 1. Cela peut se faire en diminuant la fréquence d'échantillonnage utilisée pour la représentation numérique de la chane d'un facteur 2/3 ce qui garantit l'absence d'aliasing donnant un échantillonnage résultant fréquence de 10.24 MHz. Pratiquement, le canal H n'est pas estimé dans tous les coefficients L mais seulement dans 2 des 3 coefficients (obtenenant un facteur de sous-échantillonnage moyen 2/3) et la mise à 0 de ceux mis à rebut:

$$\bar{\mathbf{h}} = (h_0 \ h_1 \ 0 \ h_3 \ h_4 \ 0 \ \dots \ h_{L-1})^T \quad (\text{A.20})$$

En fait, l'égalisation de canal dans le système OFDM n'est pas effectuée dans

le domaine temporel, mais dans le domaine des fréquences. Par conséquent, il n'importe pas d'avoir une représentation exacte dans le domaine du temps du canal à la fréquence d'échantillonnage réelle. Ce qui est important est la fonction de transfert de canal dans la bande d'intérêt.

$$\mathbf{z} = \mathbf{F}_L \bar{\mathbf{h}} =$$

$$= \begin{bmatrix} 1 & 1 & 1 & 1 & 1 \\ 1 & w^1 & w^2 & \dots & w^{(L-1)} \\ 1 & w^2 & w^3 & \dots & w^{2(L-1)} \\ 1 & w^3 & w^6 & \dots & w^{3(L-1)} \\ 1 & w^4 & w^8 & \dots & w^{4(L-1)} \\ 1 & w^5 & w^{10} & \dots & w^{5(L-1)} \\ \vdots & \vdots & \vdots & \vdots & \vdots \\ 1 & w^{N-1} & w^{2(N-1)} & \dots & w^{(L-1)(N-1)} \end{bmatrix} \begin{bmatrix} h_0 \\ h_1 \\ 0 \\ h_3 \\ h_4 \\ 0 \\ \vdots \\ h_{L-1} \end{bmatrix} \quad (\text{A.21})$$

$$\mathbf{z} = \mathbf{F}_L^{DS} \mathbf{h}^{DS} =$$

$$= \begin{bmatrix} 1 & 1 & 1 & 1 & 1 \\ 1 & w^1 & w^3 & \dots & w^{(L-1)} \\ 1 & w^2 & w^6 & \dots & w^{2(L-1)} \\ 1 & w^3 & w^9 & \dots & w^{3(L-1)} \\ 1 & w^4 & w^{12} & \dots & w^{4(L-1)} \\ 1 & w^5 & w^{15} & \dots & w^{5(L-1)} \\ \vdots & \vdots & \vdots & \vdots & \vdots \\ 1 & w^{N-1} & w^{3(N-1)} & \dots & w^{(L-1)(N-1)} \end{bmatrix} \begin{bmatrix} h_0 \\ h_1 \\ h_3 \\ h_4 \\ \vdots \\ h_{L-1} \end{bmatrix} \quad (\text{A.22})$$

$$w = e^{\frac{j2\pi}{N}} \quad (\text{A.23})$$

Comme l'a montré (A.21) et (A.22), cette approche se révèle être comme la représentation du signal reçu, les $\frac{L}{3}$ colonnes de la matrice de Fourier \mathbf{F}_L correspondant à la négligence coefficients sont multipliées par 0, de sorte que le domaine temporel le signal reçu peut être représenté en tant que:

$$\mathbf{r} = \mathbf{F}_L^H \mathbf{F}_L^{DS} \mathbf{h}^{DS} + \mathbf{w} \quad (\text{A.24})$$

o ù \mathbf{h}^{DS} est la version sous-échantillonnée du canal FIR représenté avec une longueur du vecteur résultant en $\frac{2}{3}L$. Analoguement \mathbf{F}_L^{DS} est égale à la matrice de Fourier \mathbf{F}_L o ù les colonnes correspondantes aux coefficients mis à zéro de h sont enlevées.

Encore une fois, le critère LS peut être appliqué pour obtenir l'expression de l'estimation LS du canal sous-échantillonné :

$$\hat{\mathbf{h}}_{ds} = (\mathbf{F}_p^{DS,H} \mathbf{F}_p^{DS})^{-1} \mathbf{F}_p^{DS,H} \hat{\mathbf{z}}_p \quad (\text{A.25})$$

En utilisant la matrice de Fourier correspondant à la voie sous-échantillonnée, le problème du mauvais conditionnement est résolu et en outre un gain de complexité est obtenu en raison de la taille de la matrice $(\mathbf{F}_p^{DS,H} \mathbf{F}_p^{DS})^{-1} \mathbf{F}_p^{DS,H}$ qui se révèle être $\frac{2}{3}L \times N$.

Estimateur MMSE En utilisant les équations (A.12), (A.13) et (A.14), on peut reformuler l'estimateur MMSE [53] par:

$$\mathbf{B} = \mathbf{F}_L, \mathbf{G} = \mathbf{F}_p \text{ and } \mathbf{R} = \sigma_{\mathbf{z}_p}^2 \mathbf{C}_h^{-1} \quad (\text{A.26})$$

donnant ainsi

$$\hat{\mathbf{z}}_{\text{MMSE}} = \mathbf{F}_L \left(\mathbf{F}_p^H \mathbf{F}_p + \sigma_{\mathbf{z}_p}^2 \mathbf{C}_h^{-1} \right)^{-1} \mathbf{F}_p^H \hat{\mathbf{z}}_p \quad (\text{A.27})$$

Encore, en appliquant (A.1) et (A.26) en (A.13) et (A.14), on obtient l'erreur de l'estimateur comme:

$$\tilde{\mathbf{z}}_{\text{MMSE}} = \mathbf{F}_L \left(\mathbf{I}_L - \left(\mathbf{F}_p^H \mathbf{F}_p + \sigma_{\mathbf{z}_p}^2 \mathbf{C}_h^{-1} \right)^{-1} \mathbf{F}_p^H \mathbf{F}_p \right) \mathbf{h} - \mathbf{F}_L \left(\mathbf{F}_p^H \mathbf{F}_p + \sigma_{\mathbf{z}_p}^2 \mathbf{C}_h^{-1} \right)^{-1} \mathbf{F}_p^H \tilde{\mathbf{z}}_p \quad (\text{A.28})$$

et la matrice de covariance:

$$\begin{aligned} \mathbf{C}_{\tilde{\mathbf{z}}_{\text{MMSE}}} = & \mathbf{F}_L \left(\mathbf{I}_L - \left(\mathbf{F}_p^H \mathbf{F}_p + \sigma_{\mathbf{z}_p}^2 \mathbf{C}_h^{-1} \right)^{-1} \mathbf{F}_p^H \mathbf{F}_p \right) \mathbf{C}_h \\ & \left(\mathbf{I}_L - \left(\mathbf{F}_p^H \mathbf{F}_p + \sigma_{\mathbf{z}_p}^2 \mathbf{C}_h^{-1} \right)^{-1} \mathbf{F}_p^H \mathbf{F}_p \right)^H \mathbf{F}_L^H + \\ & + \sigma_{\mathbf{z}_p}^2 \mathbf{F}_L \left(\mathbf{F}_p^H \mathbf{F}_p + \sigma_{\mathbf{z}_p}^2 \mathbf{C}_h^{-1} \right)^{-1} \mathbf{F}_p^H \mathbf{F}_p \left(\mathbf{F}_p^H \mathbf{F}_p + \sigma_{\mathbf{z}_p}^2 \mathbf{C}_h^{-1} \right)^{-1} \mathbf{F}_L^H \end{aligned} \quad (\text{A.29})$$

Estimateur MMSE desadapté Pour éviter l'estimation du canal des statistiques de second ordre \mathbf{C}_h et l'inversion en ligne d'une matrice $rmL \text{ times } L$ nécessaire à l'application pure et simple du MMSE de (A.27), la PDP du canal peut être supposée uniforme [54]. Ainsi, dans cette formulation *desadaptée* du MMSE, \mathbf{C}_h est imposée pour avoir la structure d'une matrice d'identité.

En référence à la formulation générale dans (A.12), ce approche consiste à prendre le même \mathbf{B} et \mathbf{G} de (A.26) mais en définissant $\mathbf{R} = \sigma_{\mathbf{z}_p}^2 / \sigma_h^2 \cdot \mathbf{I}_L$ pour donner l'expression

$$\hat{\mathbf{z}}_{\text{M-MMSE}} = \mathbf{F}_L \left(\mathbf{F}_p^H \mathbf{F}_p + \sigma_{\mathbf{z}_p}^2 / \sigma_h^2 \cdot \mathbf{I}_L \right)^{-1} \mathbf{F}_p^H \hat{\mathbf{z}}_p \quad (\text{A.30})$$

Fait intéressant, on constate que cet estimateur est en pratique équivalent à l'estimateur LS *régularisé* A.1.2. où la seule différence réside dans le fait que le rapport $\sigma_{\mathbf{z}_p}^2 / \sigma_h^2$ peut être estimée et donc adaptée. Pour une longueur rmL de canal donné, afin d'éviter l'inversion en ligne de la matrice $\left(\mathbf{F}_p^H \mathbf{F}_p + \sigma_{\mathbf{z}_p}^2 / \sigma_h^2 \cdot \mathbf{I}_L \right)$, l'approche pratique consisterait à diviser la plage de travail du SNR en sous-gammes et en stockant différentes versions de la matrice inversée hors ligne pour chaque sous-gamme. La formulation du MMSE désadaptée offre l'avantage que les coefficients de filtrage peuvent être calculées pour être des nombres réels parce que le PDP uniforme est symétrique. En effet, les coefficients de filtrage réels peuvent être utilisés lorsque le symbole OFDM est correctement synchronisé pour couvrir la moitié de CP de chaque cté, en réduisant fortement la complexité. En outre, puisque la longueur du canal est faible par rapport à la taille de la FFT, la matrice A_{gen} peut être considéré comme *faible densité* ne stockant que les coefficients significatifs pour réduire encore considérablement la complexité. LTE ne pas mettre en oeuvre un modèle de symboles de référence uniforme exact: en particulier, ce n'est pas le cas partout dans le DC où les symboles de référence sont inégalement espacées. Cela implique qu'un plus grand nombre de coefficients doivent être stockés.

Estimateur MMSE désadapté Exponentiel PDP de canal ééalistes sont susceptibles de décroissance exponentielle plutt que uniforme comme le suppose le MMSE *désadapté* discuté ci-dessus. Nous proposons donc une estimateur MMSE *désadapté exponentiel* qui se rapproche de \mathbf{C}_h par une matrice diagonale dont les entrées sont de forme exponentielle. Ceci est fait en utilisant (A.26) et prenant:

$$\mathbf{R} = \frac{\sigma_{\mathbf{z}_p}^2}{\sigma_h^2} \mathbf{C}_{L,\text{exp}}^{-1} \text{ and } \mathbf{C}_{L,\text{exp}} = \gamma \cdot \text{diag} \left(e^{-n \frac{\ln(2L)}{L}} \right) \quad (\text{A.31})$$

avec $0 \leq n \leq L - 1$ and $\gamma = 1 / \sum_{n=0}^{L-1} e^{-n \frac{\ln(2L)}{L}}$. Ainsi, il est représenté par:

$$\hat{\mathbf{z}}_{\text{exp-MMSE}} = \mathbf{F}_L \left(\mathbf{F}_p^H \mathbf{F}_p + \frac{\sigma_{z_p}^2}{\sigma_h^2} \mathbf{C}_{L,\text{exp}}^{-1} \right)^{-1} \mathbf{F}_p^H \hat{\mathbf{z}}_p \quad (\text{A.32})$$

À nouveau, l'erreur et la matrice de covariance d'erreur peuvent être déduites de (A.13) et (A.14) en remplaçant \mathbf{B} , \mathbf{G} et \mathbf{R} avec leurs expressions correspondantes.

Par rapport à l'hypothèse de la distribution de canal uniforme d'avant, l'estimateur révèle être moins sensible à la longueur de canal et a sa mauvaise estimation due à sa nature exponentielle décroissante et donc moins de versions de l'inverse de la matrice $\left(\mathbf{F}_p^H \mathbf{F}_p + \frac{\sigma_{z_p}^2}{\sigma_h^2} \mathbf{C}_{L,\text{exp}}^{-1} \right)$ doivent être calculées et stockées.

Estimateur MMSE simplifié Comme déjà mentionné, la mise en oeuvre directe de l'estimateur MMSE dans (A.27) exige la solution de deux problèmes:

1. L' estimation de la variance du bruit et des statistiques de deuxième ordre du canal;
2. L'inversion on-line inversion d'une large matrice $L \times L$

$$\mathbf{S}_{\text{MMSE}} = \mathbf{F}_p^H \mathbf{F}_p + \sigma_{z_p}^2 \mathbf{C}_h^{-1} \quad (\text{A.33})$$

chaque fois que la statistique du canal et du bruit changent.

En supposant que les estimations nécessaires disponibles, Nous proposons ici une solution originale à surmonter en particulier le deuxième problème. L'idée derrière notre estimateur MMSE simplifiée réside dans séparer le problème du rapprochement de (A.33) en, d'abord, l'examen d'une initialisation fixe matrice $\mathbf{S}_{\text{initialisation}}$, comme détaillé ci-dessous, puis dans l'amélioration de la première approximation par l'insertion, l'apport d'une partie du PDP correspondant aux coefficients forts, notés *coefficients capturés* dans ce qui suit, sur la diagonale de l'initialisation matrice $\mathbf{S}_{\text{initialisation}}$. Quant aux méthodes approximées précédentes,

la dépendance de la variance du bruit peut être maintenue par la quantification du SNR en sous-gammes et stocker un ensemble limité de valeurs de $\mathbf{S}_{\text{initialisation}}$. Nous définissons:

$$\mathbf{S}_{\text{init}} = \mathbf{F}_p^H \mathbf{F}_p + \sigma_{\mathbf{z}_p}^2 \mathbf{C}_{\text{init}}^{-1} \quad (\text{A.34})$$

où $\mathbf{C}_{\text{initialisation}} = \beta \mathbf{I}_L$ et β est une constante soigneusement choisie pour fournir une performance suffisamment bonne de l'estimateur.

La matrice \mathbf{S}_{MMSE} peut être approchée par:

$$\mathbf{S}_{\text{SMMSE}} = \mathbf{S}_{\text{init}} + \mathbf{D} \Delta \mathbf{S} \mathbf{D}^H \quad (\text{A.35})$$

où

1. \mathbf{D} est une matrice sélecteur $L \times M$ appelée après le rôle qu'elle joue dans la sélection des positions où les éléments du profil de PDP (qui correspondent aux M trajets capturés) vont être situés sur la diagonale de $\mathbf{S}_{\text{initialisation}}$. La première colonne de la matrice \mathbf{D} contient un 1 dans la position qui correspond à l'indice du premier trajet capturé et zéros partout ailleurs et la seconde colonne contient un 1 seulement dans la position qui correspond à l'indice du second trajet capturé et de zéros ailleurs. Et ainsi de suite.
2. $\Delta \mathbf{S}$ est une matrice diagonale contenant l'inverse de la puissance des coefficients capturés après élimination de l'effet de l'initialisation, à savoir $\Delta \mathbf{S}_{m,m} = \sigma_{\mathbf{z}_p}^2 (\mathbf{C}_{\mathbf{h}_m}^{-1} - \beta^{-1})$ où \mathbf{h}_m est un vecteur qui contient les M coefficients capturés.

Appliquant, le *Lemme d'inversion de matrice*, on peut écrire:

$$\mathbf{S}_{\text{SMMSE}}^{-1} = \mathbf{S}_{\text{init}}^{-1} - \mathbf{S}_{\text{init}}^{-1} \mathbf{D} (\mathbf{D}^H \mathbf{S}_{\text{init}}^{-1} \mathbf{D} + \Delta \mathbf{S}^{-1})^{-1} \mathbf{D}^H \mathbf{S}_{\text{init}}^{-1} \quad (\text{A.36})$$

Il est à noter que le nombre de taps importants en termes de puissance est en général très inférieur à la longueur totale du canal. Ainsi, l'importance de l'estimateur proposé découle du fait que nous profitons de cette propriété pour réduire la taille de la matrice à inverser en ligne à partir de $L \times L$ à $M \times M$ avec $M \ll L$. Sachant que le nombre d'opérations nécessaires pour inverser une matrice est proportionnelle au cube de sa taille, nous en déduisons que notre estimateur réduit de manière

significative (à partir de L^3 à M^3), la puissance de calcul par rapport à la méthode traditionnelle.

Un autre aspect important de l'estimateur proposé est que la précision de l'approximation peut être balancée avec le complexité en contrlant le nombre de coefficients capturées. Par conséquent, plus le nombre des taps capturés est grand plus est grande la taille de la matrice à inverser en ligne et vice versa.

Enfin, le CTF estimé est donné par:

$$\hat{\mathbf{z}}_{\text{SMMSE}} = \mathbf{F}_L \mathbf{S}_{\text{SMMSE}}^{-1} \hat{\mathbf{z}}_p \quad (\text{A.37})$$

En comparant (A.37) avec (A.12), le MMSE *Simplifié* consiste dans le choix de:

$$\mathbf{B} = \mathbf{F}_L, \mathbf{G} = \mathbf{F}_p \text{ and } \mathbf{R} = \sigma_{\hat{\mathbf{z}}_p}^2 \mathbf{C}_{\text{init}}^{-1} + \mathbf{D} \Delta \mathbf{S} \mathbf{D}^H \quad (\text{A.38})$$

Les expressions de l'erreur et de sa matrice de covariance peuvent être obtenue en substituant (A.38) en (A.13) et (A.14).

A.1.3 Résultats de simulation

Nous comparons les performances des estimateurs par moyen de l'erreur quadratique moyen normalisé *tronqué* (TNMSE). Pour chaque estimateur $\hat{\mathbf{Z}}$, le TNMSE est calculée à partir de sa matrice de covariance $\mathbf{C}_{\hat{\mathbf{z}}}$ et le vrai canal $\mathbf{H} = \mathbf{F}_L \mathbf{h}$ en utilisant les expressions suivantes:

$$\text{TNMSE}_{\hat{\mathbf{z}}} = \frac{\text{Ttr}(\mathbf{C}_{\hat{\mathbf{z}}})}{\text{Ttr}(\mathbf{F}_L \mathbf{C}_h \mathbf{F}_L^H)} \quad (\text{A.39})$$

où avec $\text{Ttr}\{\cdot\}$ on dénote l'operatuer tronqué de trace consistant de la matric de covariance *tronquée* en considerant seulement les K sous-porteuses utilisées.

Pour comparaison, dans la figure A.2, on utilise un filtre de pulse-shaping de la forme *raised-cosine* avec un facteur de roll-off de $\beta = 0.2$, le canal SCMA et un setup LTE pour 10 MHz de bande [28]. Pour ce qui concerne l'estimateur LS régularisé, on utilise un terme de *regularization* égale à $\alpha = 0.1$. Les lignes connectées représentent le TNMSE théorique pendant que les points représentent les résultats de simulation. On peut tout de suite conclure que les méthodes *IFFT* et d'interpolation linéaires ont les moindres performances.

En outre, l'estimateur LS *régularisé* et le MMSE *désadapté* s'avèrent performer exactement à égalité et la courbe TNMSE de ce dernier est donc omise dans la figure A.2. L'estimateur MMSE *désadapté exponentiel* et le MMSE *simplifiée* offrent un gain de performances sur tous les autres estimateurs sous-optimaux mais celui-ci se révèle être meilleur dans la région de faible SNR.

Pour mettre en évidence la robustesse de notre MMSE *simplifiée*, la figure A.3 compare sa performance à celle de du MMSE *désadapté* où le MMSE est utilisé en tant que référence.

Le TNMSE calculée sur l'ensemble des sous-porteuses cache en réalité le comportement de chaque estimateur pour un problème bien connu pour des techniques agissantes dans le domaine fréquentiel: l'effet de bande-garde. Ceci peut être représenté par le phénomène de Gibbs [66] dans l'approximation d'une série de Fourier de longueur finie; suivant cette approche, la figure A.1 montre que l'estimation de canal MMSE basée souffre le moins de dégradation aux bords de la bande bande, tandis que toutes les autres méthodes présentées sont fortement affectées.

La figure A.4 compare les performances des méthodes à base de MMSE en terme de taux d'erreur de bits avec rate un receptr MF et 1/3 Turbo Coding avec longueur de code de 4992 bits for QPSK modulation. Les performances du MMSE *simplifié* surpasse celles des autres. than 10^{-2} .

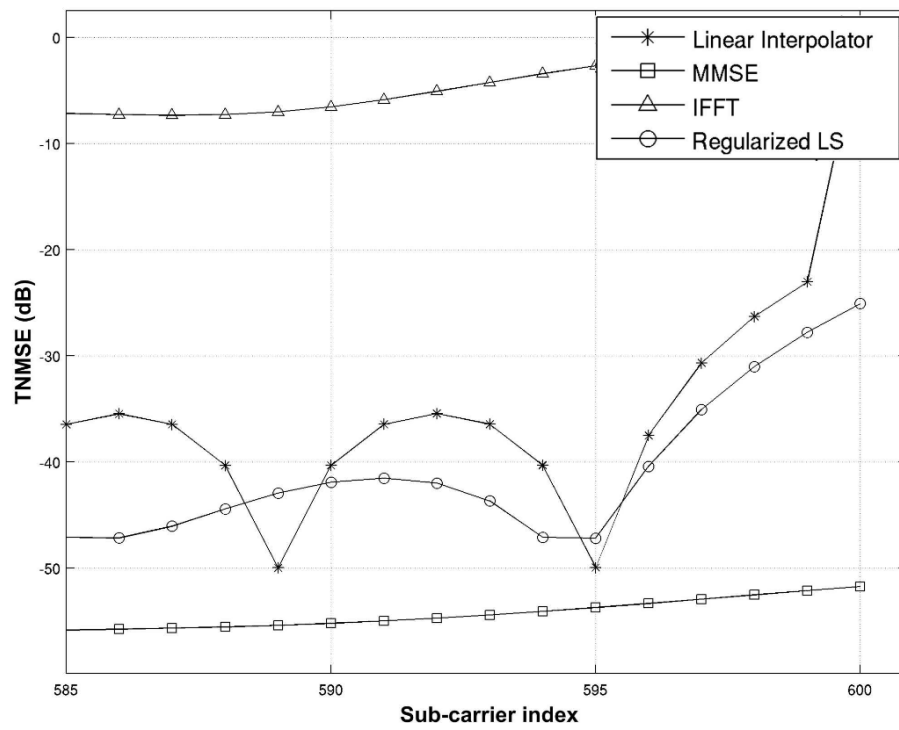


Figure A.1: Performances des estimation de canal, comportement aux bords de la bande.

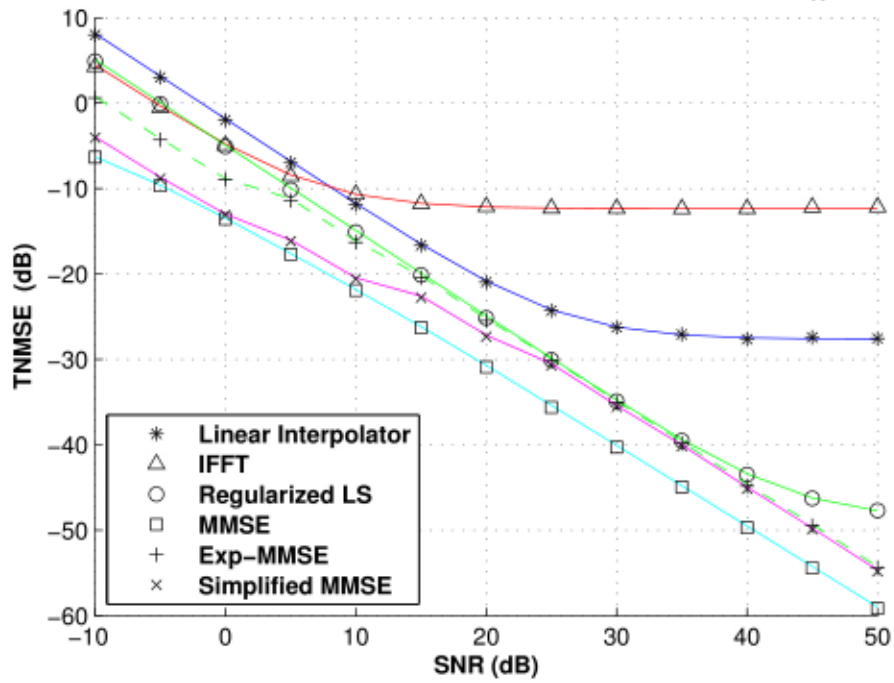


Figure A.2: CTF TNMSE versus SNR.

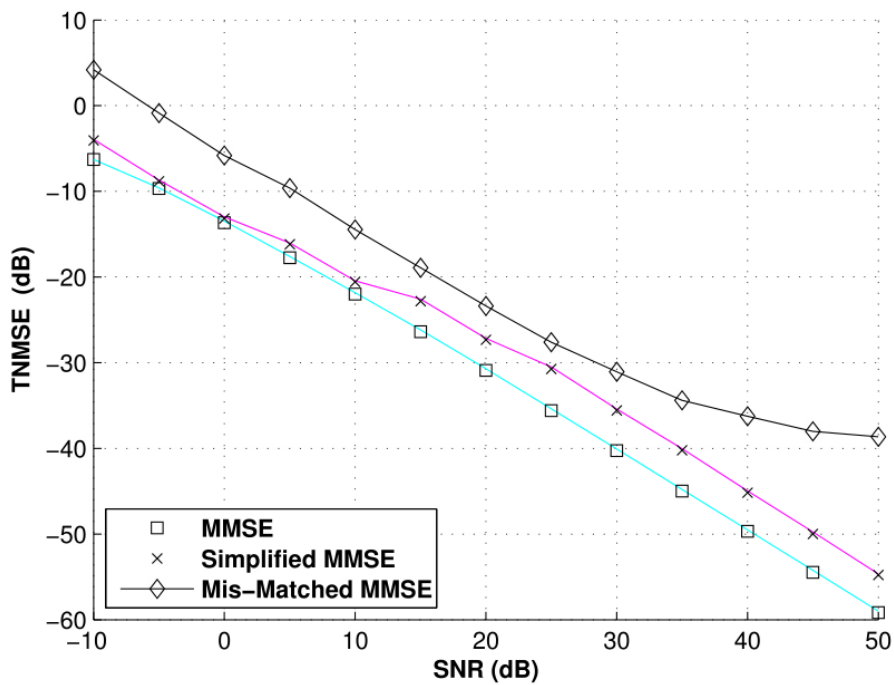


Figure A.3: CTF TNMSE versus SNR.

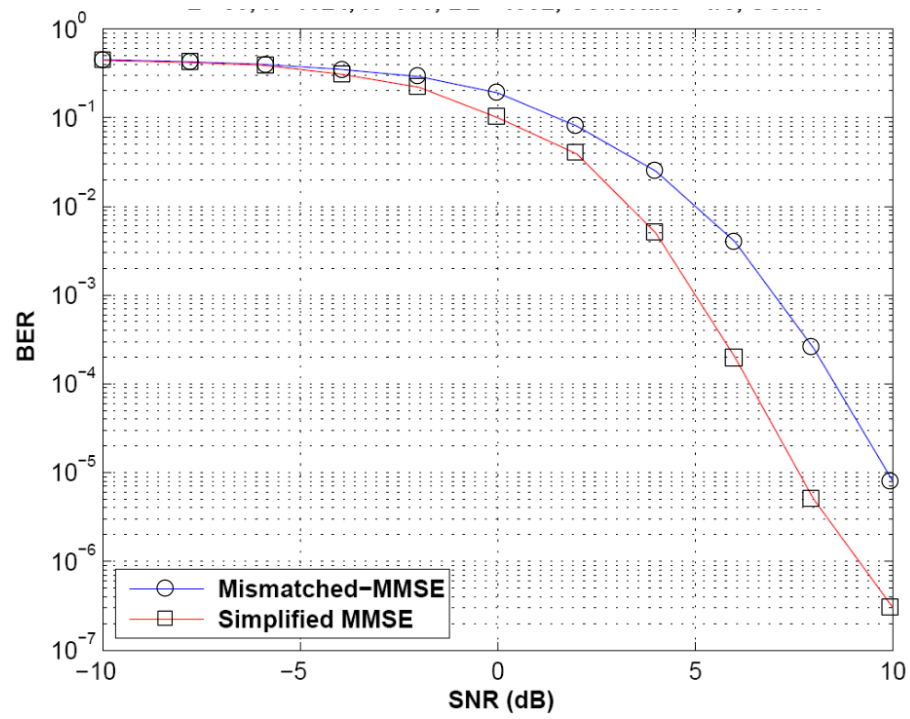


Figure A.4: BER versus SNR.

A.2 Détection OFDM avec canal variant rapidement

A.2.1 Introduction

OFDM permet une allocation flexible de la bande ainsi que architectures à faible complexité pour l'émetteur et le récepteur. Toutefois, la performance d'un récepteur OFDM à faible complexité est fortement impactée en présence d'un canal de propagation temps-variant par la hausse de l'interférence inter-porteuse (ICI). Ces conditions se produisent en présence d'un grand étalement Doppler par rapport au taux de symbole OFDM en raison de la vitesse du récepteur mobile. Le résultat variant dans le temps rapide des rendements de canaux de propagation de significatif ICI. Dans la pratique, l'augmentation ICI empêche schémas classiques de récepteurs OFDM à partir de détecter de manière fiable le signal désiré. Ainsi techniques les plus avancées de prééquilibration du récepteur sont nécessaires pour atténuer l'effet de l'ICI.

Techniques d'égalisation ICI linéaire optimale impliquent généralement inversion complète de la matrice de canal complexe. Dans les systèmes de télécommunication OFDM existants, la taille typique de la nécessaire transformation de Fourier discrète rend une telle opération d'inversion de matrice de canal complet prohibitif complexe pour la mise en oeuvre pratique. Ainsi plusieurs approches ont été adressées à réduire la complexité tout en conservant des performances acceptables. À cette fin, l'utilisation du temps-domaine fenêtrage de l'OFDM signal reçu a été montré pour limiter la durée importante de l'ICI, générant des matrices *bandeées* de transfert de canal. En outre, itératif d'égalisation et des techniques de détection ont été proposées pour réduire davantage la complexité du récepteur fonctionnant dans le domaine fréquentiel, voir par exemple [65], [67] et les références citées, ou dans le domaine temporel comme dans [68], [69].

Nous introduisons un cadre général pour itérative annulation ICI. L'analyse de la performance de détection, la vitesse de convergence, et la complexité fournissent des lignes directrices pour dériver roman rapide convergence des algorithmes itératifs

d'annulation ICI dans le temps et en fréquence. Nous montrons que la bonne *pre-conditioning* exploitant la structure intrinsèque du signal OFDM et les rendements ICI à la performance de détection quasi optimal avec très rapide de convergence et de complexité réduite algorithmes itératifs. En outre, nous interprétons techniques de fenêtrage sous une perspective plus générale par rapport à la modélisation d'extension de base (BEM) du canal variant dans le temps [77]. Dans la section A.2.2, nous introduisons le modèle de signal du modèle de système OFDM considéré envisagé d'inclure le BEM de canal variant dans le temps. Ensuite, nous rappelons techniques d'égalisation linéaires connus et nous tirons des approches itératives ICI annulation dans la section A.2.4 et A.2.5 respectivement. La performance et la complexité des techniques présentées sont discutés dans la section A.2.6 avec l'appui des résultats numériques.

A.2.2 Modèle du système et du signal

Nous considérons que la transmission sur un variant dans le temps, la fréquence sélective canal à évanouissement avec impulsion en temps continu réponse $h(t, \tau) = \sum_m \alpha_m(t) \psi(\tau - \tau_m)$ supposé obéir au modèle de diffusion stationnaire non corrélés au sens large (WSSUS) 2.3.1, où $\psi(\tau)$ représente l'émission-récepteur frontal filtre passe-bas équivalent, τ_m représente the p -ième retard de trajet, $\alpha_m(t)$ est le coefficient de canal complexe variant dans le temps associée au m -ième trajet du canal de propagation, respectivement. Nous désignerons $h[k, l]$ que la réponse impulsionnelle à temps discret correspondant passe-bas échantillonné, et assumer $h[k, l]$ pour être bien approchée par un modèle de réponse impulsionnelle finie avec un retard maximum la propagation de L échantillons. Ensuite, nous supposons un système OFDM classique avec cyclique préfixe de durée $N_{cp} \geq L$ pour éviter l'interférence inter-symbole. En laissant N représenter le nombre de sous-porteuses, la durée du symbole OFDM est donnée par $N_{block} = N + N_{cp}$. Le k -ième symbole OFDM emis $\mathbf{s}[k] = [s[kN] \dots s[kN - N + 1]]^T$, où $(\cdot)^T$ représente l'opération de transposition, comprenant le symboles codés $s[i]$ à la sortie du codage de canal, de l'entrelacement et du mappage sur une constellation finie \mathcal{S} supposé i.i.d. avec une énergie unitaire, est modulé par la $N \times N$ matrice unitaire de la transformée discrète de Fourier \mathbf{F} de manière à obtenir

$$\mathbf{x}[k] = \mathbf{F}^H \mathbf{s}[k] \quad (\text{A.40})$$

où $(\cdot)^H$ denote l'opération de transposée Hermitienne. Sans tenir compte du préfixe cyclique, le n -ième symbole reçu peut s'écrire

$$\mathbf{r}[k] = \mathbf{H}[k] \mathbf{x}[k] + \mathbf{z}[k] \quad (\text{A.41})$$

où $\mathbf{r}[k] = [r[kN] \dots r[kN - N + 1]]^T$, $\mathbf{H}[k]$ représente la $N \times N$ matrice de convolution du canal dans le domaine du temps, et $\mathbf{z}[k] = [z[kN] \dots z[kN - N + 1]]^T$ représente un bruit additif Gaussien complexe et circulairement symétrique tel que $\mathbf{z}[k] \sim \mathcal{N}_C(\mathbf{0}, \sigma_z^2 \mathbf{I})$.

Par souci de la simplicité d'écriture et sans perte de généralité, nous allons supprimer l'index de temps k par la suite. Ainsi, l'équation (A.41) peut être réécrite comme suit

$$\mathbf{r} = \mathbf{H} \mathbf{F}^H \mathbf{s} + \mathbf{z} \quad (\text{A.42})$$

Car, en général $L \ll N$, la matrice de canal \mathbf{h} aura tendance à être *clairsemée* et *bandes*. Lorsque le canal est invariante dans le temps au sein d'un symbole OFDM, $\mathbf{b} \mathbf{d} \mathbf{m} \mathbf{h}$ est circulante et donc la dans le domaine fréquentiel matrice de canal, $\mathbf{F} \mathbf{h} \mathbf{F}^H$, est diagonale.

Cette caractéristique est largement exploitée pour effectuer l'égalisation a coefficient unique dans le domaine fréquentiel.

En cas de variation en temps du canal, \mathbf{h} n'est plus circulante et cela résulte dans une matrice de canal pleine dans domaine de fréquence. Ainsi, l'approche classique d'égalisation OFDM est très égalisation sous-optimale et plus complexe est nécessaire (voir [65], [67] et les références citées).

A.2.3 Représentation BEM du canal

La matrice de convolution du canal peut être reformulée comme

$$\mathbf{H} = \sum_{l=0}^{L-1} \mathbf{Q}_l \text{diag} \{ \mathbf{h}_l \} \quad (\text{A.43})$$

où $\mathbf{h}_l = \mathbf{h}[k, l] = [h[kN, l] \dots h[kN - N + 1, l]]^T$ comprend le l -ième trajet du canal temps-variant et \mathbf{Q}_l denote la correspondante $N \times N$ matrice circulante des délais avec des uns dans la l -ième diagonale inférieure et zéros ailleurs, c.a.d. avec des éléments $[\mathbf{Q}_l]_{ij} = 1$ if $j = (i-l)_{\text{mod } N}$ et zéros autrement. Le vecteur correspondant à l'évolution temps-variante de la l -ième prise de canal peut être exprimée en fonction de la BEM comme suit

$$\mathbf{h}_l = \mathbf{B} \mathbf{v}_l = \sum_{p=0}^{P-1} v_{l,p} \mathbf{b}_p \quad (\text{A.44})$$

où le $N \times P$ matrix $\mathbf{B} = [\mathbf{b}_0 \mathbf{b}_1 \dots \mathbf{b}_{P-1}]$ denote la base déterministe engendré par les P vecteurs complexes \mathbf{b}_p for $p = 0, \dots, P-1$, et $\mathbf{v}_l = [v_{l,0} \dots v_{l,P-1}]^T$ les coefficients stochastiques décrivant les l -ième comportement du coefficient de canal pour un bloc OFDM donné sur les fonctions de base P .

Puis, en substituant (A.43) en (A.44)

$$\begin{aligned} \mathbf{H} &= \sum_{l=0}^{L-1} \left(\sum_{p=0}^{P-1} v_{l,p} \text{diag} \{ \mathbf{b}_p \} \right) \mathbf{Q}_l \\ &= \sum_{p=0}^{P-1} \text{diag} \{ \mathbf{b}_p \} \sum_{l=0}^{L-1} v_{l,p} \mathbf{Q}_l \end{aligned} \quad (\text{A.45})$$

En définissant

$$\mathbf{B}_p = \text{diag} \{ \mathbf{b}_p \}$$

et sommant sur les L coefficients de canal, cela résulte en

$$\mathbf{H} = \sum_{p=0}^{P-1} \mathbf{B}_p \mathbf{F}^H \mathbf{D}_p \mathbf{F} \quad (\text{A.46})$$

Donc, le signal reçu \mathbf{r} of (A.42) peut être exprimé en accord avec la BEM du canal comme

$$\mathbf{r} = \sum_{p=0}^{P-1} \mathbf{B}_p \mathbf{F}^H \mathbf{D}_p \mathbf{s} + \mathbf{z} \quad (\text{A.47})$$

$\sum_{l=0}^{L-1} v_{l,p} \mathbf{Q}_l$ étant une matrice circulante, alors

$$\mathbf{D}_p = \mathbf{F} \sum_{l=0}^{L-1} v_{l,p} \mathbf{Q}_l \mathbf{F}^H$$

est une matrice diagonale.

La figure A.5 dépeint le modèle du signal OFDM reçu dans la représentation BEM du canal.

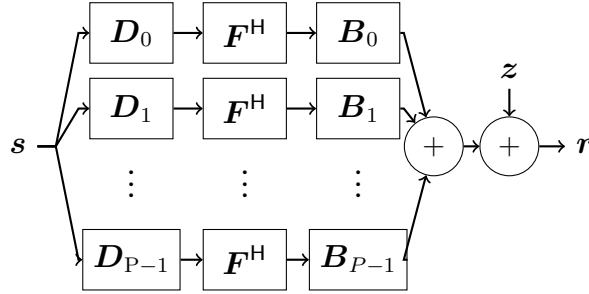


Figure A.5: Représentation BEM du signal OFDM reçu

A.2.4 Égalisation Linéaire

Dans cette section, on rappelle brièvement l'égalisation Minimum-Mean-Square-Error (Linéaire, L-MMSE), Zero Forcing (ZF), and Matched Filter (MF).

En laissant $\mathcal{H} = \mathbf{H}\mathbf{F}^H$, l'estimé de la sequence OFDM transmise devient

$$\hat{\mathbf{s}}_{\text{MMSE}} = (\mathcal{H}^H \mathcal{H} + \sigma_z^2 \mathbf{I})^{-1} \mathcal{H}^H \mathbf{r} \quad (\text{A.48})$$

$$\hat{\mathbf{s}}_{\text{ZF}} = (\mathcal{H}^H \mathcal{H})^{-1} \mathcal{H}^H \mathbf{r} \quad (\text{A.49})$$

$$\hat{\mathbf{s}}_{\text{MF}} = \mathcal{H}^H \mathbf{r} \quad (\text{A.50})$$

pour l'égalisation MMSE, ZF, and MF respectivement.

Dans l'assomption de connaissance *parfaite* du canal et de ses statistiques de deuxième ordre, les estimés MMSE et ZF (A.48) (A.49) engendrent l'inversion d'une matrice pleine qui en général nécessite une complexité de l'ordre de $\mathcal{O}(N^3)$ en utilisant des techniques classiques (comme l'élimination de *Gauss-Jordan* [76]). Dans les deux cas, des techniques itératives peuvent être adoptées pour éviter l'inversion complète de la matrice ainsi réduisant la complexité du récepteur comme détaillé dans la suite.

A.2.5 Cancellation itérative de l'ICI

Un large nombre de techniques itératives pour résoudre les systèmes linéaires ont été proposées dans la littérature, voir [71]. Pour une technique donnée, la complexité dépend du nombre d'opérations par itération et le nombre d'itérations nécessaires pour atteindre la précision voulue. Compte tenu de ces considérations, la vitesse de convergence est un aspect primordial pour la conception d'un algorithme itératif. En considérant un système linéaire générique de la forme

$$\mathbf{A}\mathbf{x} = \mathbf{b} \quad (\text{A.51})$$

où le vecteur \mathbf{x} est la séquence à estimer, \mathbf{b} est le vecteur observé, et la matrice \mathbf{A} est la matrice de transfert entrée-sortie, que l'on assume de rang plein avec dimensions $N \times N$ pour notre tractation. Ainsi, pour toute méthode d'estimation itérative, la convergence des estimés de la séquence $\hat{\mathbf{x}}^{(k)} \rightarrow \mathbf{x}$ est gouvernée par les propriétés spectrales de la matrice \mathbf{A} . Une métrique utilisée communément pour ces propriétés spectrales est le *nombre de conditionnement* (CN) $\kappa(\mathbf{A})$, défini comme le rapport entre le plus grand et le plus petit des valeurs propres de \mathbf{A} , $\kappa(\mathbf{A}) = |\lambda_{\max}(\mathbf{A})/\lambda_{\min}(\mathbf{A})|$ [71]. Le plus $\kappa(\mathbf{A})$ sera proche de 1, le plus rapidement un algorithme itératif convergera.

En particulier, les problèmes d'égalisation (A.48) et (A.49) peuvent être exprimés par la forme (A.51)

$$(\mathcal{H}^H \mathcal{H} + \sigma_z^2 \mathbf{I}) \hat{\mathbf{s}}_{\text{MMSE}} = \mathcal{H}^H \mathbf{r} \quad (\text{A.52})$$

$$(\mathcal{H}^H \mathcal{H}) \hat{\mathbf{s}}_{\text{ZF}} = \mathcal{H}^H \mathbf{r} \quad (\text{A.53})$$

Sous ces conditions, la convergence de toute approche itérative à la solution de ces deux problèmes dépendra de $\kappa(\mathcal{H}^H\mathcal{H}) = \kappa(\mathcal{H})^2$ dans la région de haut SNR ($\sigma_z^2 \rightarrow 0$). Dans le cas du système OFDM considéré, la matrice \mathcal{H} est en général de rang plein. Le problème ZF (A.53) peut être exprimé d'une façon équivalente comme

$$\mathcal{H}s_{\text{ZF}} = \mathbf{r} \quad (\text{A.54})$$

dont le CN est $\kappa(\mathcal{H})$, et comme $\kappa(\mathcal{H}) \leq \kappa(\mathcal{H}^H\mathcal{H})$, un algorithme itératif appliqué à (A.54) convergera plus rapidement qu'en appliquant (A.52) et (A.53).

On observe que le problème d'égalisation en (A.54) est caractérisé par les propriétés de la matrice du canal associée à la transmission OFDM. Au contraire, les problèmes d'égalisation MMSE et ZF de (A.52) et (A.53) sont *sur*-conditionnés dans le domaine du carré de la matrice de canal. Dans l'état d'équilibre (nombre d'itérations qui vont à l'infini en supposant convergence), la solution ZF donne généralement des performances pire que la solution MMSE en termes de performances de détection. Toutefois, lorsque les problèmes ZF et MMSE sont résolus par des techniques itératives, on doit considérer la performance réelle de détection (ou de l'exactitude de l'estimation) pour un nombre fini, limité d'itérations.

Les techniques itératives peuvent grandement profiter d'un *préconditionnement* approprié visant à réduire le CN et pour permettre une convergence plus rapide. La méthode itérative est donc appliquée à un système linéaire *préconditionné* dérivé de (A.51) dans

$$\mathbf{P}\mathbf{A}\mathbf{x} = \mathbf{P}\mathbf{b} \quad (\text{A.55})$$

avec \mathbf{P} étant la matrice de preconditionnement telle que $\kappa(\mathbf{A}) \geq \kappa(\mathbf{P}\mathbf{A}) \geq 1$ et avec $\mathbf{P}\mathbf{A} = \mathbf{I}$ if $\mathbf{P}^{-1} = \mathbf{A}$.

Plusieurs techniques de preconditionnement existent [71]. Parmi celles-ci, une méthode simple et directe est le preconditionnement de *Jacobi* où \mathbf{P} est choisi pour être diagonal et tel que $\text{diag}\{\mathbf{P}^{-1}\} = \text{diag}\{\mathbf{A}\}$ if $[\mathbf{A}]_{ii} \neq 0$ for $i = 1, \dots, N$. Le preconditionnement de *Jacobi* indique que l'opération de preconditionnement consiste à effectuer la résolution du problème de matrice inverse \mathbf{A} et transforme le problème original dans un mieux conditionné.

Égalisation itérative preconditionnée ZF À la lumière de ce qui précède, dans [68] une approche pertinente du problème ZF itératif d'annulation de ICI est proposé. Même si le travail référencé ne le mentionne pas, la méthode décrite consiste en un algorithme itératif *diagonale pré-conditionné* ZF. Le pré-conditionnement est composée d'une matrice diagonale dont les éléments sont exactement ceux de la matrice diagonale de l'inverse de la matrice de canal dans le domaine fréquentiel $\text{diag}\{\mathbf{P}\} = \text{diag}\left\{(\mathbf{F}\mathbf{H}\mathbf{F}^H)^{-1}\right\}$. La figure A.6 dépeint le diagramme a blocs de ce receveur. Notez que l'étage \mathcal{H} est réalisé utilisant la BEM du canal comme decrit par l'équation (A.46) et une base *polynomiale*. Fait intéressant, la complexité de cette approche est linéaire à la taille du bloc OFDM N .

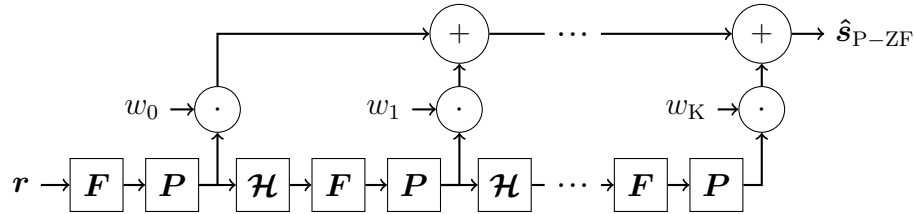


Figure A.6: Récepteur itératif ZF pré-conditionné

La performance de la méthode d'annulation d'ICI ZF préconditionné diagonale itérative [68] peut être améliorée à plusieurs égards. D'abord la diagonale de pré-conditionnement, bien que de faible complexité cède à un CN augmenté par rapport à $\kappa(\mathcal{H})$. Deuxièmement, il est intrinsèquement sous-optimale par rapport au MMSE depuis la tentative d'approcher la solution ZF. Dans ce qui suit, nous abordons plus rapide convergence des techniques itératives ICI approchant les performances de détection optimale MMSE pour une complexité comparable.

Cancellation Iterative Preconditionnée de l'ICI par BEM-MMSE Dans cette section, nous voulons nous rapprocher de la solution optimale MMSE par des techniques itératives combinant différentes formes préconditionnement *locale* MMSE et la combinaison basée sur la structure BEM. Quant à la méthode présentée dans la section A.2.5, le canal BEM nous permet de dériver ici expressions pour un pré-conditionneur amélioré encore à une complexité abordable. En effet, le canal BEM peut être exploitée sur le cté du récepteur et interprété comme un *multiple* fenêtrage du signal reçu lorsque des fonctions de fenêtrage l' correspond au conjugué de la base \mathbf{B}_p . Laissez le vecteur de sortie de chaque branche de *fenêtrage* être définie comme

la projection du signal reçu sur le p -ème fonction de base

$$\mathbf{y}_p = \mathbf{F}\mathbf{B}_p^H \mathbf{r} \quad (\text{A.56})$$

alors le vecteur *élargi* d'observation du signal reçu est obtenu en empilant chaque vecteur issu d'une branche de fenêtrage dans un vecteur $PN \times 1$ comme

$$\mathbf{y} = \begin{bmatrix} \mathbf{y}_0 \\ \mathbf{y}_1 \\ \vdots \\ \mathbf{y}_{P-1} \end{bmatrix} = \begin{bmatrix} \mathbf{F}\mathbf{B}_0^H \\ \mathbf{F}\mathbf{B}_1^H \\ \vdots \\ \mathbf{F}\mathbf{B}_{P-1}^H \end{bmatrix} \mathbf{r} = \mathbf{U}\mathbf{r} \quad (\text{A.57})$$

Compte tenu de la représentation BEM de l'équation (A.46), nous estimons le symbole $s[n]$ à la sous-porteuse n en adoptant un filtre FIR MMSE *local* \mathbf{f}_n dans tous les tons pour toute sortie de chaque base. L'exploitation de la structure particulière de ICI dans la représentation BEM du canal peut limiter la complexité d'une égalisation dans toutes les sous-porteuses, en choisissant correctement un sous-ensemble des éléments du vecteur \mathbf{y} que $\bar{\mathbf{y}}_n = \mathbf{S}_n \mathbf{y}$ avec \mathbf{S}_n être une matrice FIR de *sélection* $L \times PN$ obtenue par extraction de L_{FIR} lignes de la matrice identité \mathbf{I}_{PN} exploiter de manière optimale la structure de \mathbf{U} pour un L_{FIR} donné et sous-porteuse n pour avoir

$$\hat{s}[n] = \mathbf{f}_n^T \bar{\mathbf{y}}_n \quad (\text{A.58})$$

Donc, les coefficients du filtre MMSE *per-ton* sont calculés tels que

$$\mathbf{f}_n^T = \text{E} \{s[n] \bar{\mathbf{y}}_n^H\} \mathbf{R}_{\bar{\mathbf{y}}_n}^{-1} \bar{\mathbf{y}}_n \quad (\text{A.59})$$

où $\mathbf{R}_{\bar{\mathbf{y}}_n} = \text{E} \{ \bar{\mathbf{y}}_n \bar{\mathbf{y}}_n^H \}$

ce qui donne

$$\mathbf{f}_n^T = \mathbf{1}_n \mathcal{H}^H \mathbf{U}^H \mathbf{S}_n^T [\mathbf{S}_n \mathbf{U} (\mathcal{H} \mathcal{H}^H + \sigma_z^2 \mathbf{I}) \mathbf{U}^H \mathbf{S}_n^T]^{-1} \quad (\text{A.60})$$

avec $\mathbf{1}_n$ étant le vecteur $1 \times N$ contenant 1 dans la n -ième position et 0 ailleurs. Il est remarquable de mentionner que l'expression ci-dessus découle de la multiplication d'un vecteur $1 \times L_{\text{FIR}}$ $\text{E} \{s(n) \bar{\mathbf{y}}_n^H\}$ et une $L_{\text{FIR}} \times L_{\text{FIR}}$ matrice inverse de $\mathbf{R}_{\bar{\mathbf{y}}_n}$ qui varie selon la sous-porteuse.

Néanmoins, celui-ci peut être calculée exigeant seulement $(2L - 1) L_{\text{FIR}}^2$ multiplications en raison de la nature à bandes de $\mathbf{H}\mathbf{H}^H + \sigma_z^2\mathbf{I}$ et les L_{FIR} éléments différents de zero de $\mathbf{S}_n\mathbf{U}$.

Par ailleurs, le calcul des coefficients de filtrage MMSE peut exploiter la cohérence entre les sous-porteuses et être faite par l'application d'une méthode récursive. Une approximation suffisamment précise de l'inverse de la matrice $\mathbf{R}_{\hat{\mathbf{y}}_n\hat{\mathbf{y}}_n}$, i.e. $\|\mathbf{I}_{L_{\text{FIR}}} - \hat{\mathbf{R}}_{\hat{\mathbf{y}}_n\hat{\mathbf{y}}_n}^{-1} \mathbf{R}_{\hat{\mathbf{y}}_n\hat{\mathbf{y}}_n}\| \leq \epsilon$ avec ϵ aussi faible que souhaité, peut être calculé en utilisant l'approximation de l'inverse sur la sous-porteuse $n - 1$ que l'initialisation et en appliquant la formule suivante itérative:

$$\begin{cases} \hat{\mathbf{R}}_{\hat{\mathbf{y}}_n\hat{\mathbf{y}}_n}^{-1(0)} = \hat{\mathbf{R}}_{\hat{\mathbf{y}}_{n-1}\hat{\mathbf{y}}_{n-1}}^{-1} \\ \hat{\mathbf{R}}_{\hat{\mathbf{y}}_n\hat{\mathbf{y}}_n}^{-1(i)} = 2\hat{\mathbf{R}}_{\hat{\mathbf{y}}_{n-1}\hat{\mathbf{y}}_{n-1}}^{-1(i-1)} - \hat{\mathbf{R}}_{\hat{\mathbf{y}}_{n-1}\hat{\mathbf{y}}_{n-1}}^{-1(i-1)} \mathbf{R}_{\hat{\mathbf{y}}_{n-1}\hat{\mathbf{y}}_{n-1}} \hat{\mathbf{R}}_{\hat{\mathbf{y}}_{n-1}\hat{\mathbf{y}}_{n-1}}^{-1(i-1)} \end{cases} \quad (\text{A.61})$$

à utiliser dans (A.73) pour calculer les coefficients de filtrage.

Tous les filtres coefficients peuvent être empilés dans une matrice *clairsemée* matrice de filtrage

$$\mathbf{G} = \begin{bmatrix} \mathbf{f}_0^T \mathbf{S}_0 \\ \mathbf{f}_1^T \mathbf{S}_1 \\ \vdots \\ \mathbf{f}_{N-1}^T \mathbf{S}_{N-1} \end{bmatrix} \quad (\text{A.62})$$

La matrice résultante du produit de $\mathbf{G}\mathbf{U}$ peut donc être vue comme un préconditionneur *amélioré* de type BEM-MMSE de \mathbf{H} . En outre, la complexité associée à l'opération de filtrage est proportionnelle à $P(N + N\log_2 N)$.

En effet, cette approche permet d'obtenir beaucoup mieux préconditionnement que celui présenté précédemment en s'appuyant sur *diagonale* préconditionnement. Son efficacité est illustré à la figure A.7 où la distribution-fonction cumulative (CDF) du CN pour préconditionnement BEM-MMSE est comparée à la fois le préconditionnement diagonale expliqué ci-dessus et au canal sans préconditionnement.

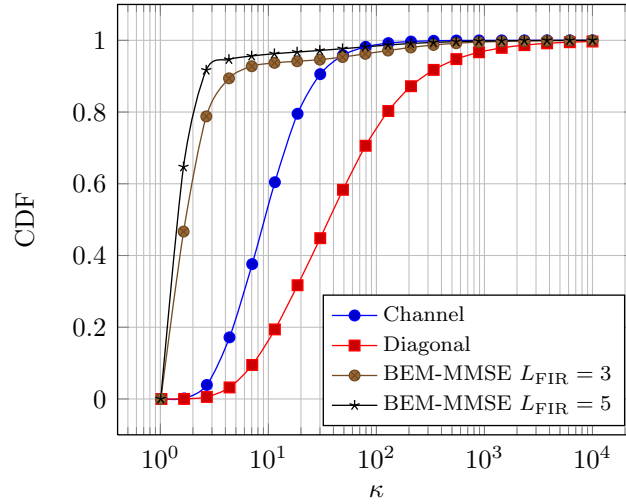


Figure A.7: Nombre de conditionnement pour preconditionnement diagonal et BEM-MMSE

Cette nouvelle approche peut être directement branché sur la méthode décrite dans la section A.2.5 pour donner le récepteur itératif polynôme *stationnaire* représenté dans la figure A.8 dont les performances sont considérablement améliorées, comme le montrent les résultats des simulations de la section A.2.6, mais encore de la complexité abordable que la méthode originale.

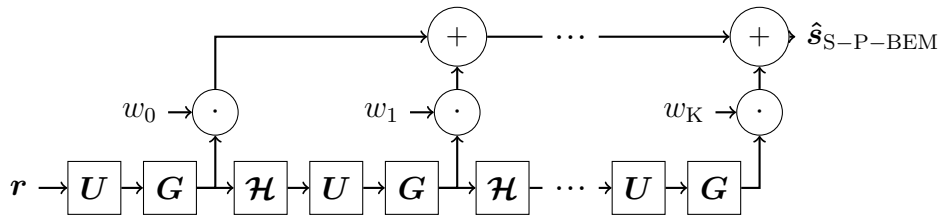


Figure A.8: Récepteur itératif polynôme preconditionné BEM-MMSE

Cancellation Iterative Non-stationnaire de ICI par preconditionnement BEM-MMSE Le même schéma de régime peut être appliqué de manière itérative dans le domaine temporel pour améliorer la performance d'annulation de ICI selon le schéma de la figure A.9.

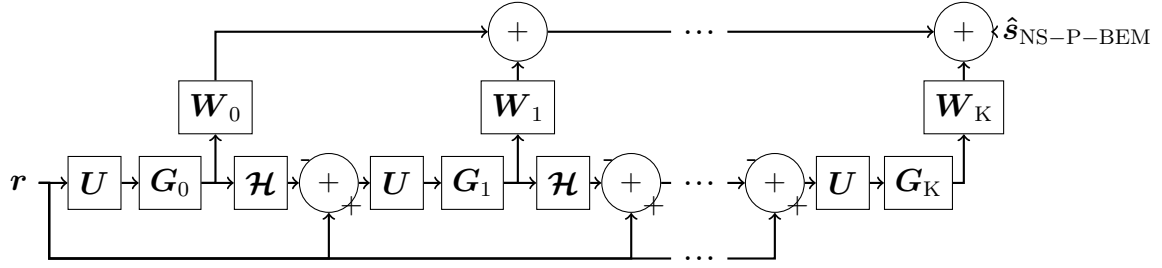


Figure A.9: Récepteur à Cancellation Iterative Non-stationnaire de ICI par préconditionnement BEM-MMSE

Dans ce cas, la matrice de filtrage MMSE \mathbf{G} est optimisée à chaque étage. Prenant le premier signal résultant de l'itération:

$$\mathbf{y}_1 = \mathbf{U} (\mathbf{r} - \mathcal{H} \hat{\mathbf{s}}_0) \quad (\text{A.63})$$

et $\hat{\mathbf{s}}_0$ calculé comme en (20), on obtient donc

$$\begin{aligned} \mathbf{y}_1 &= \mathbf{U} (\mathbf{r} - \mathcal{H} \mathbf{G}_0 \mathbf{y}_0) \\ &= (\mathbf{I} - \mathbf{U} \mathcal{H} \mathbf{G}_0) \mathbf{U} \mathbf{r} \end{aligned} \quad (\text{A.64})$$

et, en définissant $\mathbf{U}_1 = (\mathbf{I} - \mathbf{U} \mathcal{H} \mathbf{G}_0) \mathbf{U}$, nous pouvons réutiliser l'expression (18) pour trouver les coefficients MMSE de première itération. Il est facile de vérifier que lors de la deuxième itération, nous aurons

$$\begin{aligned} \mathbf{U}_2 &= (\mathbf{I} - \mathbf{U} \mathcal{H} \mathbf{G}_1 + \mathbf{U} \mathcal{H} \mathbf{G}_1 \mathbf{U} \mathcal{H} \mathbf{G}_0) \mathbf{U} \\ &= [\mathbf{I} - \mathbf{U} \mathcal{H} \mathbf{G}_1 (\mathbf{I} - \mathbf{U} \mathcal{H} \mathbf{G}_0)] \mathbf{U} \end{aligned} \quad (\text{A.65})$$

Au stade générique k , les coefficients peuvent alors être calculée par

$$\mathbf{f}_n^{\top(k)} = \mathbf{1}_n \mathcal{H}^H \mathbf{U}_k^H \mathbf{S}_n^T [\mathbf{S}_n \mathbf{U}_k (\mathcal{H} \mathcal{H}^H + \sigma_z^2 \mathbf{I}) \mathbf{U}_k^H \mathbf{S}_n^T]^{-1} \quad (\text{A.66})$$

et obtenir \mathbf{G}_k comme en (A.74).

L'estimation globale du signal après K itérations peut alors être obtenue par MMSE combinant des estimations à chaque étape. Laissez

$$\mathbf{X} = \begin{bmatrix} \mathbf{G}_0 \mathbf{U}_0 \\ \mathbf{G}_1 \mathbf{U}_1 \\ \vdots \\ \mathbf{G}_{K-1} \mathbf{U}_{K-1} \end{bmatrix} \quad (\text{A.67})$$

alors, le vecteur de coefficients $K \times 1$ pour la n -ième sous-porteuse \mathbf{c}_n^\top peut être calculée par

$$\mathbf{c}_n^\top = \mathbf{1}_n \mathcal{H}^\text{H} \mathbf{X}^\text{H} \mathbf{S}_n^\top [\mathbf{S}_n \mathbf{X} (\mathcal{H} \mathcal{H}^\text{H} + \sigma_z^2 \mathbf{I}) \mathbf{X}^\text{H} \mathbf{S}_n^\top]^{-1} \quad (\text{A.68})$$

Avec \mathbf{S}_n étant cette fois la matrice $K \times KN$ qui sélectionne la sous-porteuse n pour toute les ostries de chaque étage d'itération.

On obtient donc la matrice de pondération $N \times K$ par

$$\mathbf{W} = \begin{bmatrix} \mathbf{c}_0^\top \\ \mathbf{c}_1^\top \\ \vdots \\ \mathbf{c}_{N-1}^\top \end{bmatrix} \quad (\text{A.69})$$

et d'en tirer les matrices de pondération par-étape en prenant les colonnes de $\mathbf{W} = [\mathbf{w}_0 \cdots \mathbf{w}_{K-1}]$ pour obtenir l'estimation globale

$$\begin{aligned} \hat{\mathbf{s}}_{\text{NS-P-BEM}} &= \text{diag} \{ \mathbf{w}_0 \} \hat{\mathbf{s}}_0 + \cdots + \text{diag} \{ \mathbf{w}_{K-1} \} \hat{\mathbf{s}}_{K-1} \\ &= \mathbf{W}_0 \hat{\mathbf{s}}_0 + \cdots + \mathbf{W}_{k-1} \hat{\mathbf{s}}_{K-1} \end{aligned} \quad (\text{A.70})$$

Cancellation d'Interférence Parallèle par BEM-MMSE On pourrait penser à effectuer une détection de PIC dans le domaine temporel et la figure A.10 montre le schéma de principe du récepteur PIC en utilisant *hard-décisions* comme critère de décision non-linéaire.

En réglant $\mathcal{H}_p = \mathbf{B}_p \mathbf{F}^\text{H} \mathbf{D}_p$ and $\mathcal{H} = \sum_{k=0}^{P-1} \mathcal{H}_k = \mathbf{H} \mathbf{F}^\text{H}$, laissez

$$\mathcal{H}_{\bar{0}} = \mathcal{H} - \mathcal{H}_0 \quad (\text{A.71})$$

représenter la partie *temps-variante* de la matrice de canal assuming an orthogonal-polynomial basis, the coefficients of the PIC filtering matrix $\hat{\mathbf{G}}$ are computed according to a modified formula assuming perfect cancellation of the ICI

en supposant une base polynme orthogonal, les coefficients de la matrice de filtrage PIC $\hat{\mathbf{G}}$ sont calculés selon une formule modifiée en supposant annulation

parfaite de l'ICI

$$\begin{aligned}\hat{\mathbf{G}} &= \mathbf{H}_0^H \mathbf{U}_0^H [\mathbf{U}_0 (\mathbf{H}_0 \mathbf{H}_0^H + \sigma_z^2 \mathbf{I}) \mathbf{U}_0^H]^{-1} \\ &= \mathbf{H}_0^H [\mathbf{U}_0 (\mathbf{H}_0 \mathbf{H}_0^H + \sigma_z^2 \mathbf{I})]^{-1}\end{aligned}\quad (\text{A.72})$$

où $\hat{\mathbf{G}}$ est une matrice diagonale.

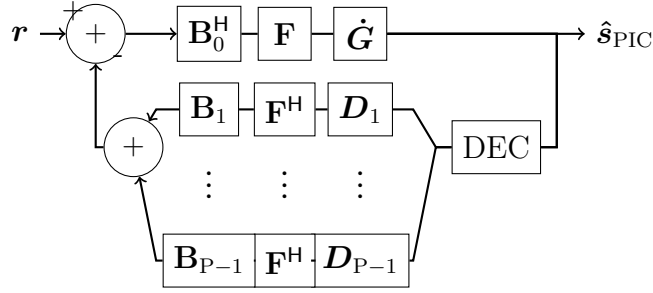


Figure A.10: Détecteur dans le domaine du temps de type PIC

Récepteur Préconditionné MMSE par méthode de gradient conjugué

Par souci d'exhaustivité et de comparaison, il est intéressant de dériver des techniques itératives d'annulation ICI opérant dans le domaine de la matrice de canal carré et résoudre le problème du MMSE l'état d'équilibre tel qu'il figure dans l'expression (A.52). Même s'il n'est pas attrayant en raison de la complexité inhérente supplémentaire requise et réduit les propriétés de convergence, elles sont toujours pertinentes pour démontrer les déclarations dans A.2.5.

Remarquant que la main gauche du système linéaire de détection MMSE dans (A.52) est hermitienne, l'algorithme de Gradient Conjugué (CG) peut être appliqué.

Une préconditionnement *bandé* calculé avec le développement similaire à celui de BEM-MMSE peut être obtenu pour un récepteur CG itératif *préconditionné* [71], dont l'algorithme est présenté dans la figure A.11. En laissant

$$\mathbf{f}_n^T = \mathbf{1}_n \mathbf{H}^H \mathbf{H} \mathbf{S}_n^T [\mathbf{S}_n \mathbf{H}^H (\mathbf{H} \mathbf{H}^H + \sigma_z^2 \mathbf{I}) \mathbf{H} \mathbf{S}_n^T]^{-1} \quad (\text{A.73})$$

et

$$\check{\mathbf{G}} = \begin{bmatrix} \mathbf{f}_0^T \mathbf{S}_0 \\ \mathbf{f}_1^T \mathbf{S}_1 \\ \vdots \\ \mathbf{f}_{N-1}^T \mathbf{S}_{N-1} \end{bmatrix} \quad (\text{A.74})$$

```

INPUT:  $\mathcal{H}$ ,  $\check{\mathbf{G}}$ ,  $\sigma_z^2$ ,  $\mathbf{r}$ ,  $K$ 
OUTPUT:  $\mathbf{s}_K$ 
# Initialize parameters
 $\mathbf{r}_0 = \mathcal{H}^H \mathbf{r}$ 
 $\mathbf{z}_0 = \check{\mathbf{G}} \mathbf{r}_0$ 
 $\mathbf{d}_0 = \mathbf{z}_0$ 
 $\mathbf{s}_0 = \mathbf{0}_N$ 
# Main loop
for  $k = 0$  to  $K - 1$  do
   $\alpha_k = \frac{\mathbf{r}_k^H \mathbf{z}_k}{\mathbf{d}_k^H (\mathcal{H}^H \mathcal{H} + \sigma_z^2 \mathbf{I}) \mathbf{d}_k}$ 
   $\mathbf{s}_{k+1} = \mathbf{s}_k + \alpha_k \mathbf{d}_k$ 
   $\mathbf{r}_{k+1} = \mathbf{r}_k - \alpha_k (\mathcal{H}^H \mathcal{H} + \sigma_z^2 \mathbf{I}) \mathbf{d}_k$ 
   $\mathbf{z}_{k+1} = \check{\mathbf{G}} \mathbf{r}_{k+1}$ 
   $\beta_k = \frac{\mathbf{r}_{k+1}^H \mathbf{z}_{k+1}}{\mathbf{r}_k^T \mathbf{z}_k}$ 
   $\mathbf{d}_{k+1} = \mathbf{z}_{k+1} + \beta_k \mathbf{d}_k$ 
end for

```

Figure A.11: Algorithme du Gradient Conjugué Preconditionné

pour un choix approprié de la matrice de selection \mathbf{S}_n et longueur du filtre L_{FIR} .

A.2.6 Resultats de simulation

Nous comparons les méthodes proposées dans ce document au moyen de simulations de Monte Carlo en supposant un préfixe cyclique OFDM configuration avec $N = 128$ sous-porteuses, un canal à trajets multiples avec $L = 4$ uniforme avec un profil de retard de puissance et de spectre Doppler Jakes avec la fréquence Doppler normalisée de 0.1 par rapport à l'espacement de sous-porteuse. Nous supposons un polynme orthogonal BEM de canal commande avec $p = 2$. La performance est mesurée en termes de taux d'erreur de bits sur séquences non codés modulés en QPSK. Le SNR est défini comme le rapport $1/\sigma_z^2$. Les méthodes présentées dans ce document sont évalués pour des longueurs de filtrage par préconditionnement BEM-MMSE de $L_{\text{FIR}} = 3$ et $L_{\text{FIR}} = 5$. Un certain nombre d'itérations $K = 1$ et $K = 3$ sont jugés pour permettre une comparaison équitable avec la méthode de [68]. Pour tous les résultats de simulation présentés dans les figures A.12 - A.15,

la technique d'annulation itérative de ICI non-stationnaire par preconditionnement BEM-MMSE (NS-P-BEM) fournit toujours les meilleures performances globales par rapport à la méthode de référence d'inversion de la matrice entière MMSE. La méthode CG preconditionnée (P-CG), en revanche, offre toujours la plus mauvaise performance avec le même nombre d'itérations et des longueurs de filtrage. Le ZF itératif Préconditionné (P-ZF) de [68] est considérablement améliorée par l'utilisation de preconditionnement stationnaire BEM-MMSE (SP-BEM) et le récepteur PIC itératif constitue un bon compromis en termes de performances et de complexité.

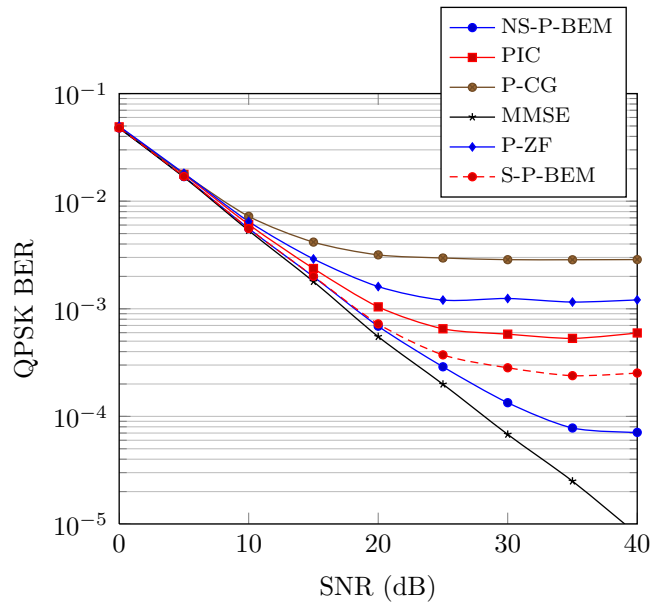


Figure A.12: Comparaison de performances des methodes iteratives avec 1 iteration, $L_{\text{FIR}} = 5$

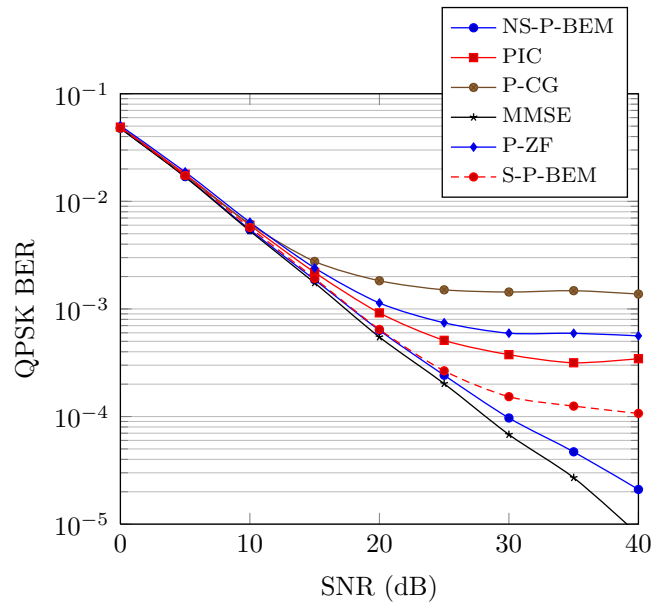


Figure A.13: Comparaison de performances des methodes iteratives avec 3 iterations, $L_{\text{FIR}} = 5$

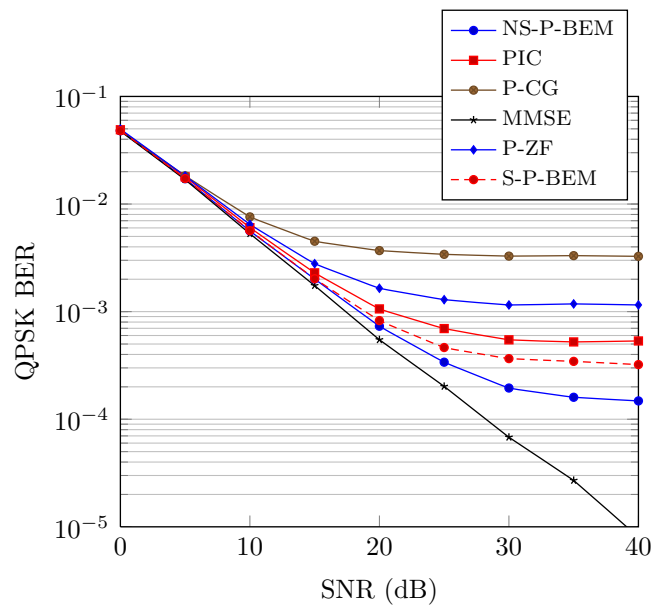


Figure A.14: Comparaison de performances des methodes iteratives avec 1 iteration, $L_{\text{FIR}} = 3$

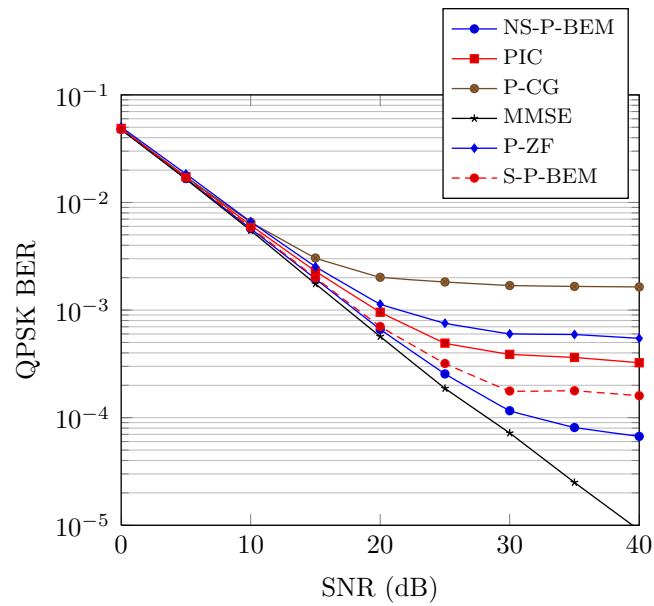


Figure A.15: Comparaison de performances des methodes iteratives avec 3 iterations, $L_{\text{FIR}} = 3$

Bibliography

- [1] R. W. Chang, *Synthesis of band-limited orthogonal signals for multichannel data transmission*, Bell Systems Technical Journal, vol. 46, pp. 1775-1796, December 1966.
- [2] B. R. Saltzberg, *Performance of an Efficient Parallel Data Transmission System*, IEEE Trans. on Communications, vol. 15, no. 6, pp. 805-811, Dec. 1967.
- [3] S. B. Weinstein and P. M. Ebert, *Data Transmission by Frequency-Division Multiplexing using the Discrete Fourier Transform*, IEEE Trans. on Communications, vol. 19, no. 5, pp. 628-634, Oct. 1971.
- [4] A. Peled, A. Ruiz, *Frequency domain data transmission using reduced computational complexity algorithms*, Proc. IEEE Int. Conf. Acoust., Speech, Signal Processing, pages: 964-967, Denver, CO, 1980.
- [5] P. Bannelli and S. Cacopardi, *Theoretical Analysis and Performance of OFDM Signals in Nonlinear AWGN Channels*, IEEE trans. on Comm., VOL. 48, No. 3, March 2000.
- [6] L. J. Cimini, *Analysis and simulation of digital Mobile Channel using Orthogonal Frequency Division Multiplexing*, IEEE Trans. in comm., vol. 33, pp. 665-675, July 1985.
- [7] X. Li and L. J. Cimini, *Effects of clipping and filtering on the performance of OFDM*, IEEE Commun. Lett., vol. 2, no. 5, pp. 131- 133, May 1998.
- [8] L. Wane and C. Tellambura, *A simplified clipping and filtering technique for PAR reduction in OFDM systems*, IEEE Signal Processing Lett., vol. 12, no. 6, pp. 453-456, June 2005.

- [9] A. Gatherer and M. Polley, *Controlling clipping probability in DMT transmission*, in 31st Asilomar Conf on Signal, System and Computers, vol. 1, Pacific Grove, CA, Nov. 2-5, 1997, pp. 578-584.
- [10] J. Armstrong, *Peak to average power reduction for OFDM by repeated clipping and frequency domain filtering*, IEE Elect. Lett., vol. 38, no. 5, pp. 246-247, Feb. 2002.
- [11] A. Jayalath, *OFDM for wireless broadband communications (peak power reduction, spectrum and coding)*, Ph D dissertation, School of Computer Science and Software Engineering, Monash University, May 2002
- [12] A. Jones, T. Wilkinson, and S. Barton, *Block coding scheme for reduction of peak to mean envelope power ratio of multicarrier transmission schemes*, IEE Elect. Lett., 01. 30, no. 25, pp. 2098-2099, Dec 1994.
- [13] H. Ochiai, *Analysis and reduction of peak to average power ratio in OFDM systems*, Ph.D dissertation, The Graduate School of Engineering, The University of Tokyo, Mar 2001.
- [14] C. Tellambura, *Use of m-sequence for OFDM peak-to-average power ratio reduction*, IEE Elect. Lett., "01. 33, no. 15, pp. 1300-1301, July 1997
- [15] J. Heiskala and J. Terry. *OFDM Wireless LANs: A theoretical and practical guide*, SAMS Publishing, 2001.
- [16] Y. Li and L. J. Cimini, *Bounds on the Interchannel Interference of OFDM in Time-Varying Impairments*, *IEEE trans. on Comm.*, VOL. 49, No. 3, March 2001.
- [17] X. Cai and G. B. Giannakis, *Bounding Performance and Suppressing Intercarrier Interference in Wireless Mobile OFDM*, *IEEE trans. on Comm.*, VOL. 51, No. 12, March 2003.
- [18] M. Russel and G. L. Stüber, *Interchannel interference analysis of OFDM in a mobile environment*, *Proc. VTC'95-Fall*, pp. 820-824, 1995.
- [19] P. Robertson and S. Kaiser, *The effects of Doppler spreads in OFDM(A) mobile radio channels*, *Proc. VTC'99-Fall*, pp. 329-333, 1999.
- [20] A. G. Burr, *Irreducible BER of COFDM on IIR channel*, *Electronics Letters*, VOL. 32, pp. 175-176, 1996.
- [21] 3GPP TS, *3GPP TS 36.211: Physical Channels and Modulation (Release 8)*, v. 8.2.0, www.3gpp.org.

- [22] J. J. Bussgang, *Cross correlation function of amplitude-distorted Gaussian signals*, *Res. Lab. Electron.*, M.I.T., Cambridge, MA, Tech. Rep. 216, Sect. 3, Mar. 26, 1952.
- [23] S. Sesia, I. Toufik and M. Baker, *LTE: The UMTS Long Term Evolution - From Theory To Practice*. Wiley and sons, 2009.
- [24] L. Hanzo and T. Keller, *OFDM and MC-CDMA: A Primer*, wiley-IEE Press 2006.
- [25] R. Nogueroles, M. Bossert, A. Donder, and V. Zyablov, *Improved performance of a random OFDMA mobile communication system*, in *Vehicular Technology Conference, 1998. VTC 98. 48th IEEE*. IEEE, 2002, vol. 3, pp. 2502–2506.
- [26] Ye Li et al., *Robust Channel Estimation for OFDM Systems with Rapid Dispersive Fading Channels*, *IEEE transactions on communications*, Vol. 46, pp. 903-912, Jul. 1998.
- [27] Frieder Sanzi et al., *An Adaptive Two-Dimensional Channel Estimator for Wireless OFDM with Application to Mobile DVB-T*, *IEEE transactions on broadcasting*, Vol 46, pp. 128-133, Jun. 2000.
- [28] 3GPP WG1, *TS 36.211: Physical Channels and Modulation (Rel. 8)*. Available: <http://www.3gpp.org/ftp/Specs/html-info/36211.htm>
- [29] 3GPP WG4, *TR 25.996: Spatial channel models for MIMO simulations*. Available: <http://www.3gpp.org/ftp/Specs/html-info/25996.htm>
- [30] Jan J. van de Beek et al., *On channel estimation in Ofdm systems*, *Vehicular Technology Conference*, Vol. 2, pp. 815-819, Jul. 1995.
- [31] M. Morelli et al., *A comparison of pilot-aided Channel estimation methods for OFDM systems*, *Signal Processing, IEEE Transactions on*, Vol. 49, pp. 3065-3073, Dec. 2001.
- [32] P. Hoher et al., *Pilot-Symbol-Aided Channel Estimation in Time and Frequency*, *Proc. Communication Theory Mini-Conf. (CTMC) within IEEE Global Telecommun. Conf. (Globecom 97)*, pp. 90-96, 1997.
- [33] G. Auer et al., *Pilot aided channel estimation for OFDM: a separated approach for smoothing and interpolation*, *Communications, 2005. ICC 2005. 2005 IEEE International Conference on*, Vol. 4, pp. 2173-2178, May 1997.

- [34] A. Ancora et al., *Down-Sampled Impulse Response Least-Squares Channel Estimation for LTE OFDMA, Acoustics, Speech and Signal Processing, 2007. ICASSP 2007. IEEE International Conference on*, Vol. 3, pp. III-293-III-296, April 2007.
- [35] A. Vosoughi and A. Scaglione, *The Best Training Depends on the Receiver Architecture in Proc. IEEE International Conference on Acoustics, Speech, and Signal Processing (ICASSP 2004)* (Montreal, Canada), May 2004.
- [36] R. Gold, *Optimal binary sequences for spread spectrum multiplexing (Corresp.)*, *Information Theory, IEEE Transactions on*, vol. 13, no. 4, pp. 619–621, 2002.
- [37] A. Vosoughi and A. Scaglione, *Everything You Always Wanted to Know about Training: Guidelines Derived using the Affine Precoding Framework and the CRB*. *IEEE Trans. on Signal Processing*, Vol. 54, pp. 940–954, March 2006.
- [38] 3GPP Technical Specification 25.211, *Physical Channels and Mapping of Transport Channels onto Physical Channels (FDD) (Release 8)*, www.3gpp.org.
- [39] N. Wiener, *Extrapolation, Interpolation, and Smoothing of Stationary Time Series*. New York: John Wiley & Sons, Ltd/Inc., 1949.
- [40] D. T. M. Slock, *Signal Processing Challenges for Wireless Communications in Proc. International Symposium on Control, Communications and Signal Processing (ISCCSP' 2004)* (Hammamet, Tunisia), March 2004.
- [41] 3GPP Technical Specification 36.211, *Physical Channels and Modulation (Release 8)*, www.3gpp.org.
- [42] R. Negi and J. Cioffi, *Pilot Tone Selection for Channel Estimation in a Mobile OFDM System*. *IEEE Trans. on Consumer Electronics*, Vol. 44, pp. 1122–1128, August 1998.
- [43] I. Barhumi, G. Leus and M. Moonen, *Optimal Training Design for MIMO OFDM Systems in Mobile Wireless Channels*. *IEEE Trans. on Signal Processing*, Vol. 51, pp. 1615–1624, June 2003.
- [44] 3GPP Technical Report 25.913, *Requirements for Evolved UTRA (E-UTRA) and Evolved UTRAN (E-UTRAN) (Release 7)*, www.3gpp.org.
- [45] 3GPP Technical Specification 36.101, *User Equipment (UE) Radio Transmission and Reception (Release 8)*, www.3gpp.org.

⁷All web sites confirmed 18th December 2008.

- [46] Motorola, Nortel, Broadcomm, Nokia, NSN, NTT DoCoMo, NEC, Mitsubishi, Alcatel-Lucent, CATT, Huawei, Sharp, Texas Instrument, ZTE, Panasonic, Philips, and Toshiba, *R1-081108: Way Forward on Dedicated Reference Signal Design for LTE Downlink with Normal CP*, www.3gpp.org, 3GPP TSG RAN WG1, meeting 52, Sorrento, Italy, February 2008.
- [47] P. Almers, *et al.* *Survey of Channel and Radio Propagation Models for Wireless MIMO Systems. EURASIP Journal on Wireless Communications and Networking*, pp. 957–1000, July 2007.
- [48] J. G. Proakis, *Digital Communications*. New York: McGraw Hill, 1995.
- [49] R. H. Clarke, *A Statistical Theory of Mobile-radio Reception. Bell Syst. Tech. J.*, pp. 957–1000, July 1968.
- [50] W. C. Jakes, *Microwave Mobile Communications*. New York: John Wiley & Sons, Ltd/Inc., 1974.
- [51] P. Hoeher, *A statistical discrete-time model for the WSSUS multipath channel in IEEE Transactions on Vehicular Technology*, Vol 41, No. 4, pp. 461–468, 1992.
- [52] J.-J. van de Beek, O. Edfors, M. Sandell, S. K. Wilson, and P. O. Börjesson, *On Channel Estimation in OFDM Systems in Proc. VTC'1995, Vehicular Technology Conference (VTC 1995)* (Chicago, USA), July 1995.
- [53] M. Morelli and U. Mengali, *A Comparison of Pilot-aided Channel Estimation Methods for OFDM Systems. IEEE Trans. on Signal Processing*, Vol. 49, pp. 3065–3073, December 2001.
- [54] P. Hoher, S. Kaiser and P. Robertson, *Pilot-Symbol-aided Channel Estimation in Time and Frequency in Proc. Communication Theory Mini-Conf. (CTMC) within IEEE Global Telecommun. Conf. (Globecom 1997)* (Phoenix, USA), July 1997.
- [55] A. Ancora, C. Bona and Slock D. T. M., *Down-Sampled Impulse Response Least-Squares Channel Estimation for LTE OFDMA in Proc. IEEE International Conference on Acoustics, Speech and Signal Processing (ICASSP 2007)* (Honolulu, Hawaii), April 2007.
- [56] J. W. Gibbs, *Fourier Series. Nature*, Vol. 59, p. 200, 1898.
- [57] D. Schafhuber, G. Matz and F. Hlawatsch, *Adaptive Wiener Filters for Time-varying Channel Estimation in Wireless OFDM Systems in Proc. IEEE International Conference on Acoustics, Speech, and Signal Processing (ICASSP 2003)* (Hong Kong), April 2003.

- [58] J. Cai, X. Shen and J. W. Mark, *Robust Channel Estimation for OFDM Wireless Communication Systems. An H_∞ Approach*. *IEEE Trans. Wireless Communications*, Vol. 3, November 2004.
- [59] H. Zhang, Y. Li, A. Reid and J. Terry, *Channel Estimation for MIMO OFDM in Correlated Fading Channels* in *Proc. 2005 IEEE International Conference on Communications (ICC 2005)* (Soeul, South Korea), May 2005.
- [60] H. Bölcskei, D. Gesbert and C. Papadias, *Space-time Wireless Systems: From Array Processing to MIMO Communications*. Cambridge: Cambridge University Press, 2006.
- [61] S. Sesia, I. Toufik and M. Baker, *LTE: The UMTS Long Term Evolution - From Theory To Practice*. Wiley and sons, 2009.
- [62] E. Isaacson and H. B. Keller, *Analysis of numerical methods*, New York: Wiley, 1966.
- [63] C. D. Meyer, *Matrix Analysis and Applied Linear Algebra*, Society for Industrial Mathematics, 2000.
- [64] D. T. M. Slock, *Signal processing challenges for wireless communications, Control, Communications and Signal Processing, 2004. First International Symposium on*, pp. 881–892, 2004.
- [65] L. Rugini, P. Banelli, RC Cannizzaro, and G. Leus, *Channel Estimation and Windowed DEF for OFDM with Doppler Spread*, in *2006 IEEE International Conference on Acoustics, Speech and Signal Processing, 2006. ICASSP 2006 Proceedings*, 2006, vol. 4.
- [66] J. W. Gibbs, *Fourier Series*. *Nature*, Vol. 59, p. 200, 1898.
- [67] P. Schniter and H. Liu, *Iterative frequency-domain equalization for single-carrier systems in doubly-dispersive channels*, in *Signals, Systems and Computers, 2004. Thirty-Eighth Asilomar Conference on*, 2004, vol. 1.
- [68] C.Y. Hsu and W.R. Wu, *A low-complexity ICI mitigation method for high-speed mobile OFDM systems*, in *2006 IEEE International Symposium on Circuits and Systems, 2006. ISCAS 2006. Proceedings*, 2006, p. 4.
- [69] T. Hrycak and G. Matz, *Low-complexity time-domain ICI equalization for OFDM communications over rapidly varying channels*, in *Proceedings of the 40th Asilomar Conference on Signals, Systems and Computers (ACSSC'06)*, pp. 1767–1771.

- [70] G.H. Golub and C.F. Van Loan, *Matrix computations*, Johns Hopkins University Press, 1996.
- [71] R. Barrett, *Templates for the solution of linear systems: building blocks for iterative methods*, Society for Industrial Mathematics, 1994.
- [72] R.R. Muller and S. Verdu, *Design and analysis of low-complexity interference mitigation on vector channels*, *IEEE Journal on Selected Areas in Communications*, vol. 19, no. 8, pp. 1429–1441, 2001.
- [73] A. Grant and C. Schlegel, *Convergence of linear interference cancellation multiuser receivers*, *IEEE Transactions on Communications*, vol. 49, no. 10, pp. 1824–1834, 2001.
- [74] L. Cottatellucci and R.R. Muller, *A systematic approach to multistage detectors in multipath fading channels*, *IEEE Transactions on Information Theory*, vol. 51, no. 9, pp. 3146–3158, 2005.
- [75] A. Bastug and D.T.M. Slock, *Polynomial expansion WCDMA receivers refined by local MMSE functionalities*, in *Signal Processing and Communications Applications Conference, 2004. Proceedings of the IEEE 12th*, 2004, pp. 387–390.
- [76] G.H. Golub, *Matrix computations*, J. H. University Press, 1996.
- [77] G.B. Giannakis and C. Tepedelenlioglu, *Basis expansion models and diversity techniques for blind identification and equalization of time-varying channels*, *Proceedings of the IEEE*, vol. 86, no. 10, pp. 1969–1986, 1998.
- [78] L. Zheng and D. Tse, *Diversity and multiplexing: a fundamental trade-off in multiple-antenna channels*, *IEEE Trans. Info. Theory*, vol. 49, no. 5, pp. 1073–1096, May 2003
- [79] S. M. Alamouti, *A simple transmit diversity technique for wireless communications*, *IEEE J. Selected Areas of Communications*, vol. 16, pp. 1451–1458, Oct. 1998
- [80] J. G. Proakis, *Digital Communications*, 4th ed., New York: McGraw-Hill, 2001, pp. 824–825
- [81] Vielmon et al., *Performance of Alamouti Transmit Diversity Over Time-Varying Rayleigh-Fading Channels*, *IEEE Transactions On Wireless Communications*, vol.3,no.5, Sept. 2004
- [82] D. B. Lin, *Performance Analysis of Two-Branch Transmit Diversity Block-Coded OFDM systems in Time Varying Multi-path Rayleigh-Fading Channels*, *IEEE Transactions On Vehicular Technology*, vol. 54, No. 1, Jan. 2005

- [83] M. Vu and A. Paulraj, *Linear Precoding for MIMO Channels with Non-zero Mean and Transmit Correlation in Orthogonal Space Time Coded Systems*, *Vehicular Technology Conference*, 2004. VTC2004-Fall. 2004 IEEE 60th Volume 4, Issue , 26-29 Sept. 2004 Page(s): 2503 - 2507 Vol. 4
- [84] D. T. M. Slock, *Diversity and Coding Gain of Linear and Decision-Feedback Equalizers for Frequency-Selective SIMO Channels* *Information Theory, 2006 IEEE International Symposium on*, July 2006 Page(s):605 - 609
- [85] D. J. Foschini, *Simplified processing for wireless communication at high spectral efficiency* *IEEE J. Selected Areas of Communications*, vol. 17, no. 11, pp. 1841-1852,1999
- [86] L. Lovász, *An algorithmic theory of numbers, graphs and convexity*, Society for Industrial Mathematics, 1986.
- [87] B.A. Lamacchia, *Basis Reduction Algorithms and Subset Sum Problems*, Technical report, MSc Thesis, Massachusetts Institute of Technology, 1991.
- [88] E. Agrell, T. Eriksson, A. Vardy, and K. Zeger, *Closest point search in lattices*, *Information Theory, IEEE Transactions on*, vol. 48, no. 8, pp. 2201–2214, 2002.
- [89] B. Hassibi and H. Vikalo, *On the expected complexity of integer least-squares problems*, in *Acoustics, Speech, and Signal Processing, 2002. Proceedings.(ICASSP'02). IEEE International Conference on*. IEEE, 2002, vol. 2, pp. 1497–1500.
- [90] J. Von Zur Gathen and J. Gerhard, *Modern computer algebra*, Cambridge Univ Pr, 2003.
- [91] C. Windpassinger and R.F.H. Fischer, *Low-complexity near-maximum-likelihood detection and precoding for MIMO systems using lattice reduction*, in *Information Theory Workshop, 2003. Proceedings. 2003 IEEE*. IEEE, 2003, pp. 345–348.
- [92] Y.H. Gan, C. Ling, and W.H. Mow, *Complex lattice reduction algorithm for low-complexity full-diversity MIMO detection*, *Signal Processing, IEEE Transactions on*, vol. 57, no. 7, pp. 2701–2710, 2009.